The Abdus Salam
International Centre for Theoretical Physics

United Nations
Educational, Scientific and
Cultural Organization

IAEA
International Atomic Energy Agency

2132-16

Winter College on Optics and Energy

8 - 19 February 2010

Fundamental limits and issues in BHJ-PSCs

K.S. Narayan
Jawaharlal Nehru Centre for Advanced Scientific Research
India

Lecture 2

Length scales

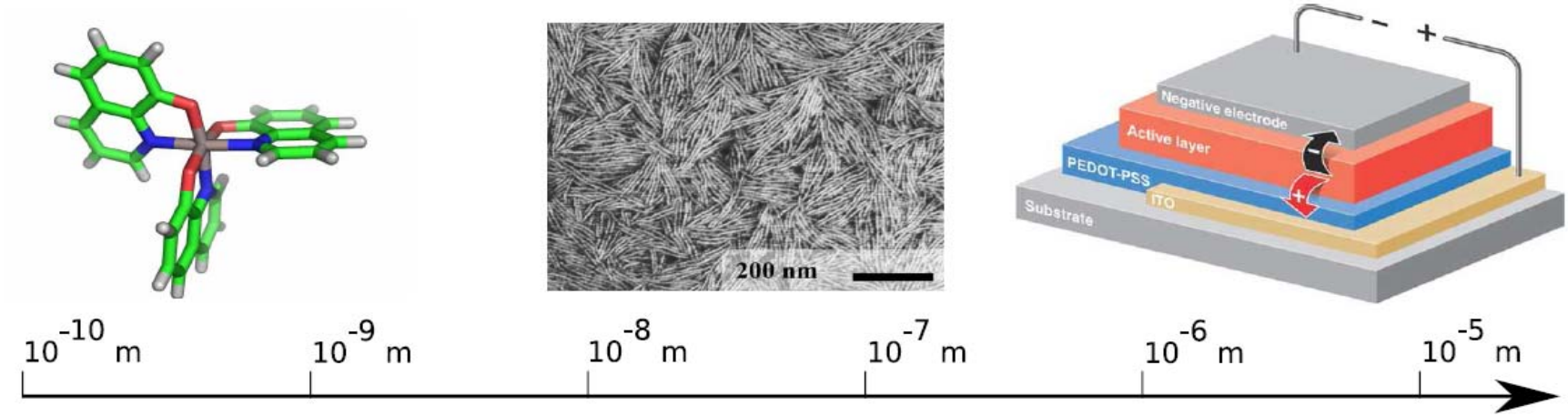

	Experimental techniques:	
Spectroscopy	*Microscopy, Crystallography*	*Device characterisation*

	Models:	
Molecular models	*ToFeT*	*'Macroscopic models'*

(Kwiatkowski, Doctoral thesis, 2008, Imperial College, London)

Inherently a multiple-length, time scale problem.

Ohmic Contacts ?

- What is the maximum current that can flow in a semiconductor ?

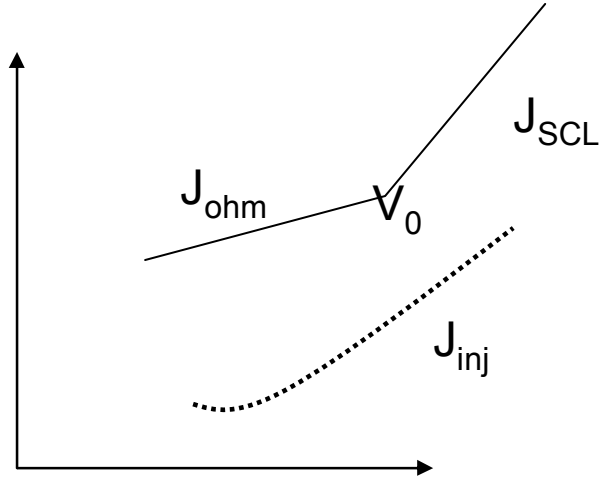

$J_{ohm} = eN\mu V/L$

$J_{SCL} = 9/8\varepsilon\varepsilon_0 \mu V^2/L$

$\eta = J_{inj}/J_{bulk}$

I-V Response:

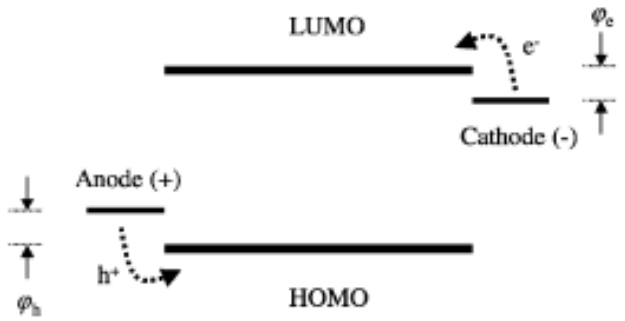

At low V : ohm's law $J = eN\mu V/l$

When $N > CV$

Then $J_{SCL} \sim \varepsilon\varepsilon_0\mu V^2/L^3$ Mott-Gurney

But, then contact comes into play also

And then the traps….

$$JP-F = B(T)E\exp[-\frac{\varphi_F - \beta_F E^{1/2}}{kT}] \qquad Poole-Frenkel$$

$$JS = A(T)T^2\exp[-\frac{\varphi_S - \beta_S E^{1/2}}{kT}] \qquad SchottkyEm\ ission$$

$$I_{DS} = I_{DS}(y) = W\mu Q_{channel}(y)E(y) = W\mu Q_{channel}(y)\frac{-dV(y)}{dy}$$

$$\int_0^L I_{DS}\,dy = \int_0^L W\mu Q_{channel}(y)\frac{-dV(y)}{dy}dy$$

$$I_{DS} = \frac{W}{L}\mu C_{ins}\left[\left(V_{GS} - V_T\right)V_{DS} - \frac{V_{DS}^2}{2}\right]$$

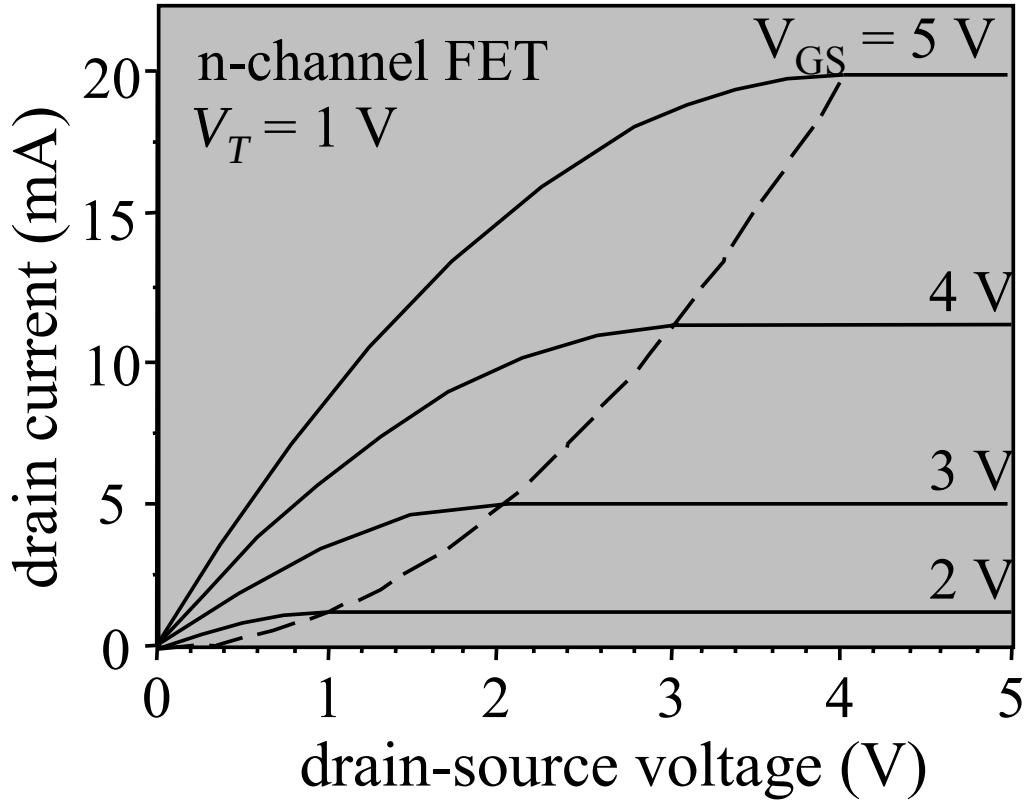

Mobility Is an Important Figure of Merit

μ= velocity/ (Electric field)

Charge Carrier Mobility Measurement By Time-Of-Flight Method

Schematics Of The Experiment

- Polymer layer is sandwiched between gold/ITO and semitransparent Al electrode.

- A narrow sheet of electron-hole pairs is produced by short-duration laser pulse near Al electrode.

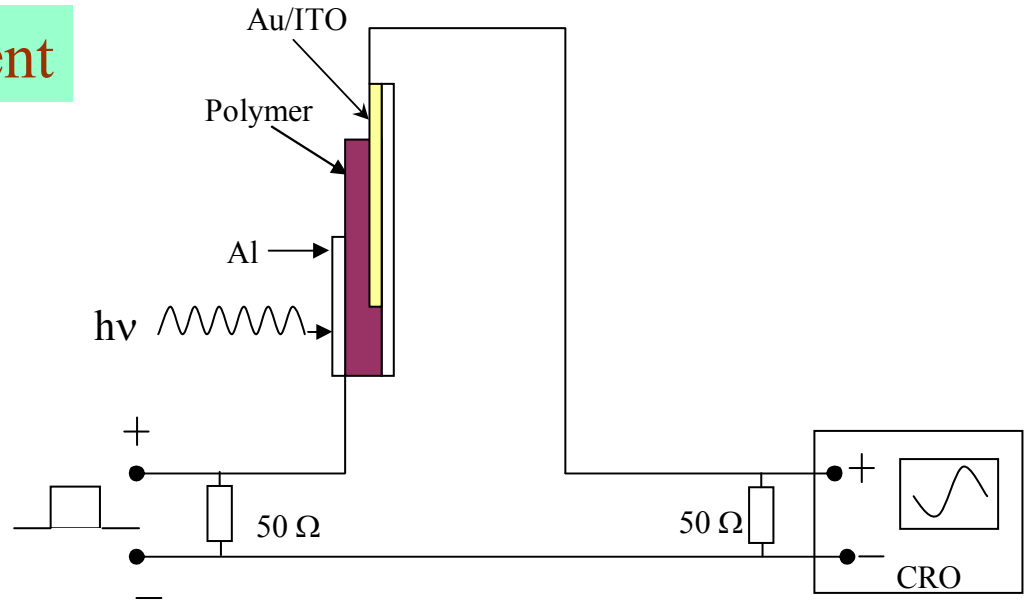

- According to the applied field holes drift across the polymer layer and get collected in the bottom electrode.

- Measurement of the transit time τ_{tr} permits a determination of mobility.

Different Modes Of Operation

- Current mode.

  $RC << \tau_{tr}$

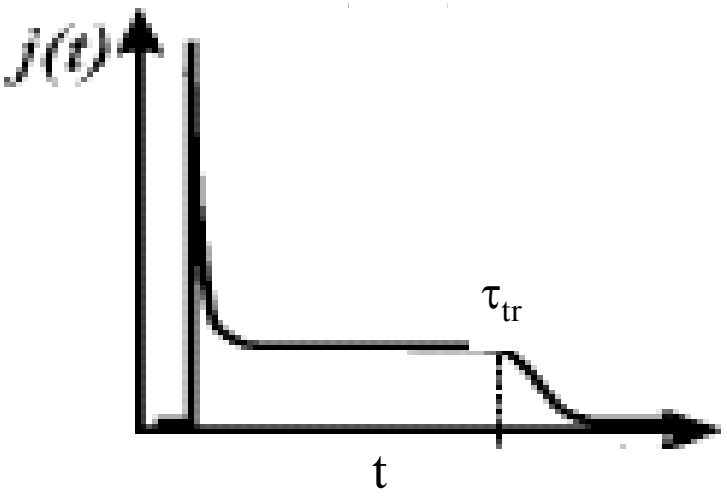

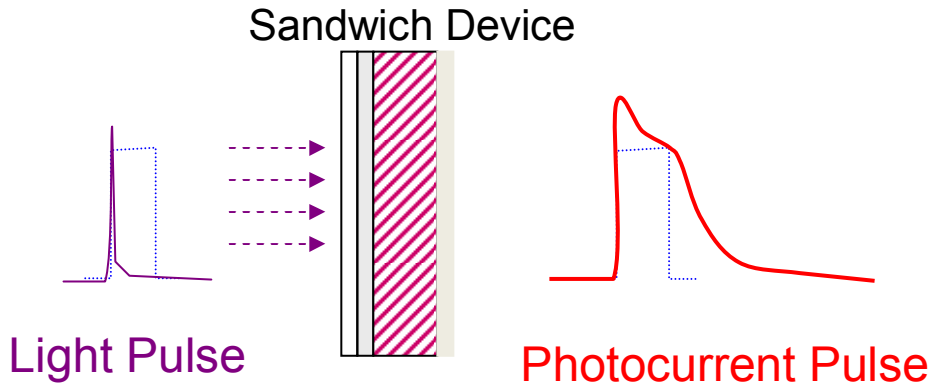

The transit time is determined from the inflection point.

Time of Flight.

Technique to study charge carrier transport in sample with low conductivity.

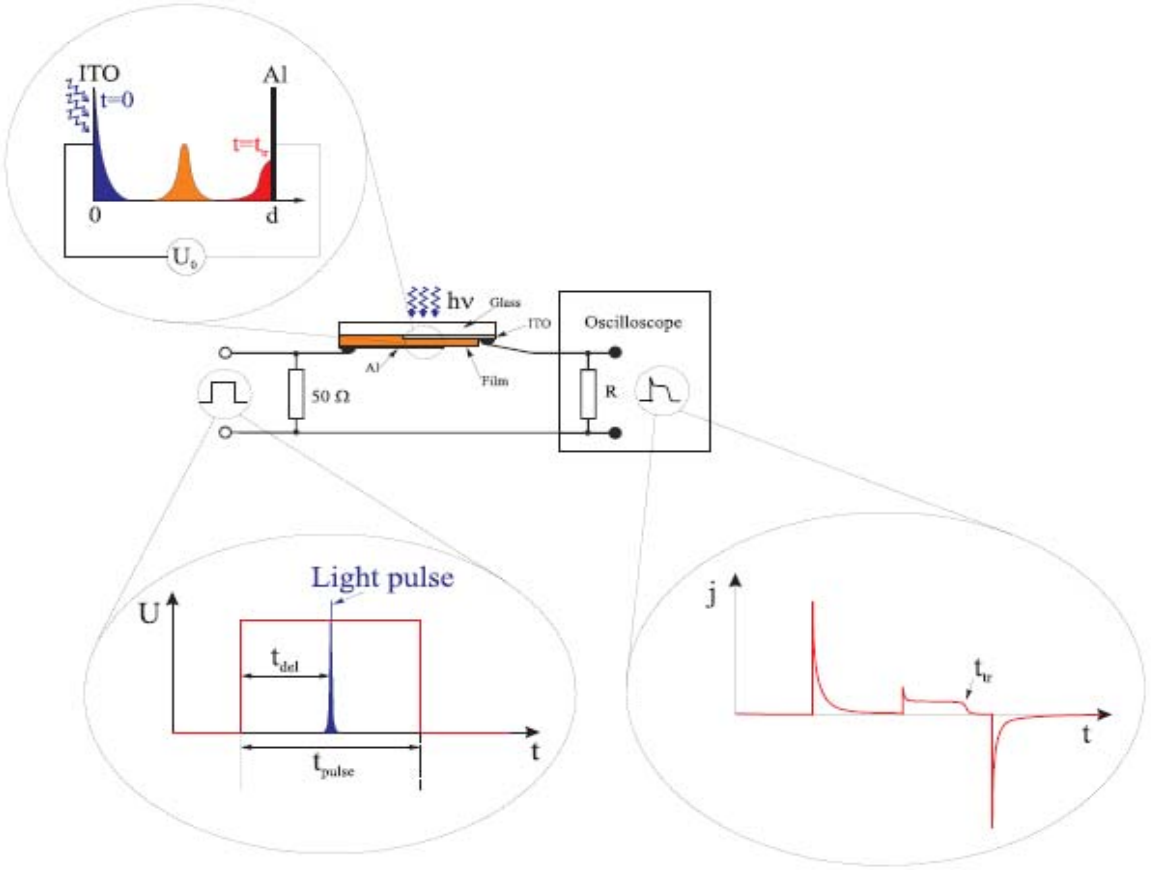

Schematic of set-up with pulse timing and charge transport in the film.

TOF is used in 2 modes based on transit time and sample time constant.

1) Differential (Current)
2) Integral(Charge)

PHILOSOPHICAL TRANSACTIONS OF THE ROYAL SOCIETY A

Phil. Trans. R. Soc. A (2007) **365**, 1473–1487
doi:10.1098/rsta.2007.2027
Published online 11 April 2007

What determines the mobility of charge carriers in conjugated polymers?

By Frédéric Laquai[1], Gerhard Wegner[1] and Heinz Bässler[2,*]

"mobility of charge carriers in a random organic solid is not a well-defined material parameter as it is in a crystalline inorganic semiconductor" depends on

- Traversal distance
- Temporal observation window
- Sample morphology

Macroscopic models

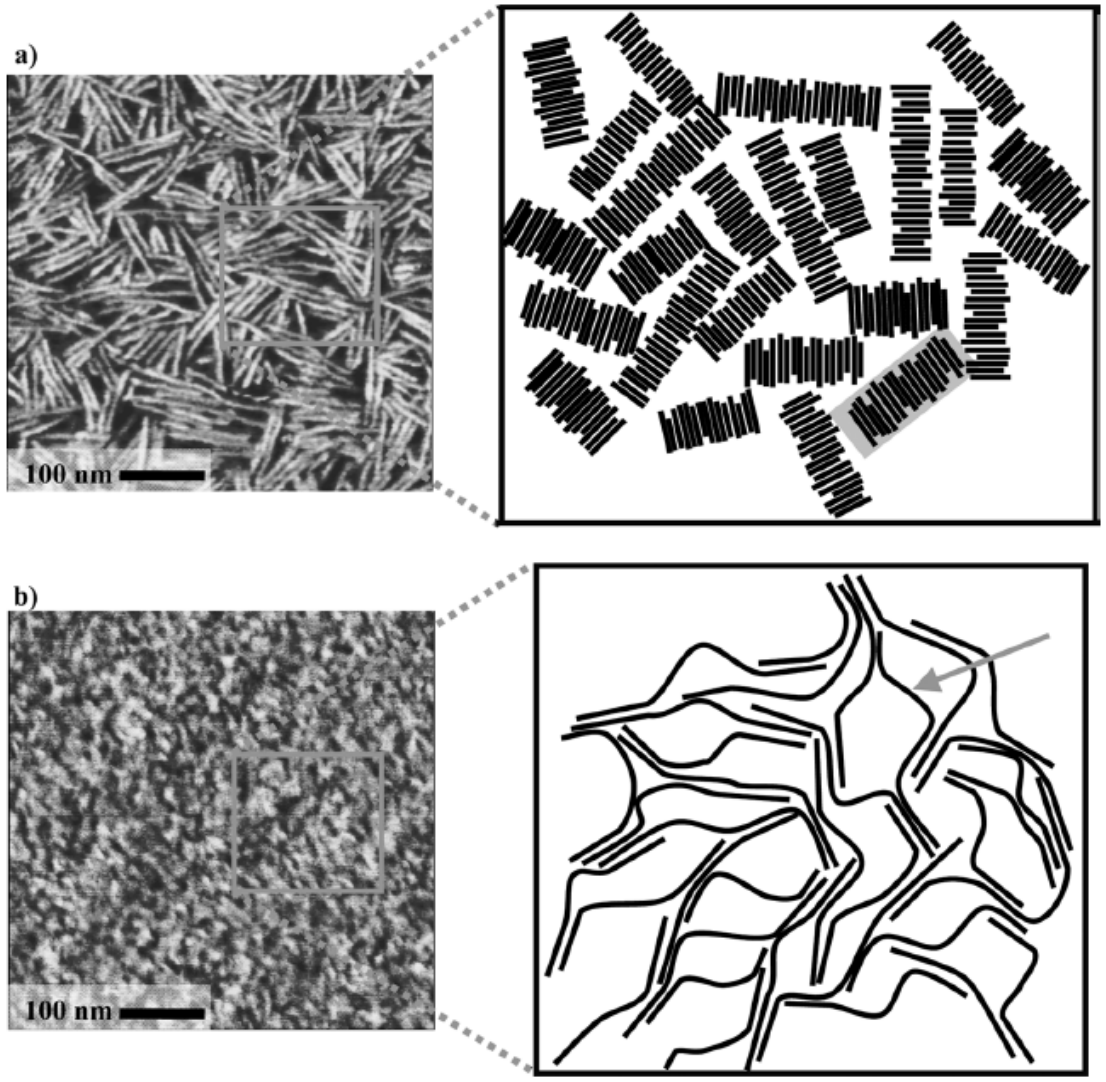

Low MW case

High MW case

(Kline, McGhee, Polymer Reviews (2006)).

Macroscopic models

- Probability evolution equation – Master equation approach

$$\frac{dP_m(t)}{dt} = \sum_n \left[A_{mn}\, P_m\,(t) - A_{nm}\, P_n\,(t)\right]$$

$P_m(t)$: Probability of molecule m being occupied at time t
A_{mn} : Rate of charge transfer from m to n

Recombination term $-\lambda_m P_m(t)$ could be added if necessary.

(Tessler et al, Adv. Mat, 21, 2741-2761 (2009).)
(Coropceanu et al, Chem.Rev. 2007, 107, 926-952)

Inputs for Macroscopic models

- Directed weighted graph (morphology)
- Hopping rates
  - Miller-Abraham (phonon-assisted)

$$\kappa_{ij} = \nu \exp(-2\gamma R_{ij}) \begin{cases} \exp\left(-\frac{\epsilon_j - \epsilon_i}{k_B T}\right) & \epsilon_j > \epsilon_i \\ 1 & \epsilon_j < \epsilon_i \end{cases}$$

ν : Attempt hopping frequency , γ: inverse localization radius / Overlap factor
$\varepsilon_i, \varepsilon_j$: energy levels of respective siteswhere; *v is the attempt-to-jump frequency,*
R_{ij}*is the distance between the states iand*
The wave function overlap of states *i and j is described by the first exponential term in*
while the second exponential termaccounts for the temperature dependence of
the phonon density

Reorganization energy neglected

(Coropceanu et al, Chem.Rev. 2007, 107, 926-952)

(Tessler et al, Adv. Mat, 21, 2741-2761 (2009).)

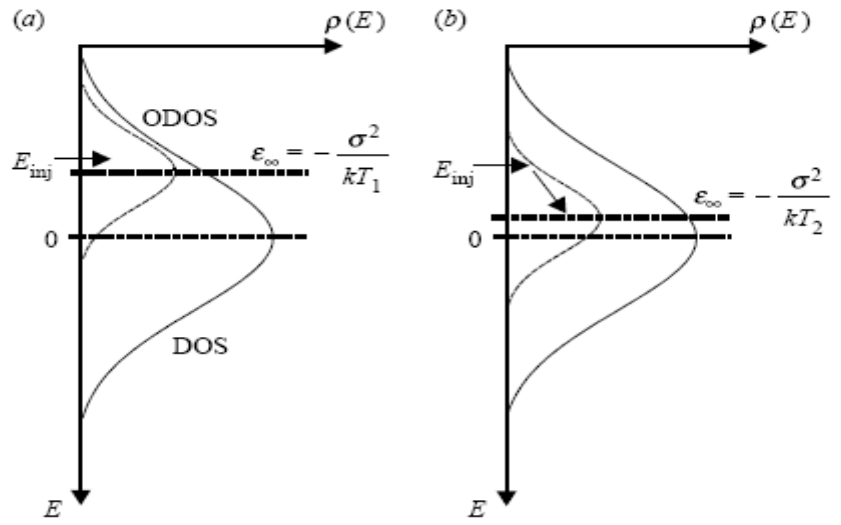

- carrier hops from site-to-site of an empty DOS of Gaussian profile with variance σ. If the carrier is initially generated randomly within the DOS, it tends to relax towards tail states.
- On average, the probability density of occupied states (ODOS) is also a Gaussian with variance σ yet displaced σ by an energy σ 2/kT relative to the centre of the DOS

$$\mu(T,F) = \mu_0 \exp\left[-\left(\frac{2\sigma}{3kT}\right)^2\right] \exp\, C_0\left[\left(\frac{\sigma}{kT}\right)^2 - \Sigma^2\right]\sqrt{F}.$$

Basslerdescribed the transport in disordered organic systems as a hopping process in a system with both positional and energetic disorder

H. B¨assler, Phys. Status Solidi B **175, 15 (1993).**

$$\mu = \mu_\infty e^{-\left(\frac{2\sigma}{3k_BT}\right)^2} \begin{cases} \exp\left(C\left[(\sigma/k_BT)^2 - \Sigma^2\right]\sqrt{F}\right) & \Sigma \geq 1.5 \\ \exp\left(C\left[(\sigma/k_BT)^2 - 2.25\right]\sqrt{F}\right) & \Sigma < 1.5, \end{cases}$$

σ - width of Gaussian distribution energy distribution
μ_∞ is the mobility in the limit $T \rightarrow \infty$,
C is a constant that is related to the lattice spacing
Σdescribes the positional disorder.

Inputs for Macroscopic models

- Hopping rates
  - Semi-classical Marcus theory/Mott
  - Electron transfer reaction description

$$\kappa_{ij} = \frac{t^2}{\hbar}\left[\frac{\pi}{k_B T \lambda_{reorg}}\right]^{1/2} \exp\left[-\frac{(\lambda_{reorg} + \epsilon_j - \epsilon_i)^2}{4\lambda_{reorg} k_B T}\right]$$

$$t = t_0 \exp(-\gamma R_{ij})$$

$\lambda_{\rho eorg}$: Reorganization energy / Polaron binding energy

(Tessler et al, Adv. Mat, 21, 2741-2761 (2009).)
(Coropceanu et al, Chem.Rev. 2007, 107, 926-952)

Equivalent circuit Approach

- Hopping network Resistor network

$$G_{ij} \approx \frac{q\upsilon_0}{kT}\exp(-2\gamma|R_{ij}|)$$
$$\exp\left(-\frac{|\varepsilon_j - E_F| + |\varepsilon_i - E_F| + |\varepsilon_j - E_i|}{2kT}\right)$$

- Solution of resistor network
  - Ambegaokar Percolation approach
  - Spreading impedance approach

(Tessler et al, Adv. Mat, 21, 2741-2761 (2009).)

Polymer Solar Cell: device structure ("plastic solar cell"):

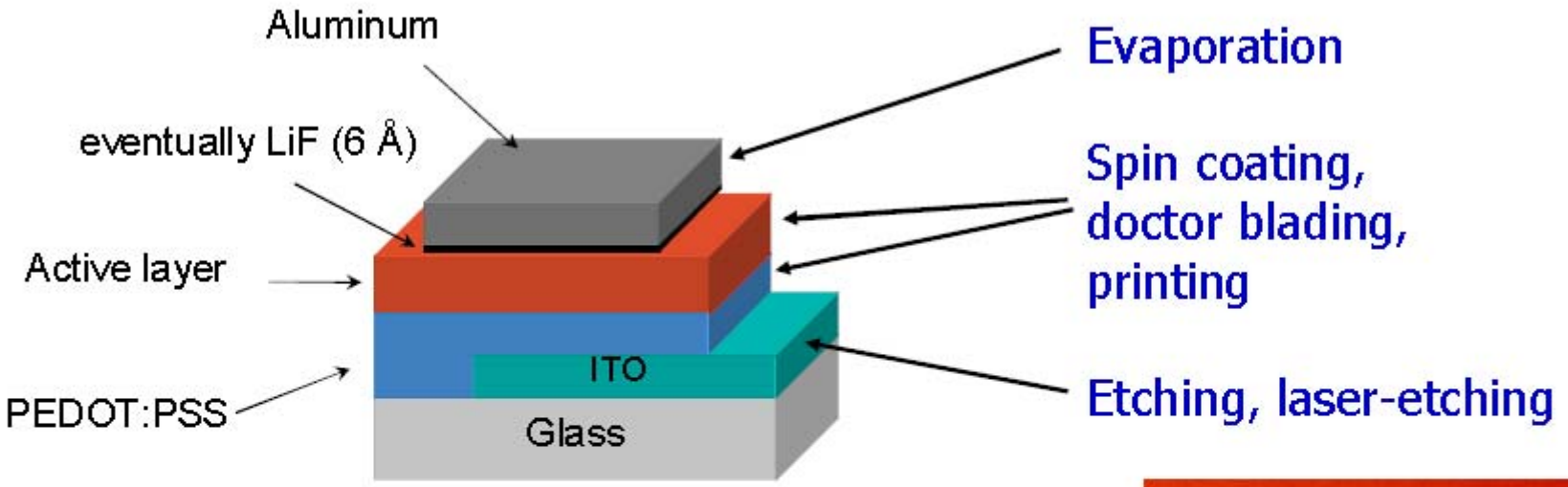

- **active layer**: conjugated polymer / fullerene blend
- **selective contacts**:

  electrons: Al/LiF

  holes: ITO/ PEDOT:PSS

  (poly[3,4-(ethylenedioxy) thiophene] : poly(styrene sulfonate))

or flexible plastic substrates

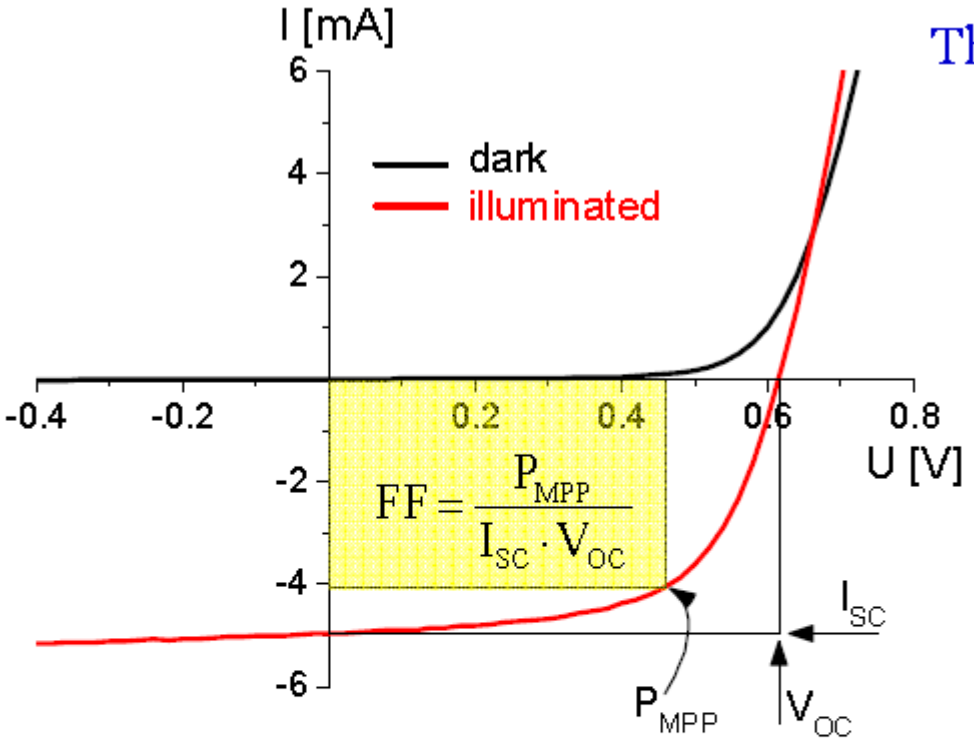

The power conversion efficiency η :

$$\eta = \frac{FF \cdot I_{SC} \cdot V_{OC}}{P_{in}}$$

Where:

1.) V_{OC}: open circuit voltage
2.) I_{SC}: short circuit (photo)current
3.) FF: fill factor
4.) MPP: maximum power point
5.) V_{MPP}: voltage at MPP
6.) I_{MPP}: photocurrent at MPP

more

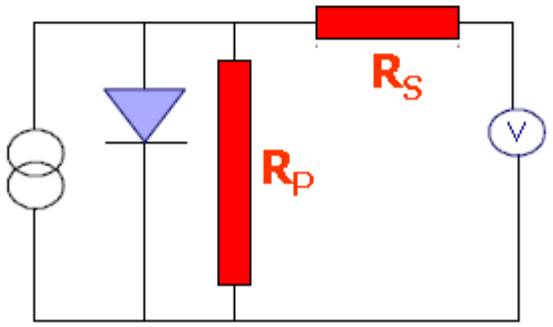

replacement circuit of a solar cell teaches us

keep

- the parallel resistance R_P as large as possible
- the serial resistance R_S as small as possible

η_{CC} and FF

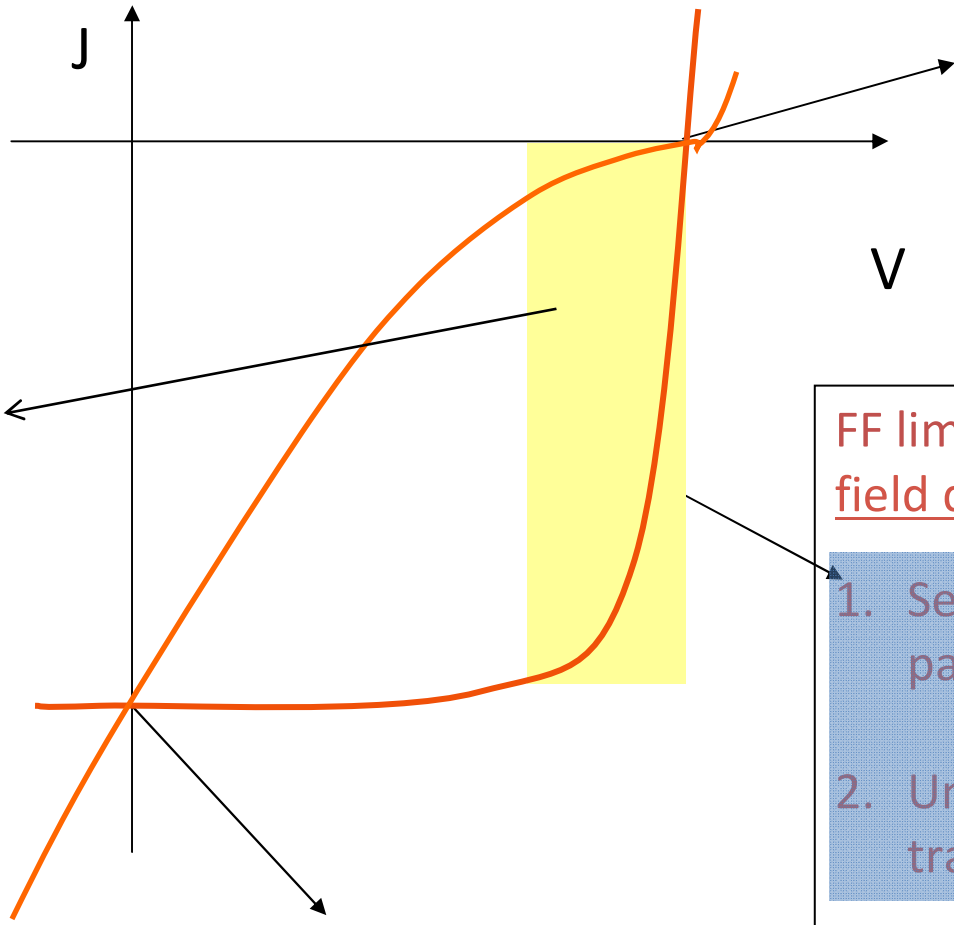

V_{oc} limited by:
Donor-acceptor energy levels

$V_{sat} < V < V_{OC}$
Low effective field region, strong field dependence of exciton dissociation rate changes the curvature

FF limited by:
field dependence of η_{CC}

1. Separation of geminate e-h pair to form free carriers.

Transport (Bulk)

2. Unbalanced 'e' and 'h' transport.

3. Inefficient collection at the metal-polymer interface.

Collection (Interface)

J_{sc} limited by: η_{IPCE}

$$J_{sc} = q\int \text{photon flux density}(\lambda) \times \eta_{\text{IPCE}}(\lambda)\, d\lambda$$

V_{OC} depends on the effective band gap E_g of the Donor – Acceptor combination, but it is independent of electrode used or the optical band gap of each polymer/fullerene molecules

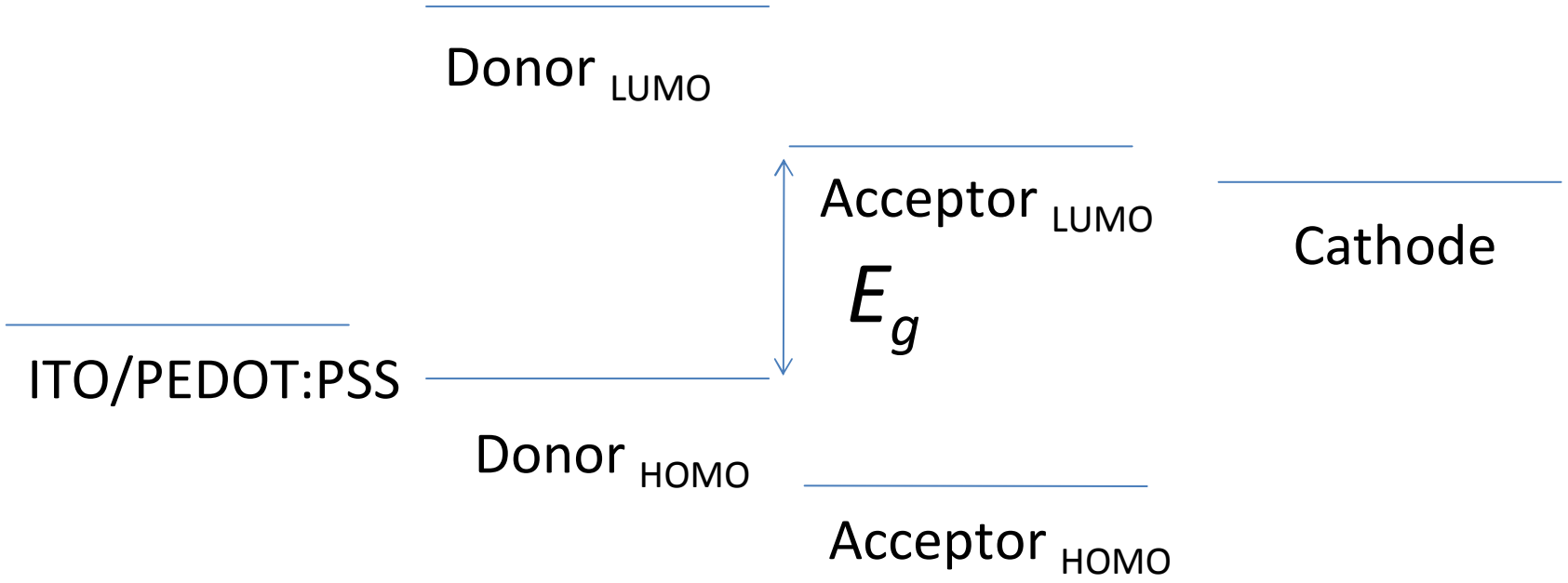

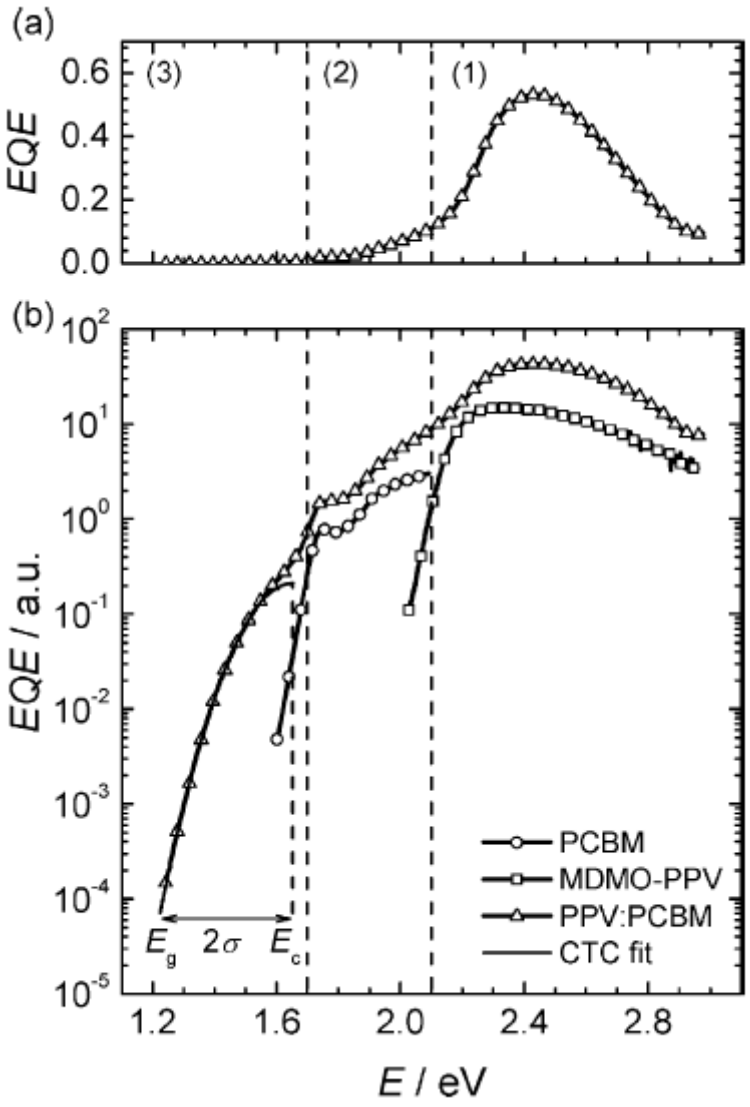

Figure 1. The external quantum efficiency (EQE) as a function of the energy (E) of the incident light of the MDMO-PPV:PCBM (1:4) photovoltaic device measured by FTPS presented on a) a linear and b) a logarithmic scale. The different spectral regions (1)–(3) are described in the text. In figure (b) the FTPS spectra of the pure materials are also represented (in arbitrary units). The non-additive CTC band can be fitted with a Gaussian function centred at E_c and with a standard deviation σ. We define the effective band gap Eg as $E_g = E_c - 2\sigma$, as shown in the figure

Vandewal *et.al*. Adv. Funct. Matter. 18, (2008)

Effect of HOMO level

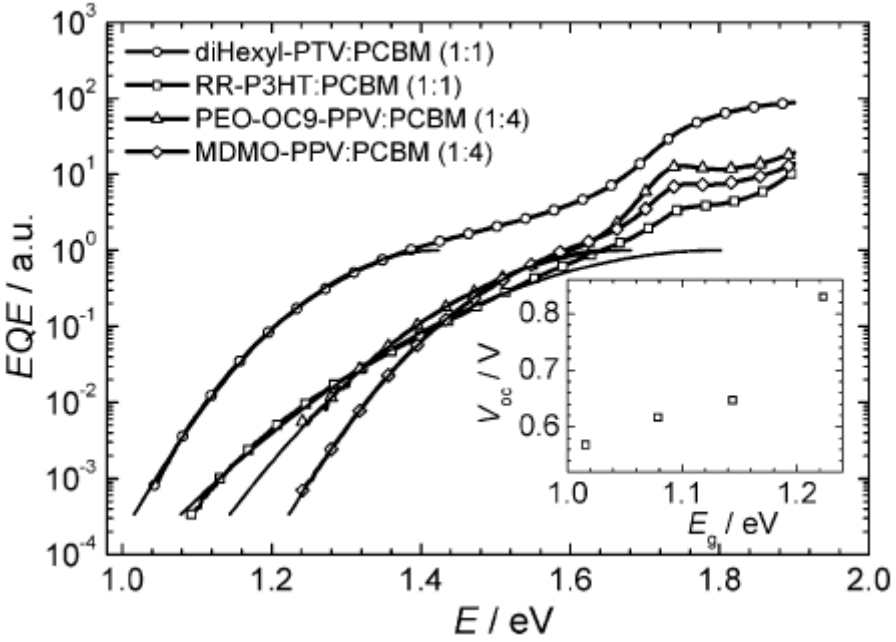

Charge Transfer band can be fitted with Gaussian function

$$A(E) = A_0 \exp\left[\left(E - E_c\right)/2\sigma^2\right]$$

$$E_g = E_c - 2\sigma$$

FTPS spectra of different types donor polymers blended with PCBM in the spectral area 1.0 eV<E<2.0 eV. The CT absorption band was fitted with a Gaussian and the band gap was determined as described in the text. The inset shows the open-circuit voltage Voc versus the effective band gap Eg.

Vandewal *et.al*. Adv. Funct. Matter. 18, (2008)

Effect of Morphology

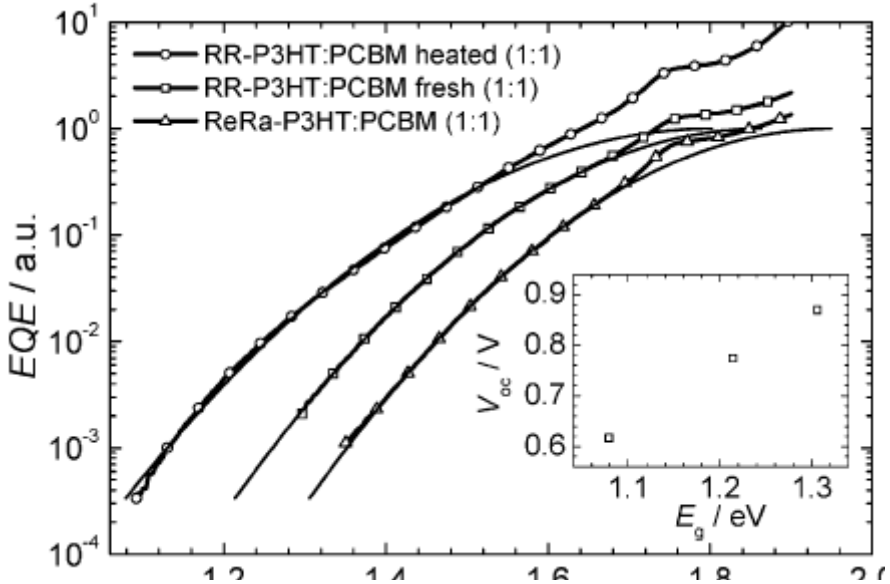

FTPS spectra of different types of P3HT blended with PCBM in the spectral area 1.0<E<2.0 eV. The CT absorption band was fitted with a Gaussian and the effective band gap was determined as described in the text. The inset shows the open-circuit voltage Voc versus the effective band gap Eg.

Table 2. Solar cell characteristic parameters for photovoltaic bulk hetero-junction devices consisting of P3HT with a different degree of crystallinity.

Donor Polymer	Heat treatment	J_{sc} [mA.cm^{-2}]	V_{oc} [V]	FF	E_c [eV]	E_g [eV]
ReRa-P3HT	no	0.73	0.87	0.29	1.95	1.31
RR-P3HT	no	3.5	0.77	0.36	1.86	1.21
RR-P3HT	yes	7.9	0.62	0.56	1.80	1.08

Vandewal *et.al*. Adv. Funct. Matter. 18, (2008)

Effect of optimum composition

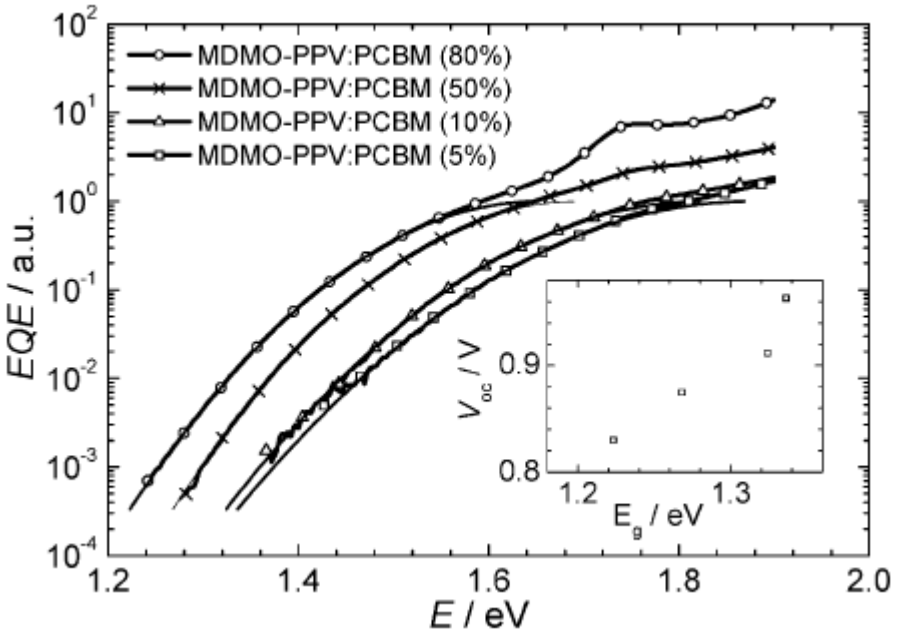

FTPS spectra of MDMO-PPV blended with different weight fractions of PCBM in the spectral area 1.2<E<2.0 eV. The CT absorption band was fitted with a Gaussian and the effective band gap was determined as described in the text. The inset shows the open-circuit voltage Voc versus the effective band gap Eg.

Table 4. Solar cell characteristic parameters for photovoltaic BHJ devices consisting of freshly prepared MDMO-PPV:PCBM blends with a different weight fractions of PCBM.

PCBM weight fraction [%]	J_{sc} [mA.cm^{-2}]	V_{oc} [V]	*FF*	E_c [eV]	E_g [eV]
5	0.062	0.97	0.23	1.87	1.34
10	0.13	0.91	0.23	1.83	1.32
50	2.6	0.88	0.30	1.69	1.27
80	3.9	0.83	0.53	1.65	1.22

Vandewal *et.al*. Adv. Funct. Matter. 18, (2008)

Relation between V_{OC} and E_g

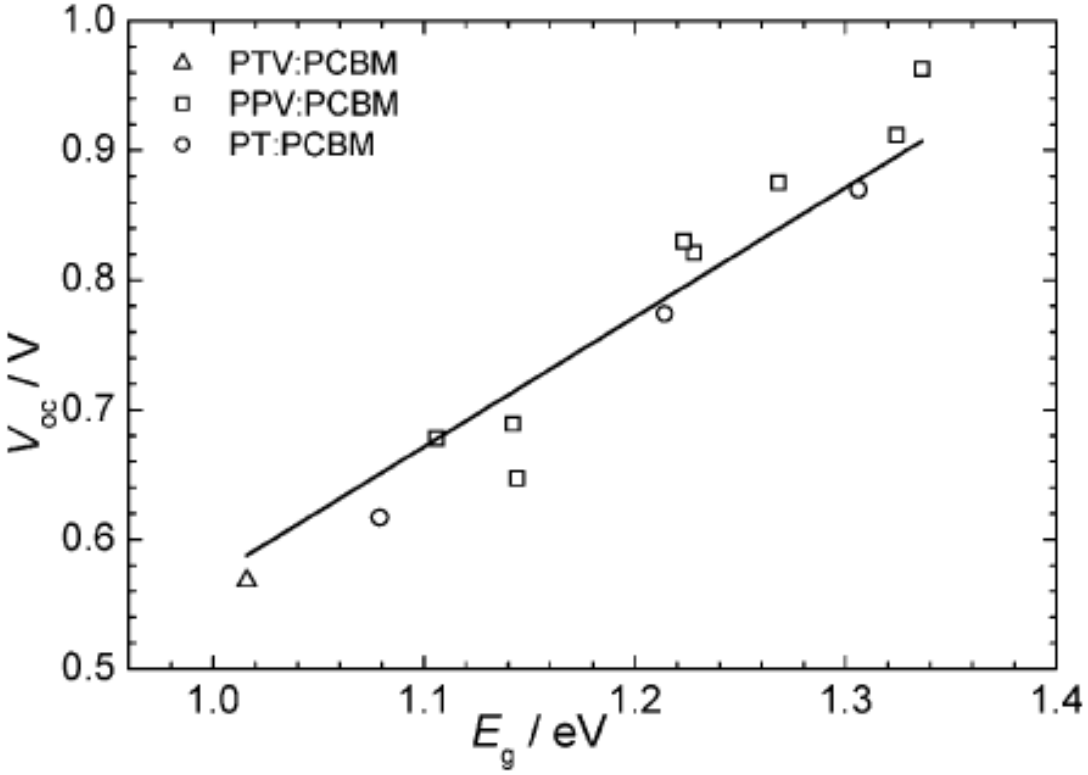

$$V_{OC} \sim E_g/e - 0.43\ \text{V}$$

The effective band gap E_g versus V_{oc} of all the studied photovoltaic devices

Vandewal *et.al*. Adv. Funct. Matter. 18, (2008)

Table 1 | Measured J_{sc}, V_{oc} and calculated J_0 for all of the devices studied in this work.

Material	J_{sc} (A m^{-2})	V_{oc} (V)	J_0 (A m^{-2})
P3HT-$PC_{61}BM$ (1:1)			
annealed	81 (±8)	0.62 (±0.01)	1.3 (±0.9) E-9
as prepared	35 (±8)	0.76 (±0.03)	5.6 (±3.0) E-12
PCPDTBT-$PC_{61}BM$ (1:2)			
with octyldithiols	100 (±5)	0.64 (±0.01)	1.9 (±1.1) E-9
without octyldithiols	66 (±7)	0.67 (±0.01)	6.7 (±5.3) E-11
LBPP5-$PC_{71}BM$ (1:3)			
	45 (±9)	0.73 (±0.015)	5.4 (±2.1) E-12
MDMO-PPV-$PC_{61}BM$			
1:4	34 (±7)	0.83 (±0.02)	2.2 (±0.8) E-13
1:1	14 (±2)	0.88 (±0.01)	1.1 (±0.4) E-14
4:1	3 (±0.6)	0.92 (±0.02)	3.8 (±2.2) E-15
APFO3-$PC_{61}BM$			
1:4	45 (±5)	1.02 (±0.01)	1.6 (±0.6) E-16
1:1	28 (±4)	1.08 (±0.015)	2.7 (±1.0) E-18
4:1	10 (±1)	1.16 (±0.01)	1.3 (±0.8) E-19
APFO3-$PC_{71}BM$			
1:4	35 (±5)	0.98 (±0.01)	1.5 (±0.3) E-16
1:1	30 (±3)	1.00 (±0.01)	1.0 (±0.2) E-16
4:1	10 (±2)	1.13 (±0.01)	6.6 (±4.4) E-19

J_0 was calculated using the $EQE_{PV}(E)$ and $EQE_{EL}(E)$ spectra by means of equation (3). The errors on J_{sc} and V_{oc} are experimental errors obtained by measuring different devices. For the errors on J_0, the variation of J_0 over the spectral range of the CTC was taken into account as well as the experimental error on EQE_{EL}.

Vandewal *et.al*. Nature Matter. 8, (2009)

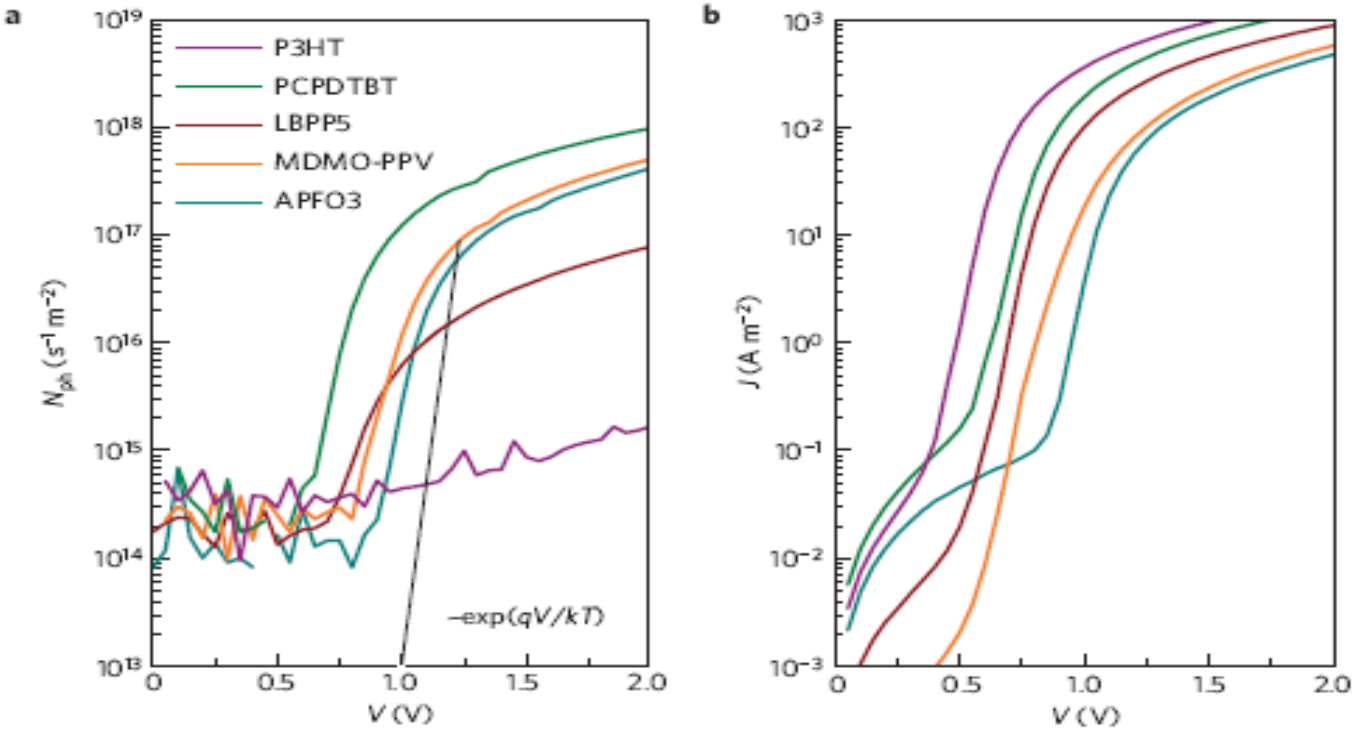

Electroluminescence emission and corresponding injected current versus voltage curves of polymer–fullerene devices. The active layers of the devices are: P3HT–$PC_{61}BM$ (1:1) (annealed), PCPDTBT–$PC_{61}BM$ (1:2), LBPP5–$PC_{71}BM$ (1:3), MDMO-PPV–$PC_{61}BM$ (1:4) and APFO3–$PC_{61}BM$ (1:4). a, The number of detected photons by a silicon detector versus the applied voltage over the device. The black line represents a curve proportional to exp(*qV/kT). An onset proportional to this curve is measurable for all polymer–fullerene devices, except for the annealed P3HT–PC61BM device, because* of its low-efficiency electroluminescence. b, The corresponding injection current versus voltage curves.

Vandewal *et.al*. Nature Matter. 8, (2009)

TABLE I. Open-circuit voltage (V_{OC}), short-circuit current density (J_{SC}), fill factor (FF), and power conversion efficiency under broadband illumination (η) of solar cells with the geometry ITO/donor/C_{60}/BCP/Al, in which the donor material was varied. Shockley parameters derived from fitting the electrical characteristics in the dark with the equivalent circuit model: diode ideality factor (n), reverse saturation current density (J_0), series resistance (R_SA), and shunt resistance (R_PA).

Donor	V_{OC} (V)	J_{SC} (mA/cm^2)	FF	η (%)	n	J_0 (μA/cm^2)	R_SA (Ω cm^2)	R_PA (kΩ cm^2)
Pentacene	0.35	11.0	0.53	2.1	1.68	1.37	0.480	110
CuPc	0.47	6.45	0.62	1.9	2.00	0.33	1.98	43.9
TiOPc	0.60	3.99	0.51	1.2	2.02	0.023	0.413	1970

Kippelen Appl. Phys. Lett. 93 (2008)

Recent advances in plastic solar cell field

Low bandgap polymer-PCBM

poly[2,6-(4,4-bis-(2-ethylhexyl)-4H-cyclopenta[b;3,4-b']dithiophene)-alt-4,7-(2,1,3-benzothiadiazole)]
(PCPDTBT) made of alternating electron-rich and electron-deficient units.

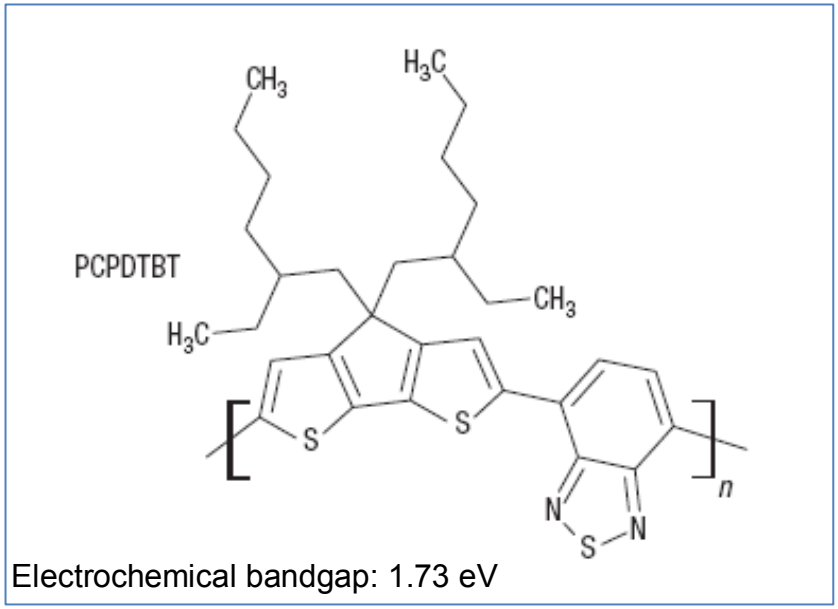

Electrochemical bandgap: 1.73 eV

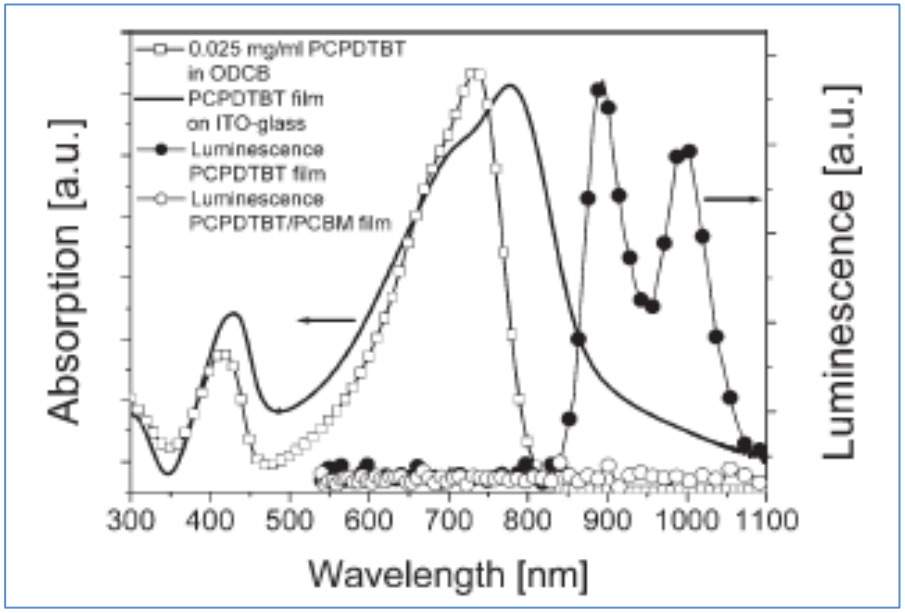

Synthesis: Z. Zhu, D. Waller, R. Gaudiana, D. Mühlbacher, M. Morana, M. C.Scharber, C. Brabec, Macromolecules, **40**, 1981 (2007).

Photovoltaic: D. Mühlbacher, M. Scharber, M. Morana, Z. Zhu, D. Waller,R. Gaudiana, C. Brabec, Adv. Mater., **18**, 2884 (2006).

Efficiency enhancement in low-bandgap polymer solar cells by processing with **alkanedithiols**

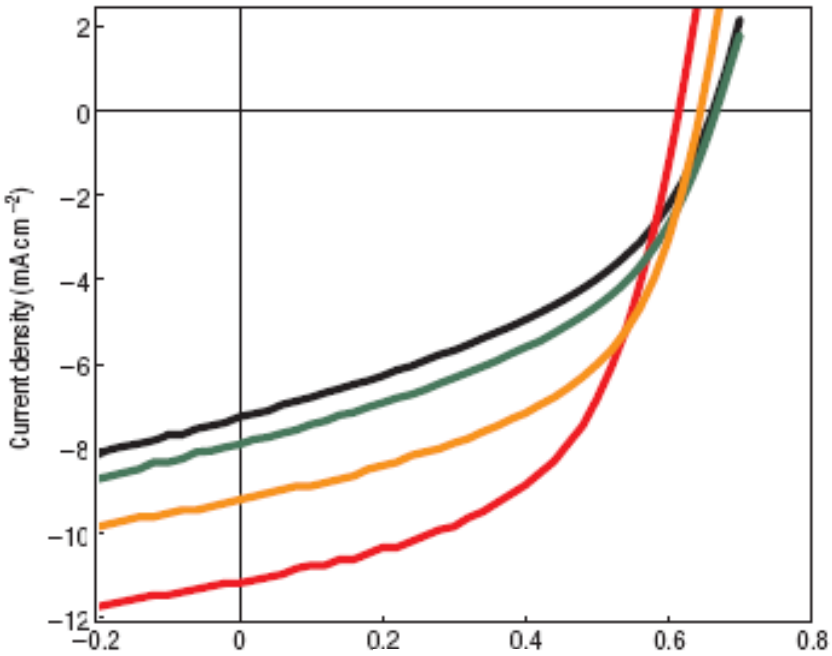

Figure 2 Device *I–V* characteristics. Current density versus voltage curves (under simulated air-mass 1.5 global, AM 1.5G, radiation at 80 mW cm^{-2}) for a series of PCPDTBT:C_{71}-PCBM solar cells. The PCPDTBT:C_{71}-PCBM films were cast at 1,200 r.p.m. from pristine chlorobenzene (black line) and chlorobenzene containing 24 mg ml^{-1} butanedithiol (green line), hexanedithiol (orange line) or octanedithiol (red line).

J. Peet, J. Y. Kim, N. E. Coates, W. L. Ma, D. Moses, A. J. Heeger, G. C. Bazan, Nature Materials, **6,** 497 (2007).

Efficient Tandem Polymer Solar Cells Fabricated by All-Solution Processing

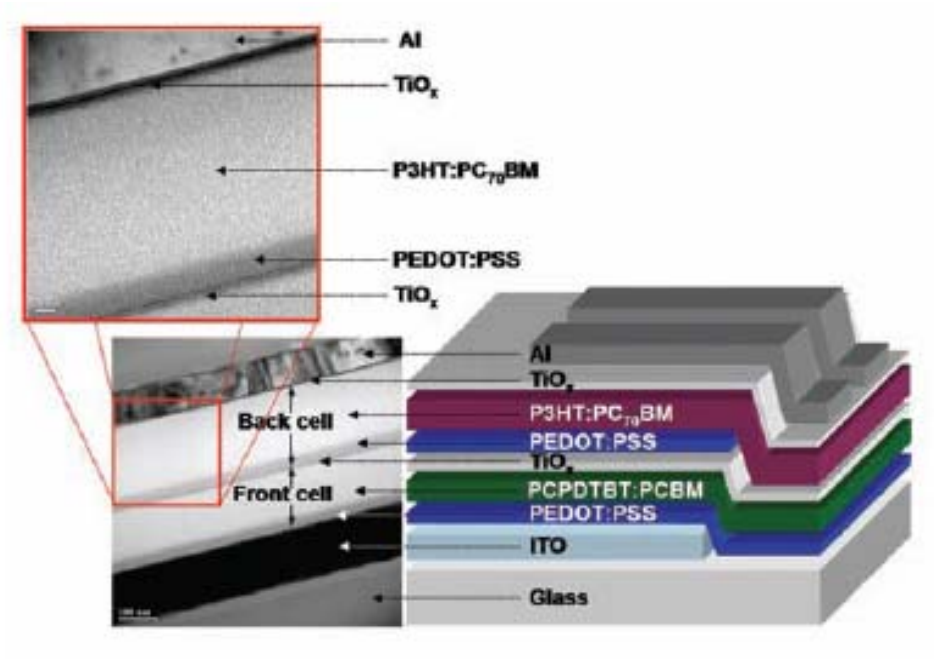

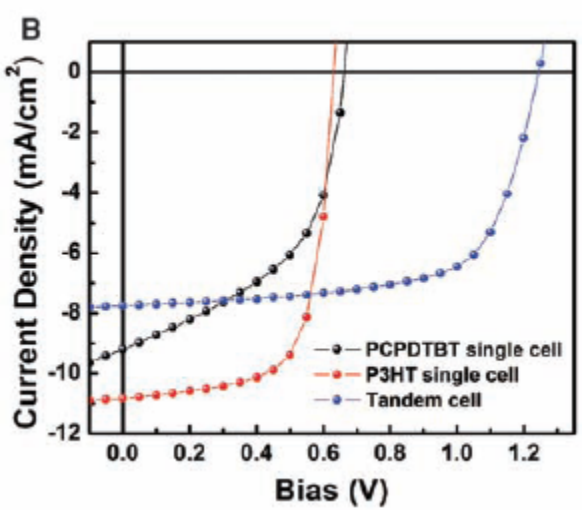

The PCPDTBT:PCBM single cell shows J_{sc} = 9.2 mA/cm^2, V_{oc} = 0.66 V, FF = 0.50, and **η_e= 3.0%**

The P3HT:PC70BM single cell shows J_{sc} = 10.8 mA/cm^2, V_{oc} = 0.63 V, FF = 0.69, and **η_e= 4.7%;**

The tandemcell shows J_{sc} = 7.8 mA/cm^2, V_{oc} = 1.24 V, FF = 0.67, and **η_e= 6.5%.**

J. Y. Kim, K. Lee, N. E. Coates, D. Moses, T-Q. Nguyen, M. Dante, A. J. Heeger, Science, **317**, 222 (2007).

Air-stable devices using TiO_x: K. Lee, J. Y. Kim, S. H. Park, S. H. Kim, S. Cho, A. J. Heeger, Adv. Mater., **19**, 2445 (2007).

Materials

poly[2-methoxy-5-(2-ethylhexyloxy)-1,4-phnylene vinylene] or MEHPPV

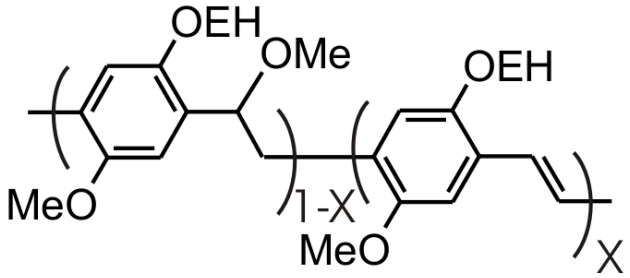

EH=

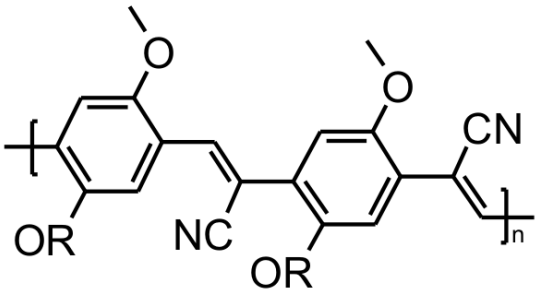

R =

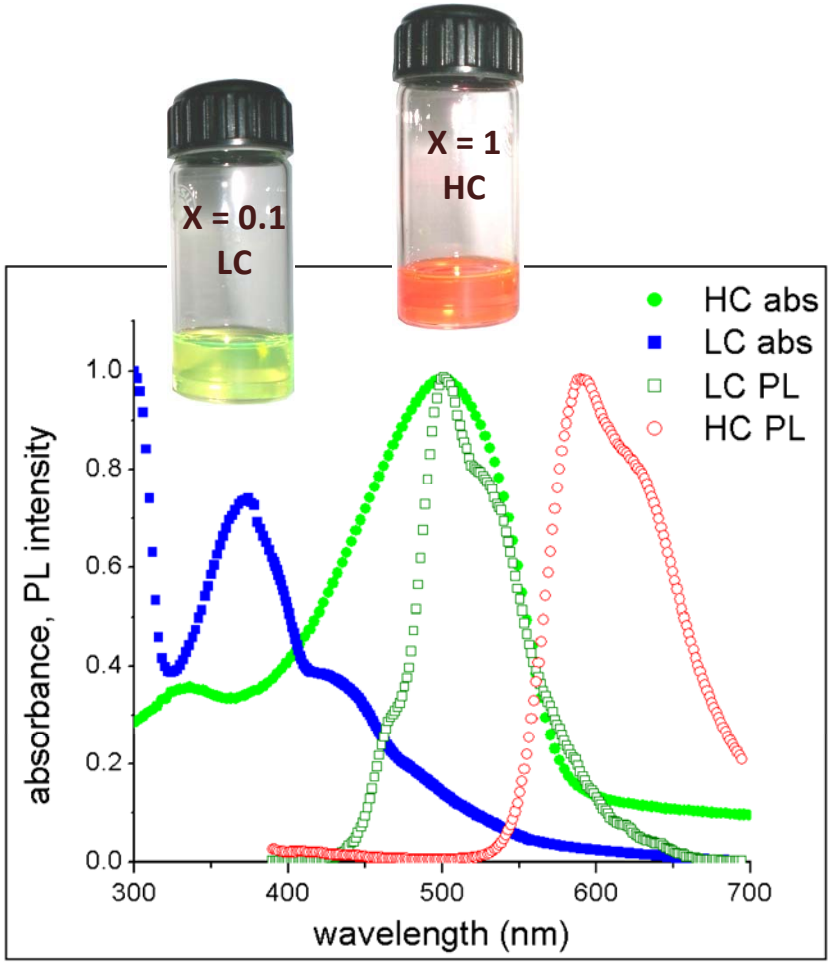

G. Padmanaban, S. Ramakrishnan, J. Am. Chem. Soc. **121** (2000), 2244.
G.Padmanaban, K. Nagesh, S. Ramakrishnan, J. Polym. Sci. Poly. Chem. , **41** (2003), 3929.

Energy transfer in the blend film

High Conjugated (HC): X = 1
Low Conjugated (LC): X= 0.1

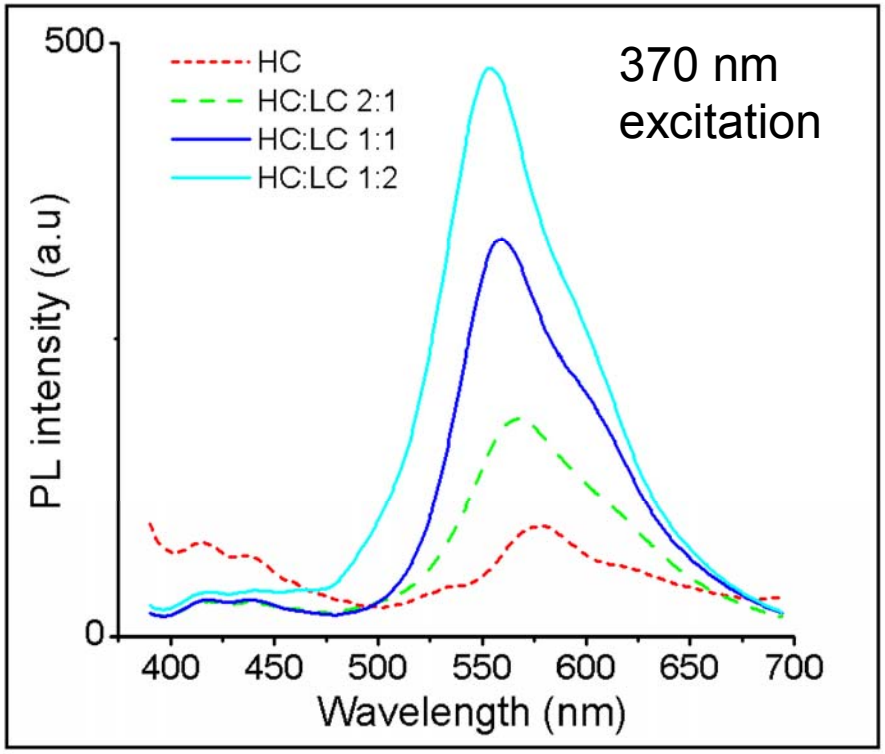

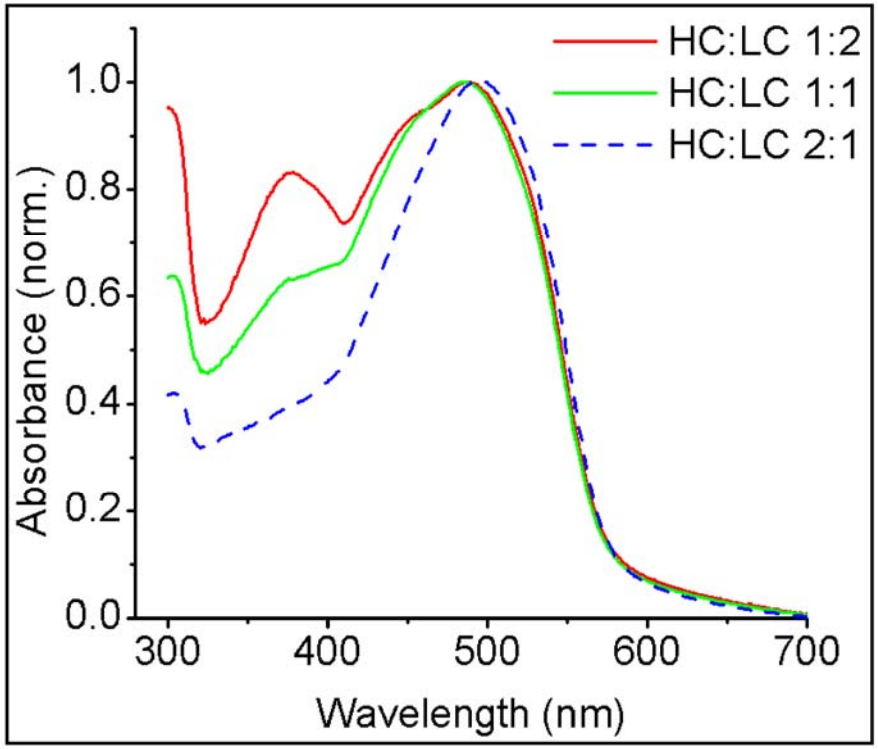

From the PL spectrum it is evident that efficient energy transfer takes place from LC phase to HC phase.

K. Nagesh, D. Kabra, K. S. Narayan, S. Ramakrishnan, Synth. Met. **155** (2005), 295.

IPCE spectrum

$$\eta_{IPCE}(\lambda) \propto \{1-\exp[-\mu\tau V_{bi}/d]\}\times\left(1-e^{-\alpha(\lambda)d}\right)$$

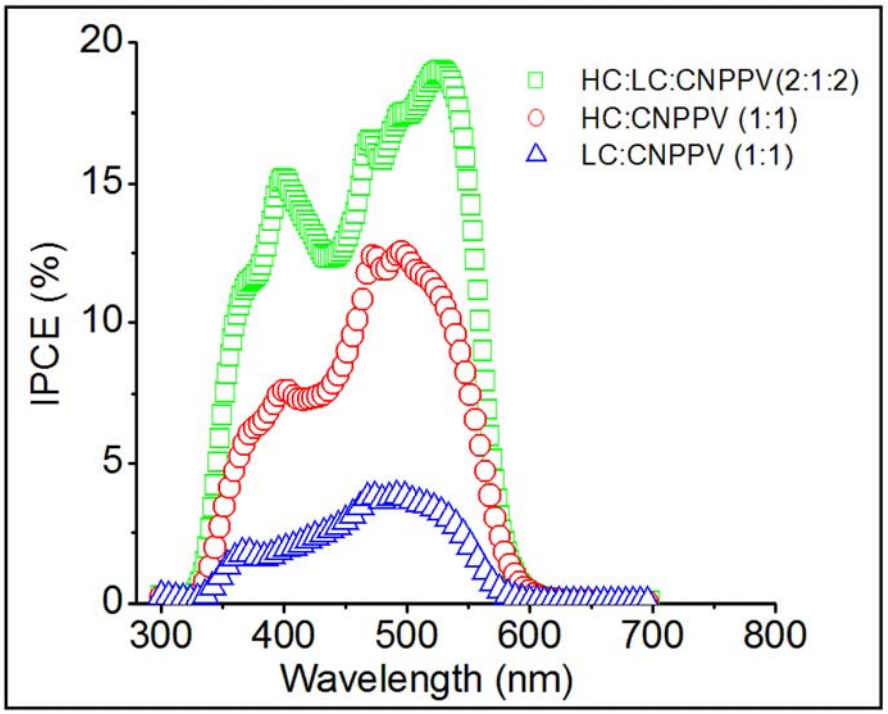

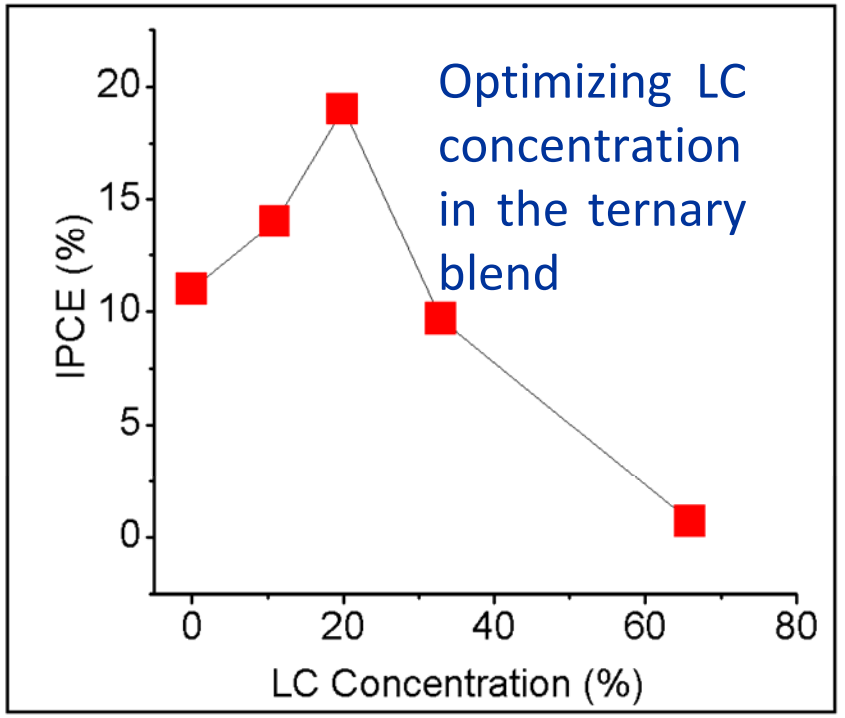

For LC polymer $\mu\tau \sim 10^{-13}$ cm^2/V

For HC polymer $\mu\tau \sim 10^{-11}$ cm^2/V

$V_{bi} = 10^5$ V/cm

Quantum efficiency enhancement in blue region

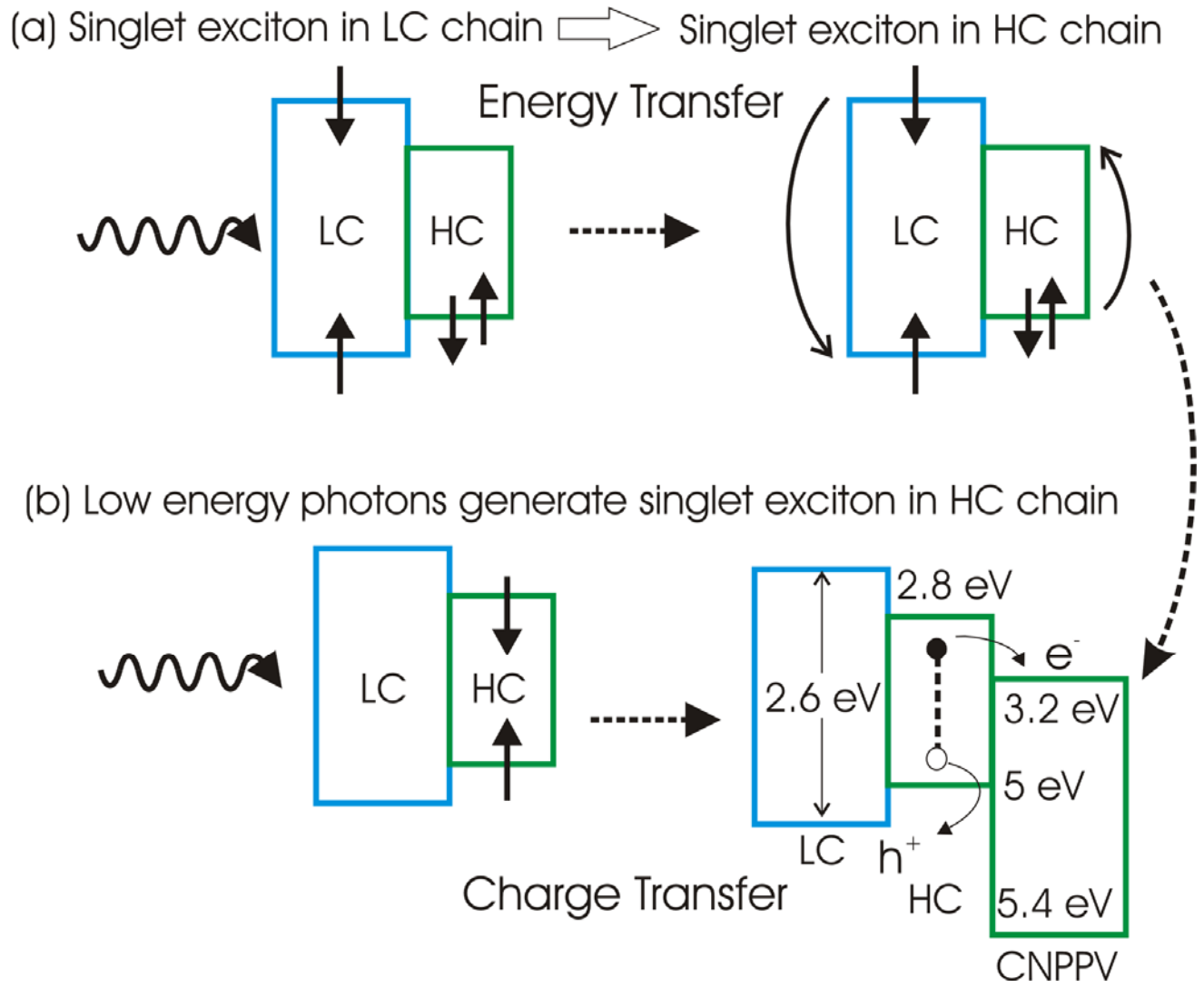

Energy Transfer Cascade in Ternary Blend System

(a) Singlet Exciton in the LC Chain → Singlet Exciton in the HC Chain

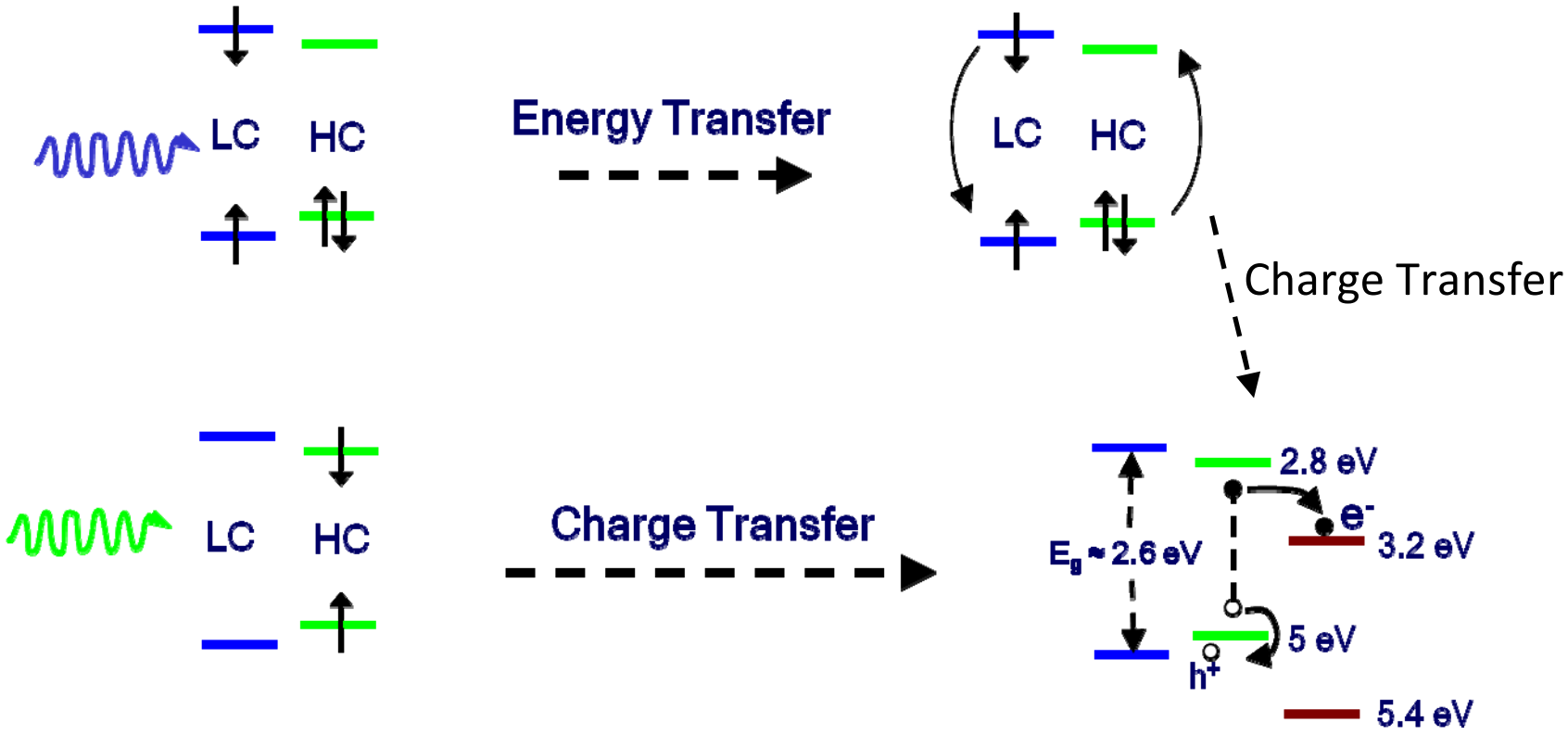

(b) Low Energy Photons Generate Singlet Exciton in the HC Chain

Variable Band-gap MEHPPV

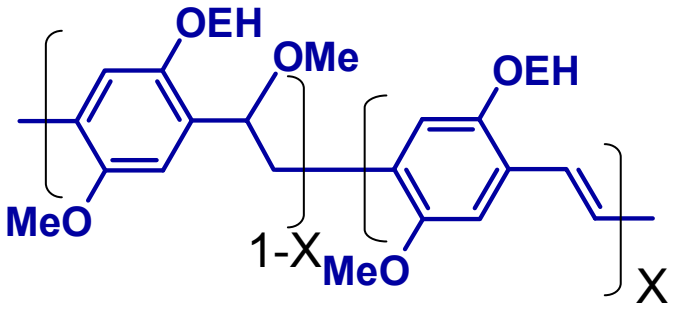

EH =

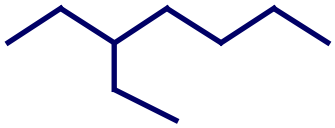

ethylhexyloxy

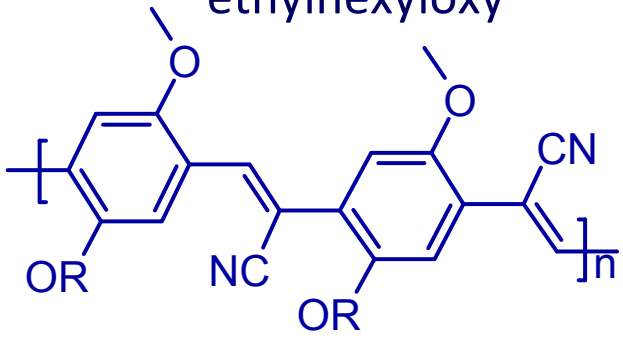

R =

CNPPV

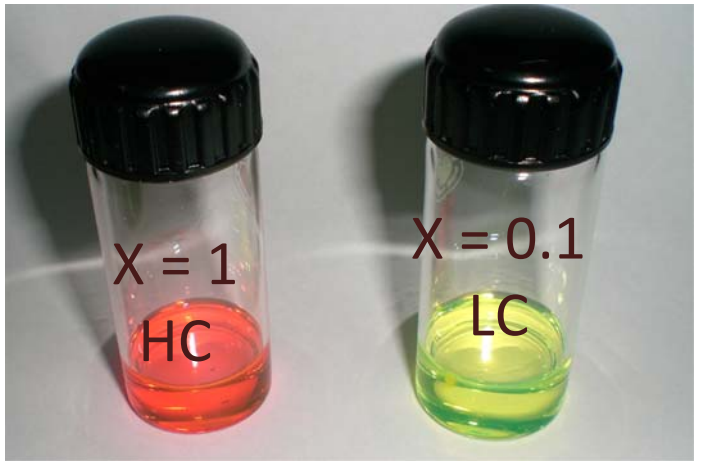

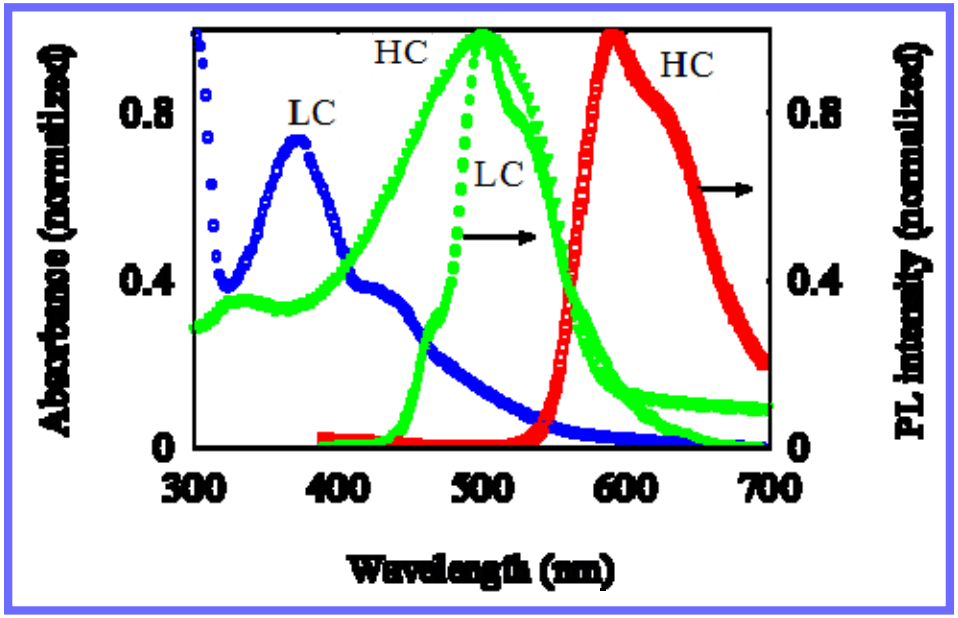

G. Padmanaban, S. Ramakrishnan, J. Am. Chem. Soc. **121** (2000), 2244.
G.Padmanaban, K. Nagesh, S. Ramakrishnan, J. Polym. Sci. Poly. Chem. , **41** (2003), 3929.

MEHPPV (HC+LC)-CNPPV Solar Cell

$$\eta_{IPCE}(\lambda) \propto \{1-\exp[-\mu\tau V_{bi}/d]\} \times \left(1-e^{-\alpha(\lambda)d}\right)$$

For LC polymer $\mu\tau \sim 10^{-13}$ cm^2/V
For HC polymer $\mu\tau \sim 10^{-11}$ cm^2/V
$V_{bi} = 10^5$ V/cm

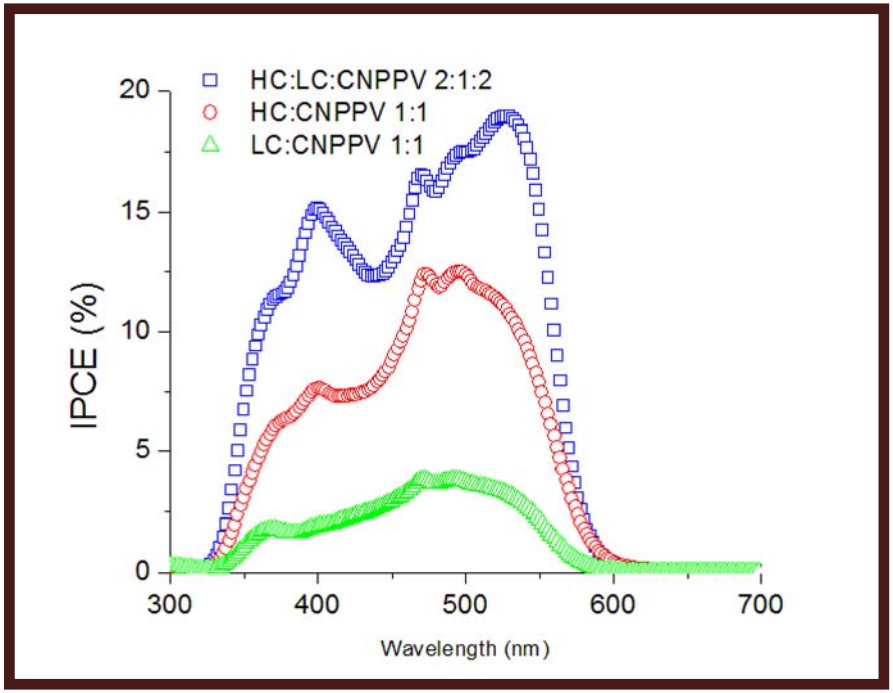

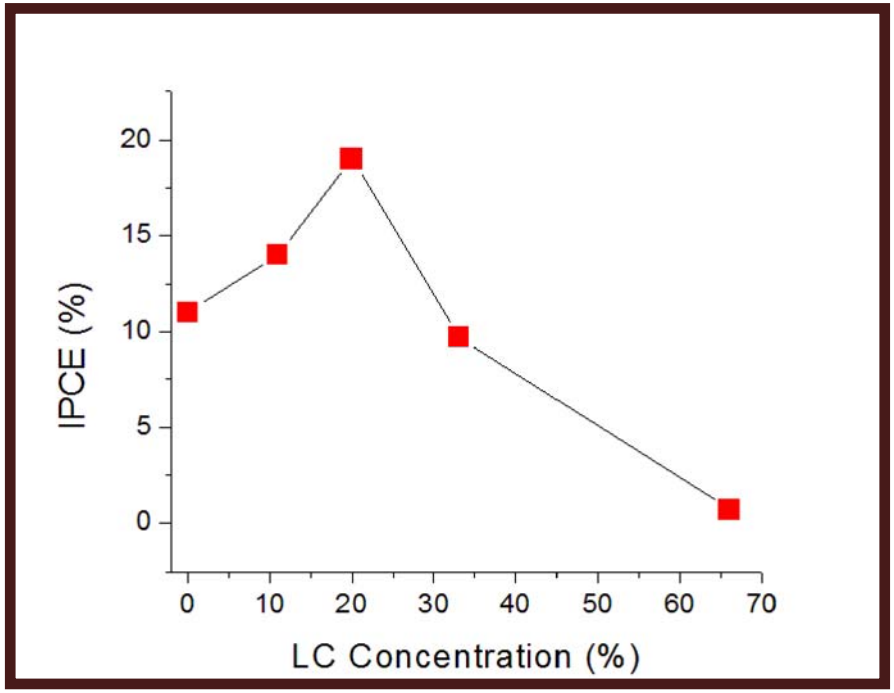

Optimizing LC concentration in the ternary blend

D. Gupta, D. Kabra, K. Nagesh, S. Ramakrishnan and K. S. Narayan,
Adv. Func. Mat. **17**, 226 (2007).

Origin of concave I(V) ?

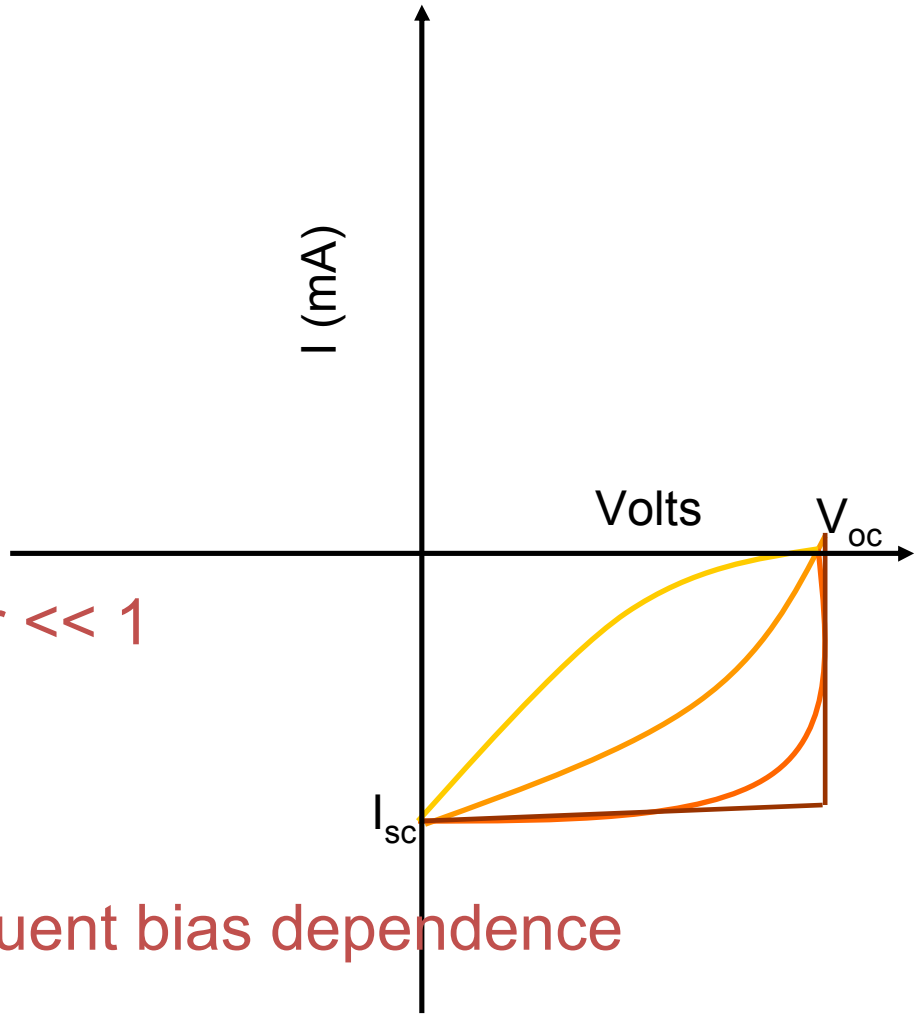

1. Bulk effect if $\mu_e\tau_e/\mu_h\tau_h$ is >> 1 or << 1
signature of unbalanced transport

⇓

space charge effects and consequent bias dependence

2. Charge generation (exciton dissociation is bias dependent)

3. Some other source such as interfacial effects…

Donor-Acceptor Pairs with Balanced μτ

P3HT

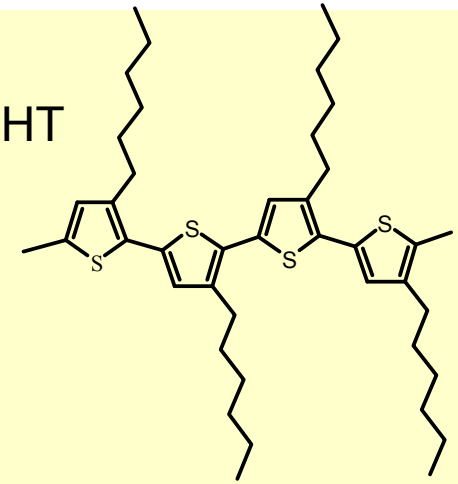

$\mu_h \sim 10^{-4}$ cm^2/Vs

Balanced transport : Good FF (> 50%). No Bulk limiting factors

Occurrence of SCL-J_{ph} limits FF

MEHPPV

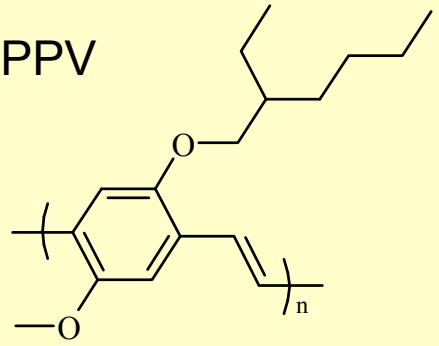

$\mu_h \sim 3.2\times10^{-5}$ cm^2/Vs

FF is expected to be good, but so far reported FF≈ 30%. Low mobility is responsible.

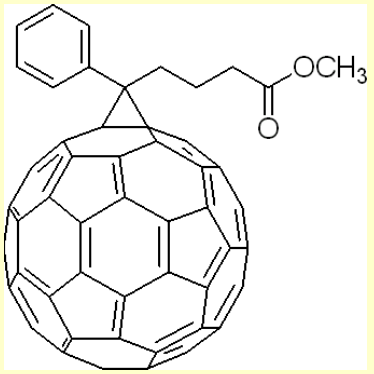

PCBM

$\mu_e \sim 4\times10^{-3}$ cm^2/Vs

CNPPV

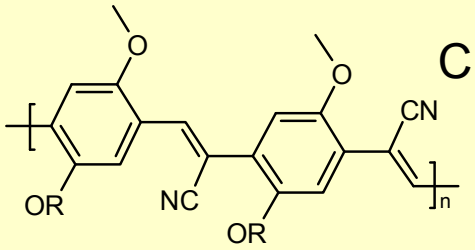

R =

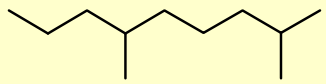

$\mu_e \sim 10^{-5}$ cm^2/Vs

Mobility (μ)-Lifetime (τ) Product: Effect on J_{ph}

Effect of Bulk Material Property on Photocurrent

Drift Length (L_D) ratio (b) of electrons and holes = $\mu_e\tau_e/\mu_h\tau_h$

For balanced transport b ~ 1

Unbalanced Transport:

1. b < 1 or b > 1 (photocurrent is μτ limited, $J_{ph} \propto P$).
2. b << 1 or b >> 1 (photocurrent is space charge limited, $J_{ph} \propto P^{3/4}$).

For an set of ohmic contact (noninjecting in the reverse bias mode)
At low V, $I \propto V$
At higher voltage $I \propto V^{1/2}$
At very high voltage I = constant = qGd (when $L_D = \mu\tau E$, becomes equal d).

SCL photocurrent decreases the FF drastically, maximum possible FF being 40%.

A. M. Goodman, A. Rose, *J. Appl. Phys.,***42**, 2823 (1971).
V. D. Mihailetchi, L. J. A. Koster, J. C. Hummelen, P. W. M. Blom, *Phys. Rev. Lett.,***93**, 216601 (2004).
V. D. Mihailetchi, J. Wildeman, P. W. M. Blom, *Phys. Rev. Lett.,***94**, 126602 (2005).

Field-Dependence of Photocurrent

$$\frac{\left(J_{ph}\right)_{High V_{eff}}}{\left(J_{ph}\right)_{Low V_{eff}}} \approx 6$$

Exciton Dissociation rate is field independent

J_{SC} = 0.18 mA/cm^2,
V_{OC} = 0.44 Volts
V_0 = 0.54 Volts and
FF = 53%
P_{inc}= 2 mW/cm^2
(White Light)

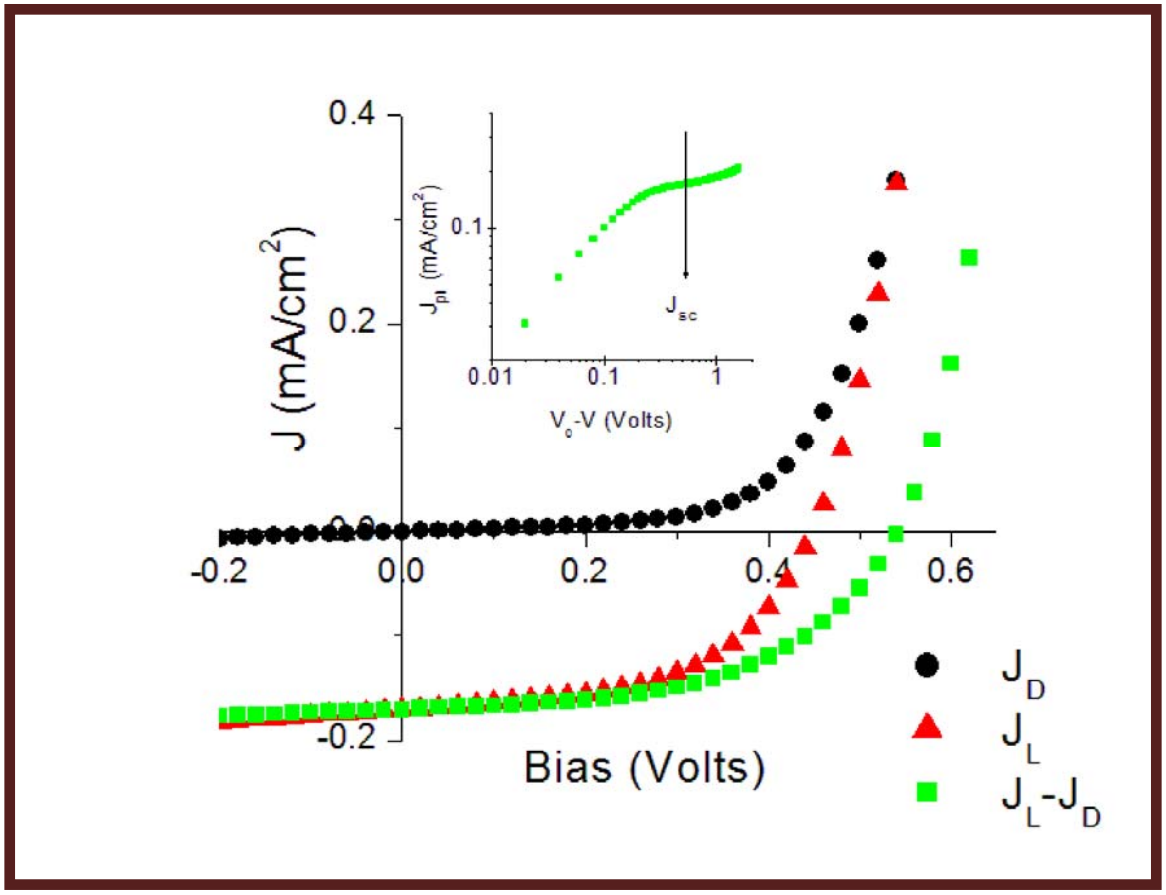

At low effective field (V_0-V < 0.1), $J_{ph} \propto$ V
At high effective field (V_0-V > 0.1), $J_{ph} \approx$ constant

No Space Charge Effect
$J_{SC} \propto$ Incident Power

D. Gupta, M. Bag and K. S. Narayan, (Appl. Phys. Lett. 2008)

Effect of Cathode-Polymer Interface: Al Cathode

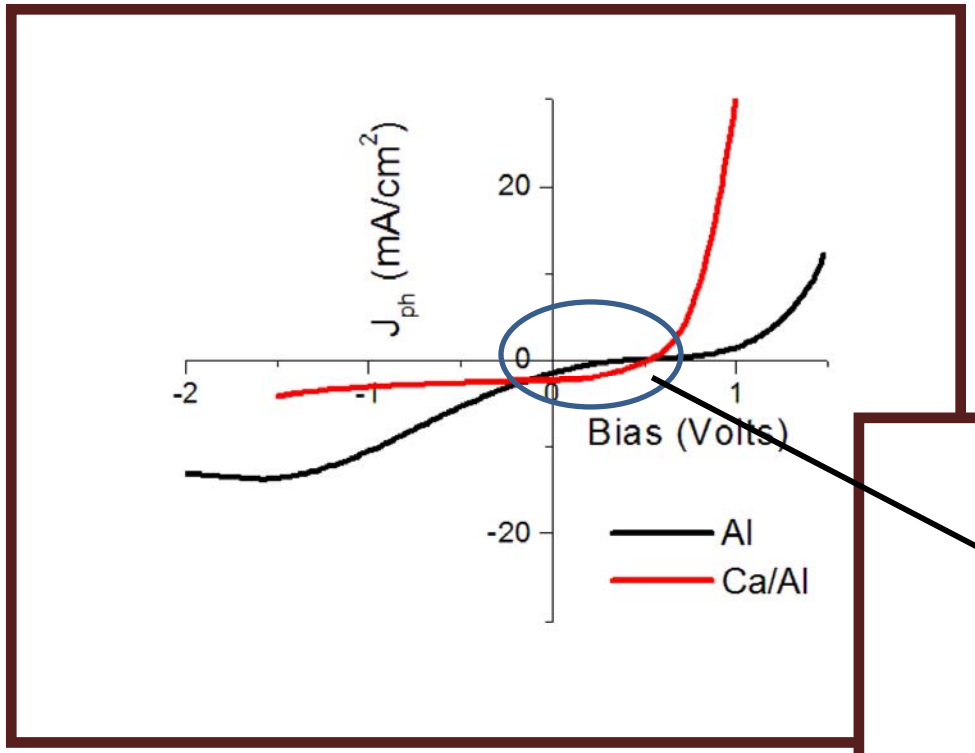

Al device
FF = 12.5 %.
J_{SC} =1.47 mA/cm^2,
V_{OC}= 0.46 Volt.

Unbalanced Extraction

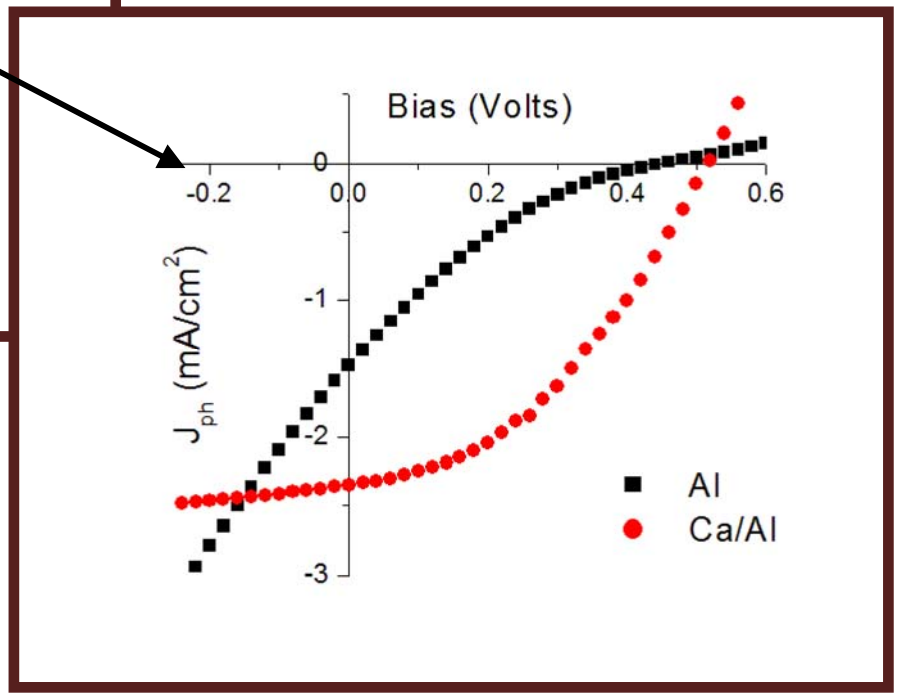

$$\eta_{IPCE} = \eta_A \eta_{ED} \eta_{CT} \eta_{CC}$$

$$\eta_{CC} = \left(1 - e^{-\alpha(\lambda)W}\right)$$

W = Width of the depletion region

Presence of Al_2O_3 layer in the Al-polymer interface

Deposition Rate of Al

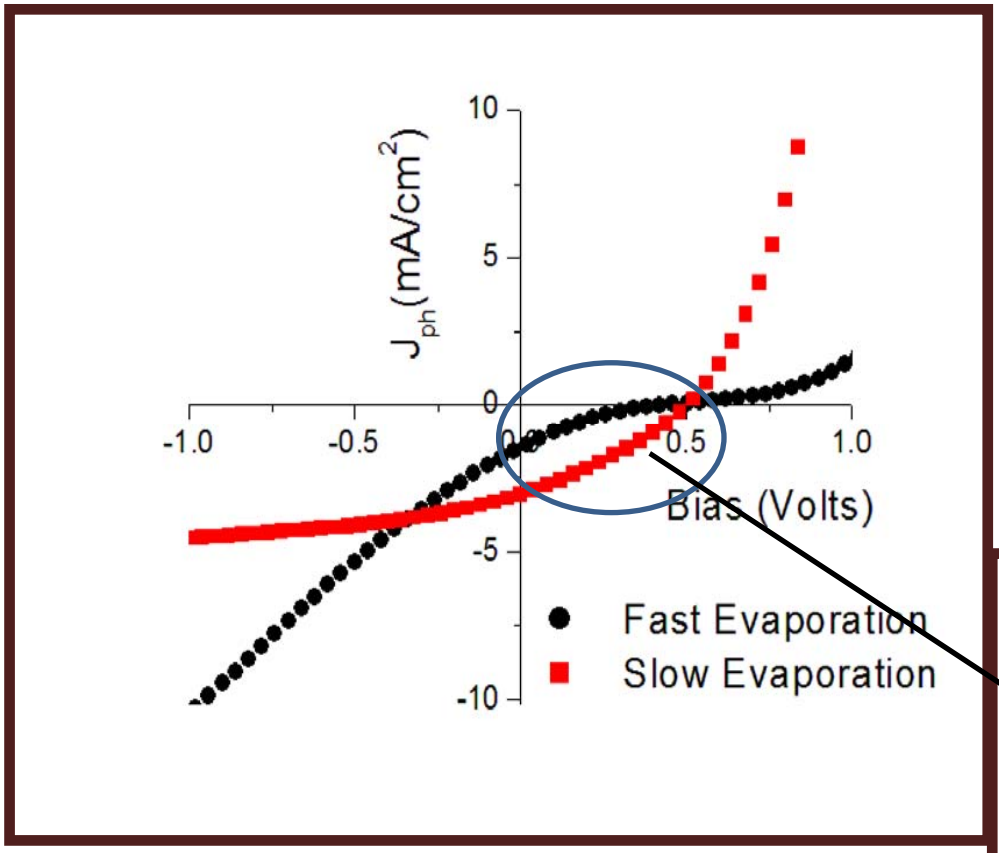

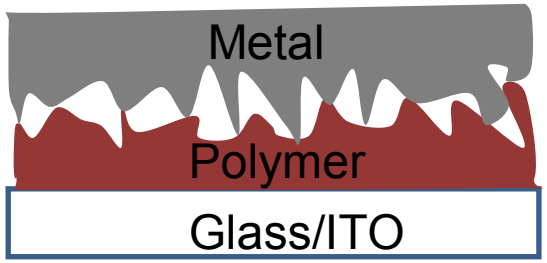

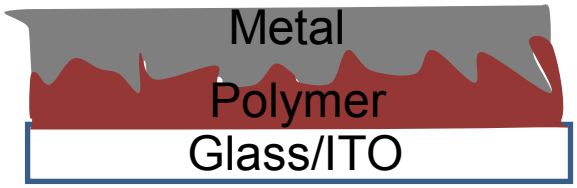

Conformal Coating

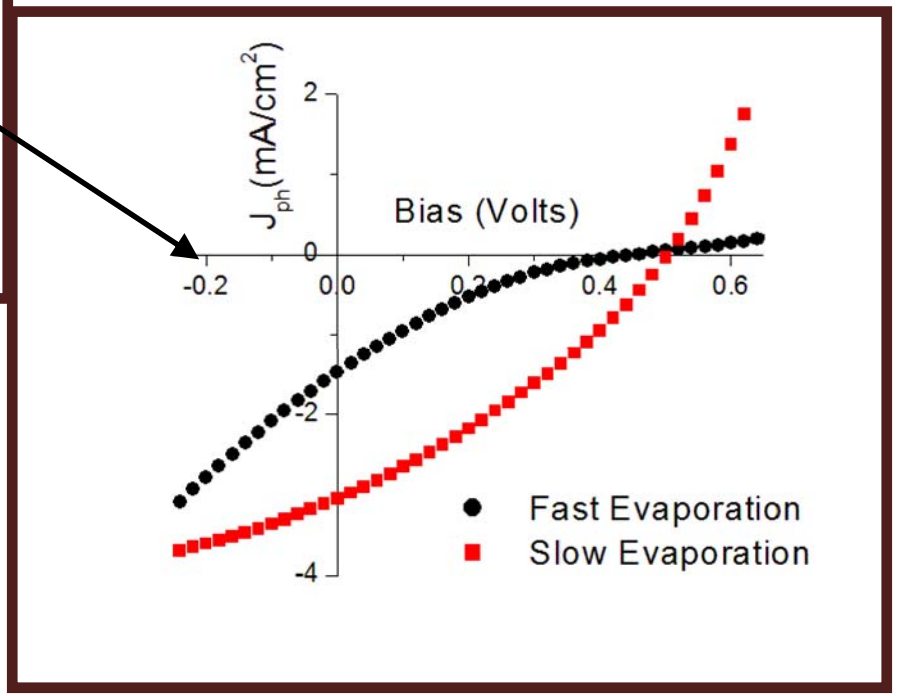

FF improves from 12.5% to 30%

Gupta and Narayan – Appl. Phys. Lett. 2008

Origin of Poor Fill Factor

Bulk Limited

1. Occurrence of Space Charge Limited-J_{ph} and square root dependence of J_{ph} on Voltage.

$$J_{ph} \propto (V_0 - V)^{1/2} \Rightarrow J_{SC} \propto V_0^{1/2}$$

$$\left[\frac{\partial}{\partial V}\left(J_{ph}V\right)\right]_{V=V_{max}} = 0 \Rightarrow$$

$$V_{max} \propto \frac{2}{3}V_0, J_{max} \propto \left(\frac{1}{3}V_0\right)^{1/2}$$

$$FF = 100 \times \frac{J_{max}V_{max}}{J_{SC}V_{OC}} \approx 40\%$$

2. Strong electric field dependence of exciton dissociation rate.
This gives rise to a linear or concave JV-response in the fourth quadrant.

Contact Limited

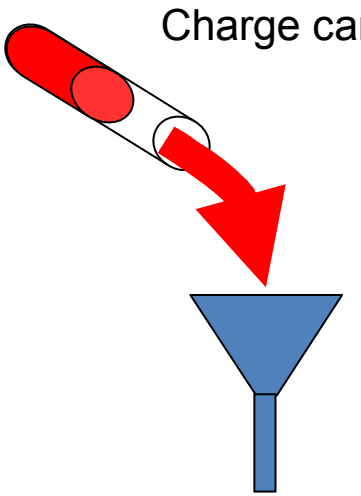

Charge carrier accumulation takes place due to inefficient collection

Cathode-polymer interface morphology determines the charge collection efficiency

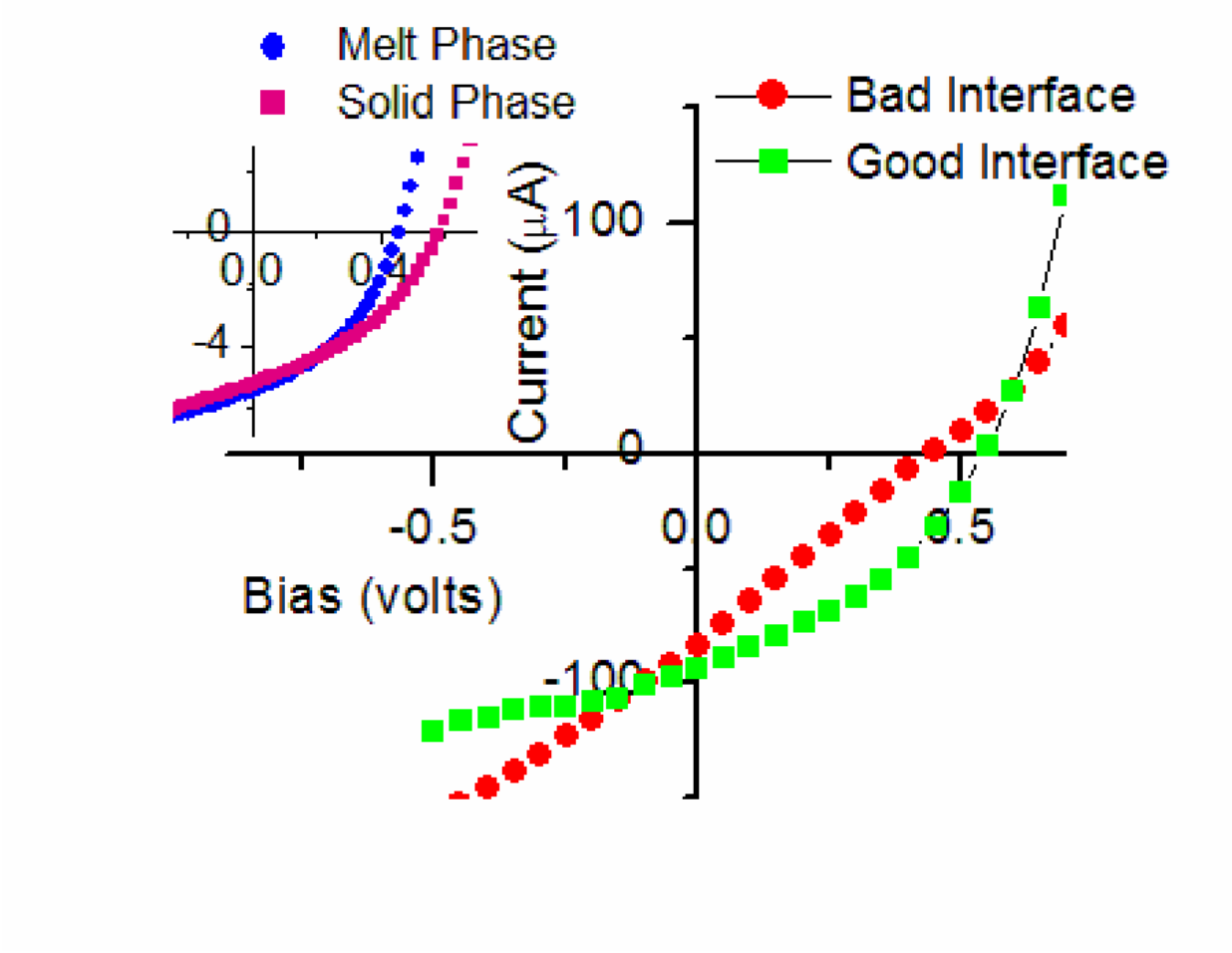
Melt Phase
Solid Phase
Bad Interface
Good Interface
Current (μA)
100
0
-100
-0.5
0.0
0.5
Bias (volts)
0
-4
0.0
0.4

- Solar Cell dimensions and pixelation
- Light trapping strategies
- Photocarrier multiplication

- Baldo et. al.
- Eutectic mixture
- Upconversion
- multiexciton

benzodithiophene polymer PBDTTT (PBDTTT-E): poly(4,8-bis-alkyloxybenzo(1,2-b:4,5-b′)dithiophene-2,6-diyl-alt-(alkyl thieno(3,4-b)thiophene-2-carboxylate)-2,6-diyl) (Liang et. al. Adv. Mat. published Online: 4 Jan 2010 with 7.4% efficiency),

PCPDTBT poly[2,6-(4,4-bis-(2-ethylhexyl)-4H-cyclopenta[2,1-b;3,4-b'_]-dithiophene)-alt-4,7- (2,1,3-benzothiadiazole)], Peet, J. Y. Kim, N. E. Coates, W. L. Ma, D. Moses, A. J. Heeger& G. C. Bazan, Nature Materials 6, 497 - 500 (2007)

PCDTBT poly[N-9'- heptadecanyl-2,7-carbazole-alt-5,5-(4',7'-di-2-thienyl-2',1',3'-benzothiadiazole)], Nicolas Blouin, Alexandre Michaud, and Mario Leclerc, Adv. Mater. 19, 2295–2300 (2007).

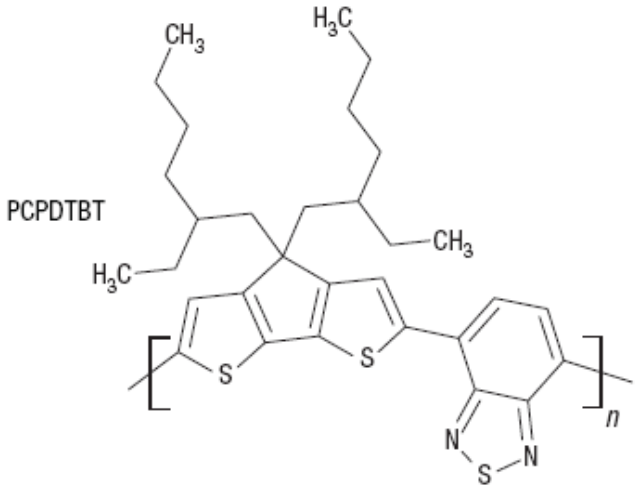

Poly[2,6-(4,4-bis- (2-ethylhexyl)-4*H-cyclopenta[2,1-b;3,4-b]-dithiophene)-alt-4,7-* (2,1,3-benzothiadiazole)] (**PCPDTBT**)

E_g = 1.4 eV HOMO = 4.9 e LUMO = 3.5 eV

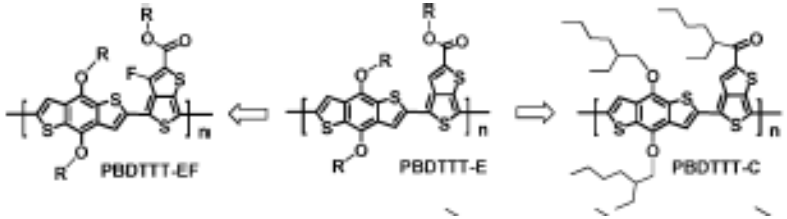

benzo(1,2-*b*:4,5-*b*')dithiophene (BDT)

poly(4,8-bis-alkyloxybenzo(1,2-*b*:4,5-*b*')dithiophene- 2,6-diyl-alt-(alkyl thieno(3,4 *b*)thiophene-2-carboxylate)-2,6-diyl) (PBDTTT-E)

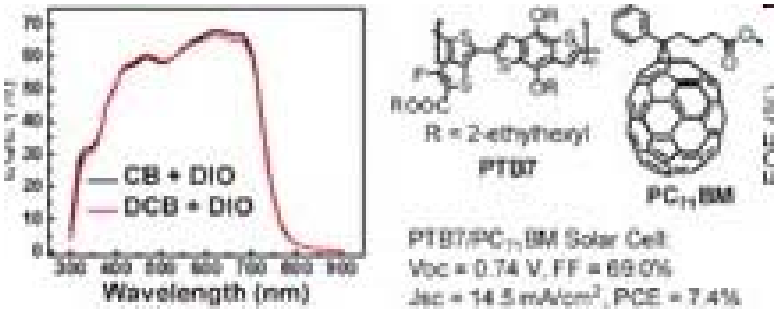

benzodithiophene polymer (PTB7)
a power conversion efficiency of 7.4%

Band diagram

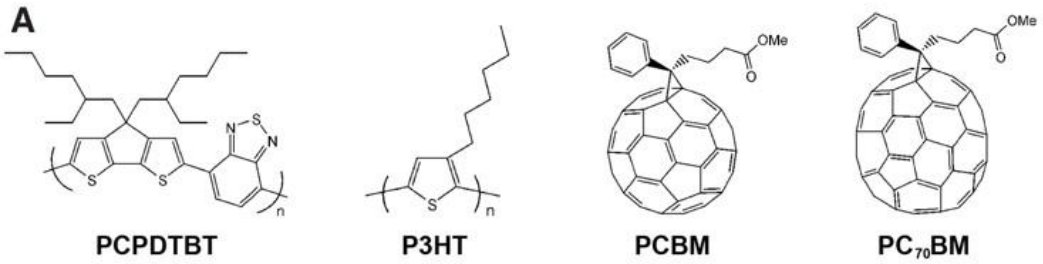

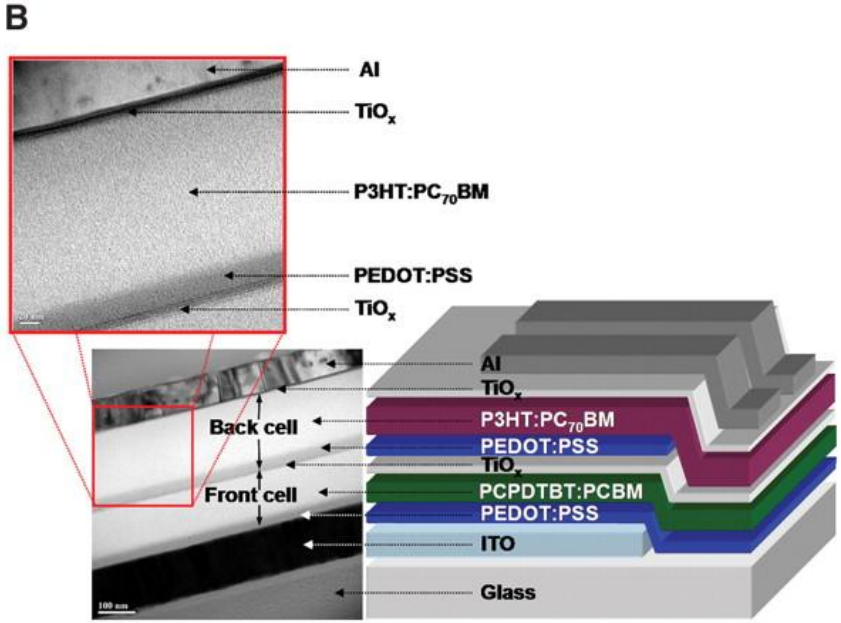

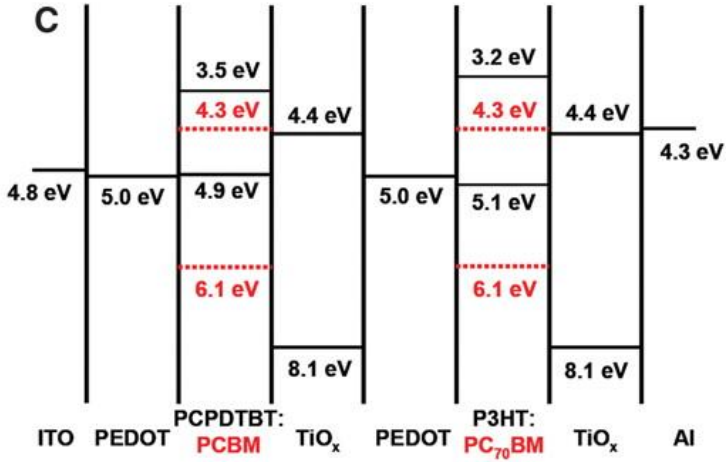

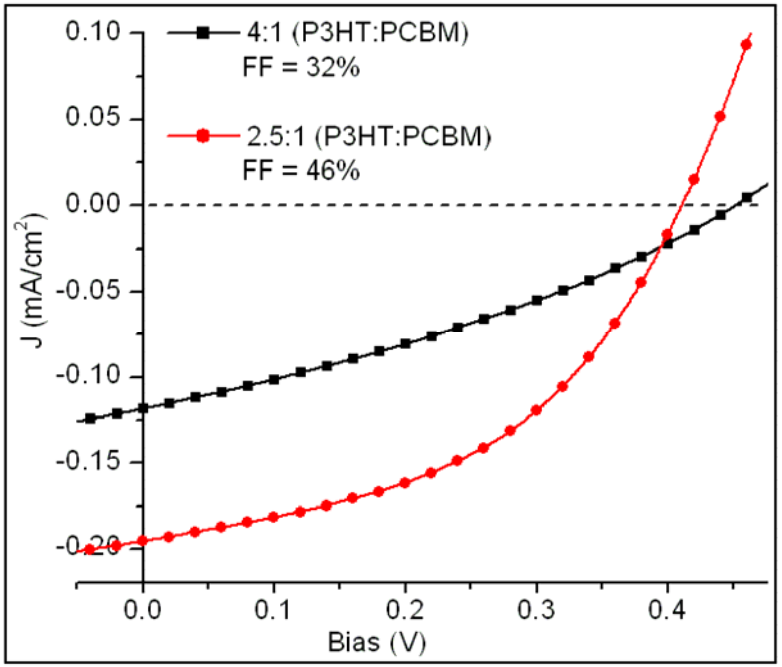

Photo Induced Charge Generation and Transport Studies in Semiconducting Polymers

Transport:

- Poisson's Eqⁿ
- Current Density Eqⁿ
- Continuity Eqⁿ

$$\frac{\partial n_p}{\partial t} = \underbrace{G_n - \frac{n_p - n_{p0}}{\tau_n}}_{\text{Generation \& Recombination Rate}} + \underbrace{n_p \mu_n \frac{\partial E}{\partial x} + \mu_n E \frac{\partial n_p}{\partial x}}_{\text{Drift}} + \underbrace{D_n \frac{\partial^2 n_p}{\partial x^2}}_{\text{Diffusion}}$$

$$\frac{\partial n_p}{\partial t} = G_n - \frac{n_p - n_{p0}}{\tau_n} + n_p \mu_n \frac{\partial E}{\partial x} + \mu_n E \frac{\partial n_p}{\partial x} + D_n \frac{\partial^2 n_p}{\partial x^2}$$

$$n_p(x) = n_{p0} + \left[n_p(0) - n_{p0} \right] \exp(-x/L_n)$$

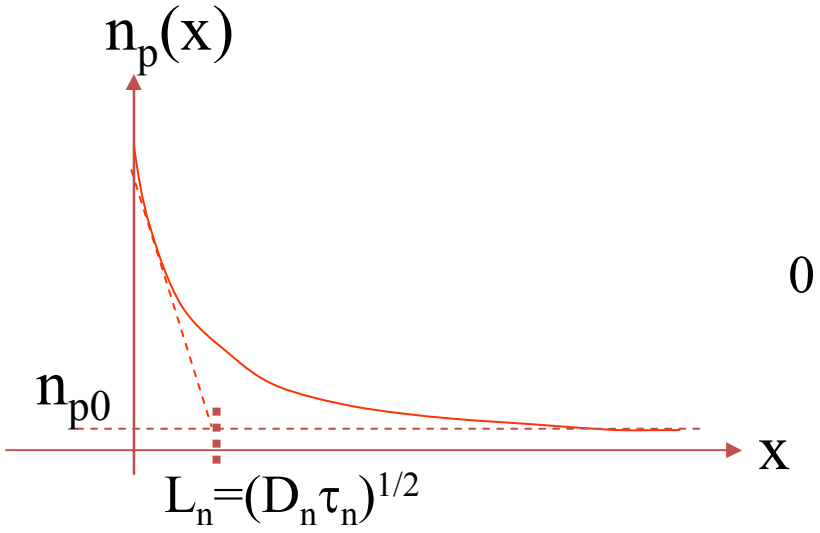

$$\langle L \rangle = (D_n . \tau)^{1/2} = \left(\frac{k_B T \mu_n . \tau}{e} \right)^{1/2}$$

Einstein Relation: $D_n = \mu_n k_B T/e$?

For Polymer Semiconductors
Lateral Diffusion coefficient D_l = ??

- Measure of mobility in ambipolar systems

(regimes: $\mu_e\tau_e/\mu_h\tau_h >> 1$ **or** $<< 1$ and $\mu_e\tau_e/\mu_h\tau_h \approx 1$)

- Bulk versus lateral mobility

(transverse-lateral correlation)

- Mobility in 2D systems, anisotropic linear systems…
- Solar cell dimensions and optimized efficiencies.

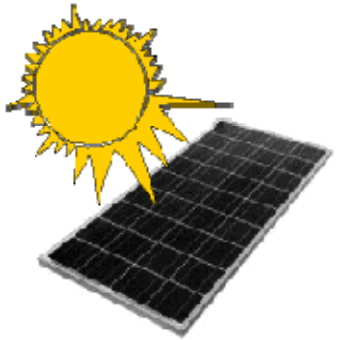

Conversion Efficicency
Spectral Response

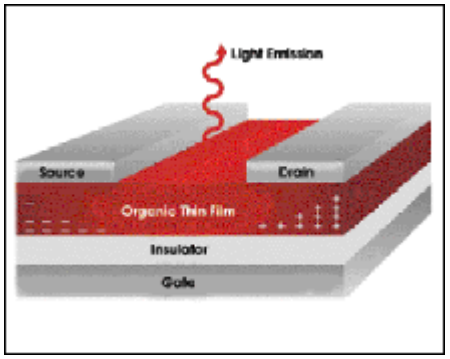

Switching action
(Subthreshold regime)

Diffusion length (cm)	Si & Ge	GaAs	a:Si	organics
L_d	~ 1	~ 10^{-2}	~ 10^{-7}	….?? ?

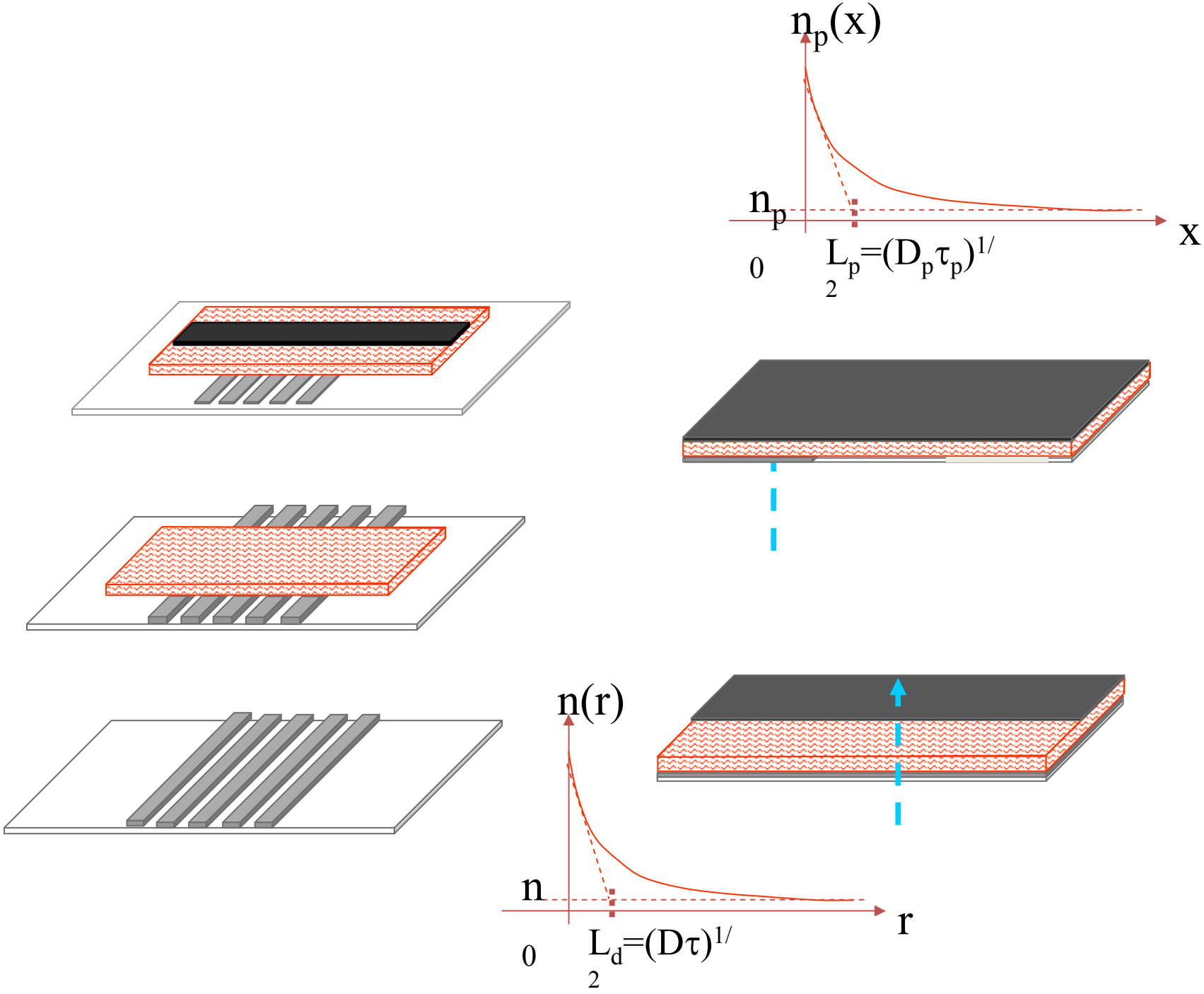
$n_p(x)$
n_p
0
$L_p=(D_p\tau_p)^{1/2}$
x
n(r)
n
0
$L_d=(D\tau)^{1/2}$
r

Experiments.....(Spatial Dependence)

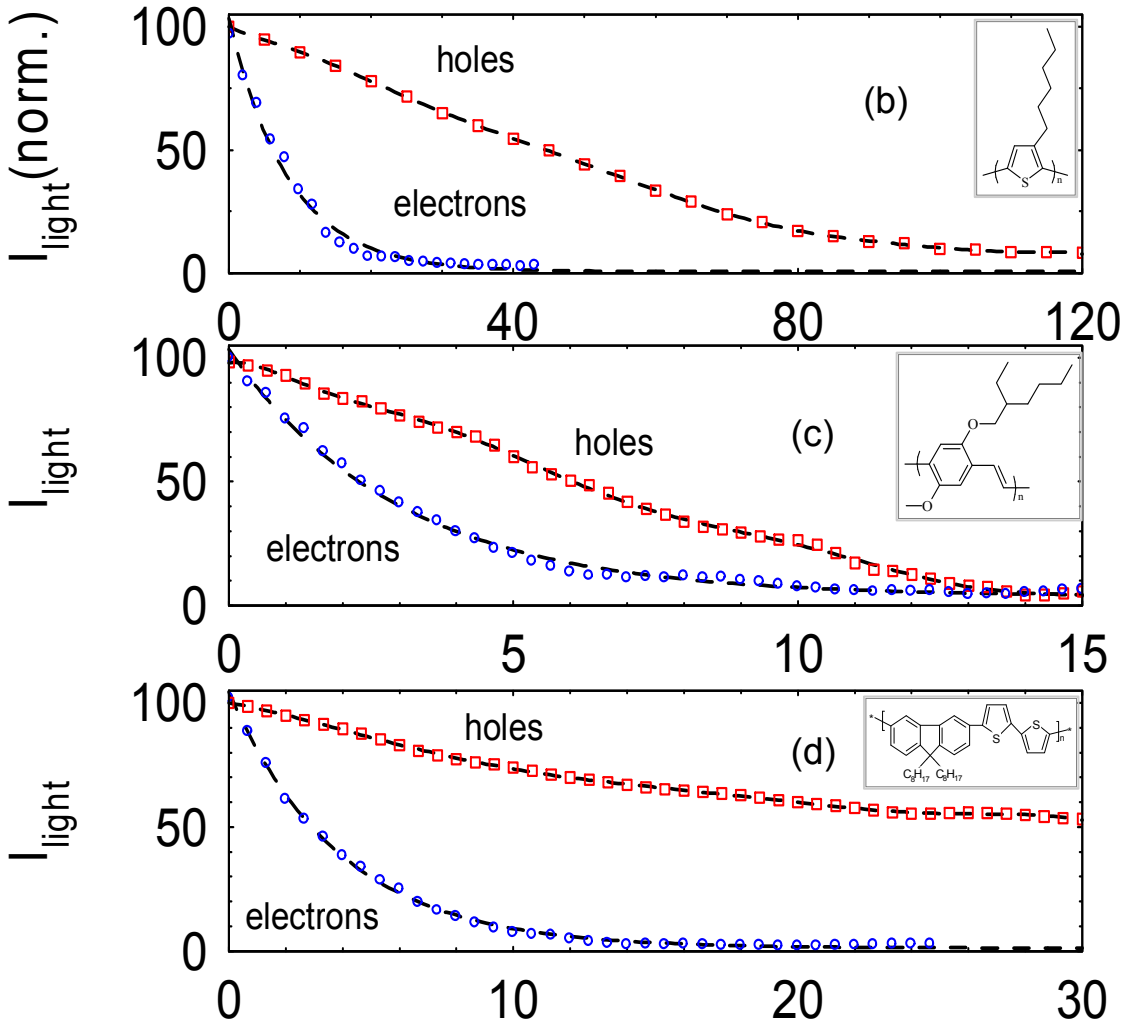

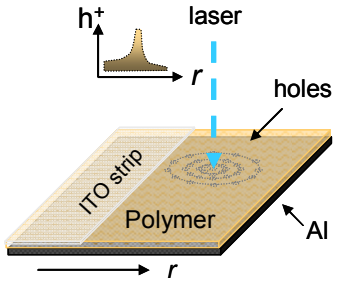

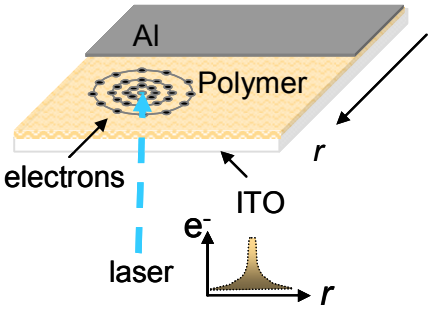

Kabra & Narayan Adv. Mat. 2007

Photocurrent decay profile near the Al edge.

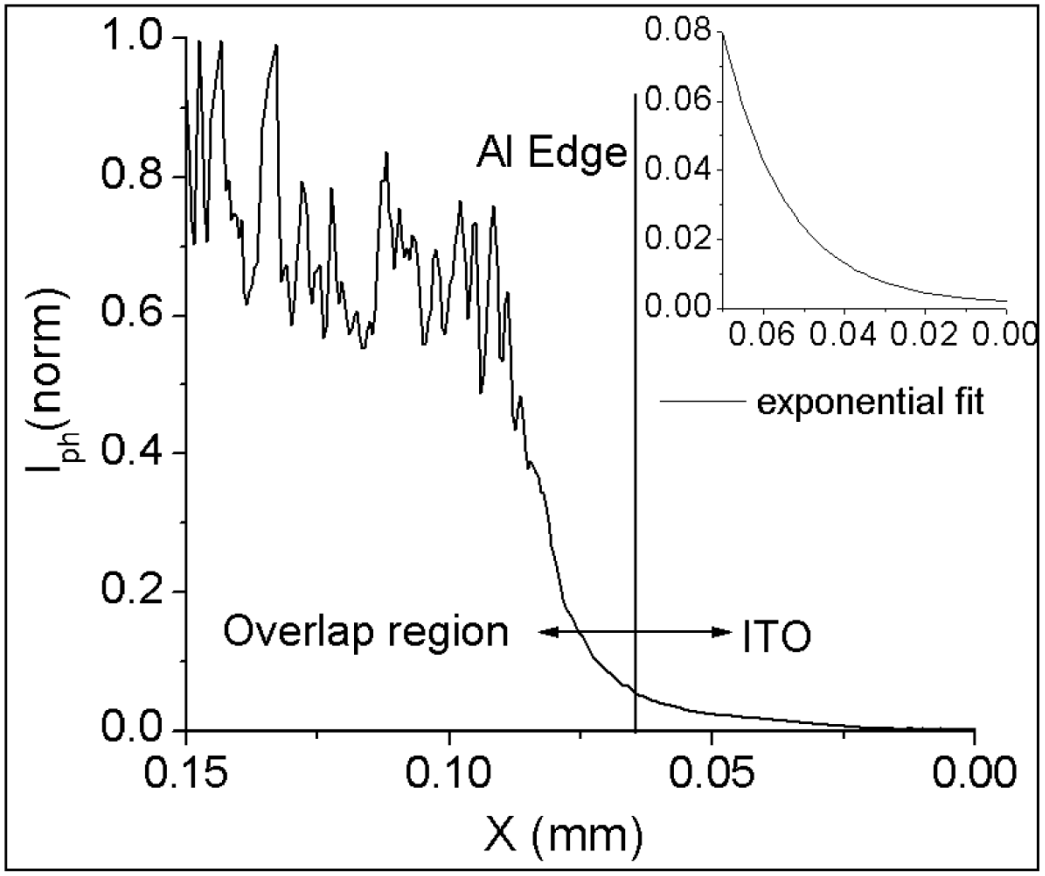

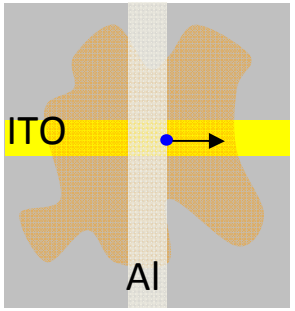

$(L_d)^{electrons} \sim 16\ \mu m$

Narayan, Gupta, Vidhyadhiraja Proc. Of IEEE 2009

Optimum Size of Solar "Cell" …… ?

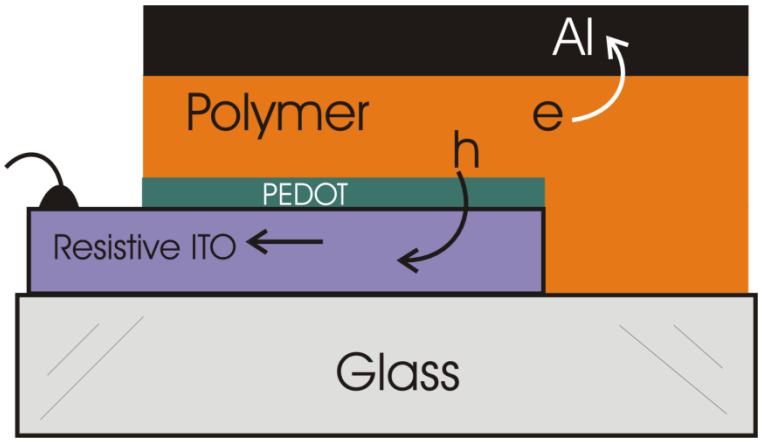

Large area means, ITO layer has to drain larger current so more I^2R drop

$$P_{loss} = J^2 R^{Sheet} a \int_0^L x^2 dx = J^2 R^{Sheet} a \frac{L^3}{3}$$

Alternative is Pixilation

Underlying unpatterned PEDOT works as an anode and efficiency measurement becomes erratic

Patterning PEDOT is difficult

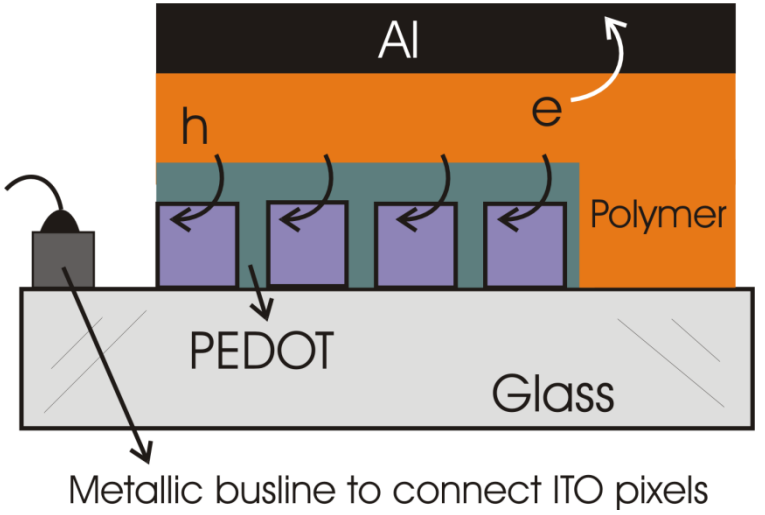

Complete and restricted illumination

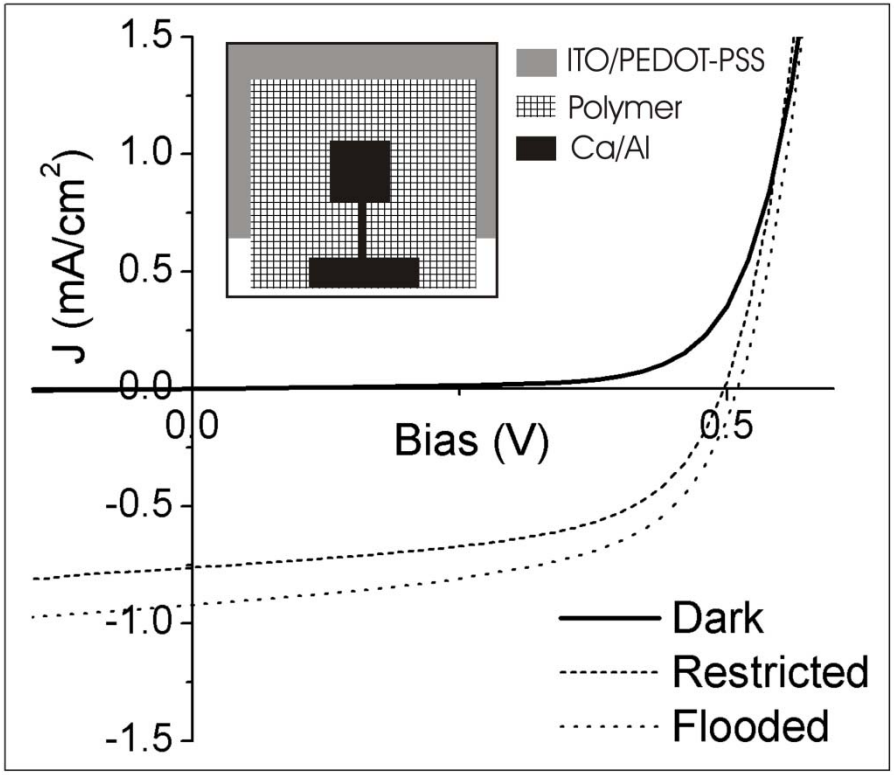

Flooded illumination

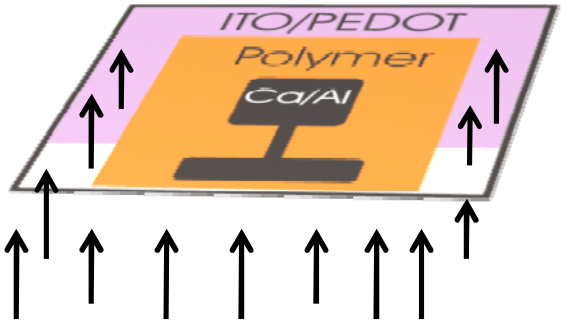

Restricted Illumination

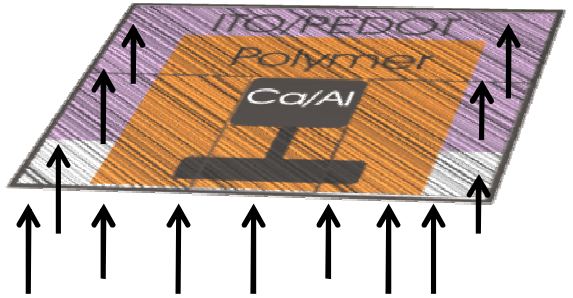

J_{SC} increases by 15% for 0.25 cm^2 device

The increase in current from the peripheral regions can not solely be attributed to the optical effects.

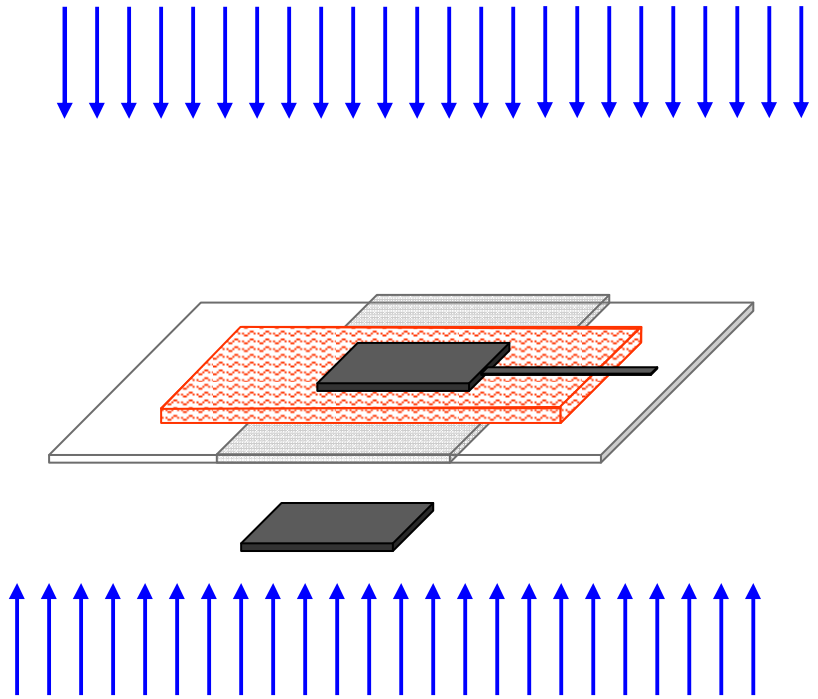

Possible sources for the current from the periphery

1. Optical effects
   i) Scattering from rough surface
   ii) Waveguiding of emitted PL from the polymer region

2. Finite extent of electric field outside the overlap region.

3. Lateral diffusion of charge carriers.

Optical scattering and waveguiding

Since $n_2 \approx n_3$ reflectivity is very low, $R_{ITO\text{-}polymer} \sim 10^{-4}$ for near normal incidence.

Haze parameter = diffused/(diffused+specular) $\propto$ (surface RMS roughness σ, λ)

For λ (400 nm) >> σ (1 nm), H_T << 10%

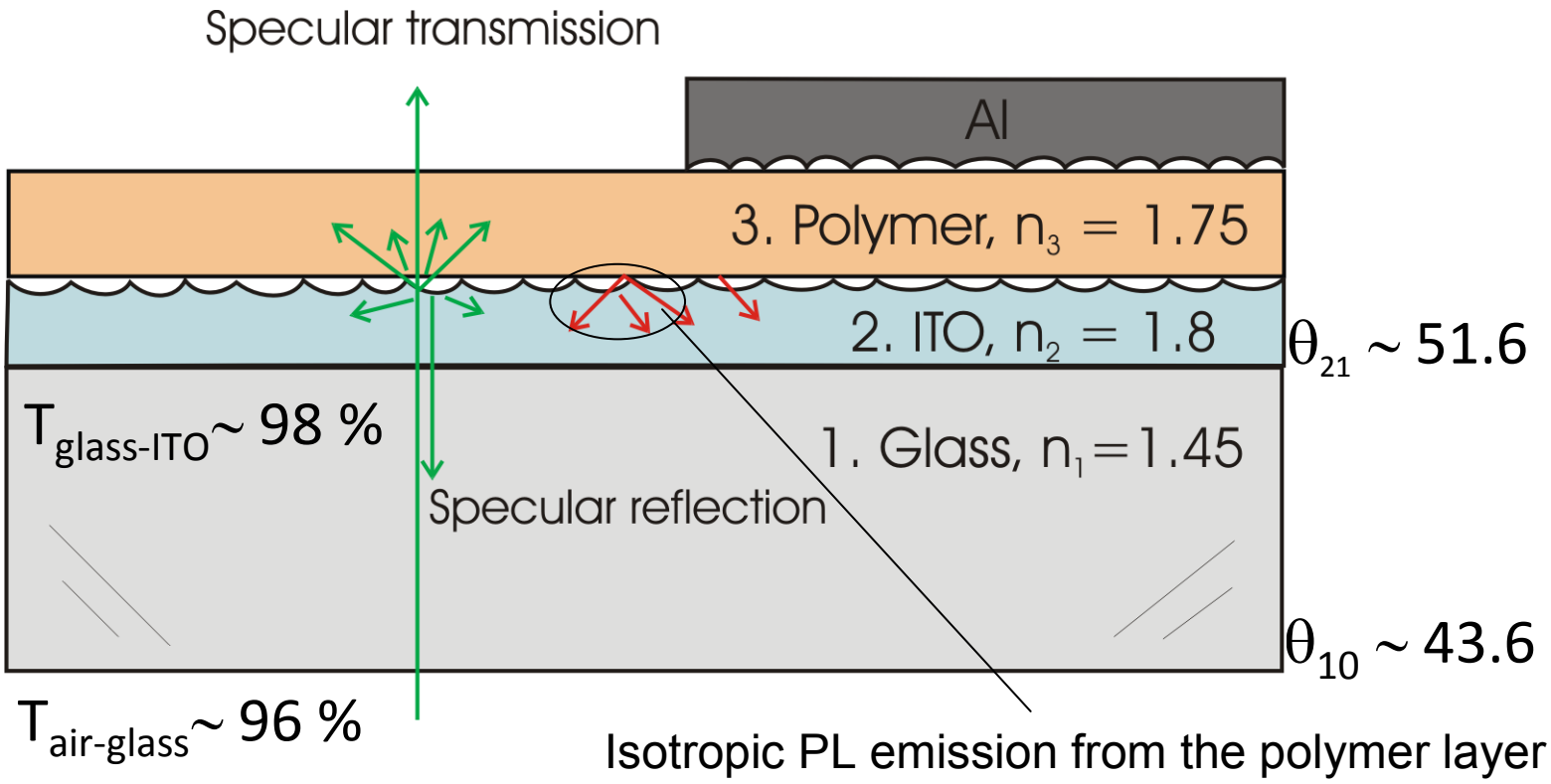

Finite fringing field outside the electrode

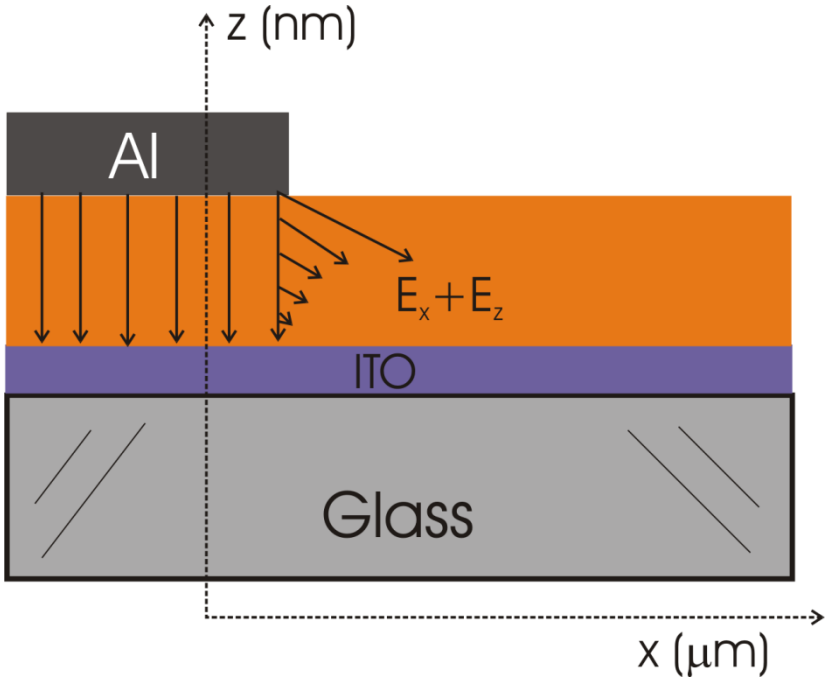

The estimated decay lengths for the electric field to decay to strength of ~ 10 - 100 V/cm are quite small (< 50 nm)

Different Active area devices under complete illumination

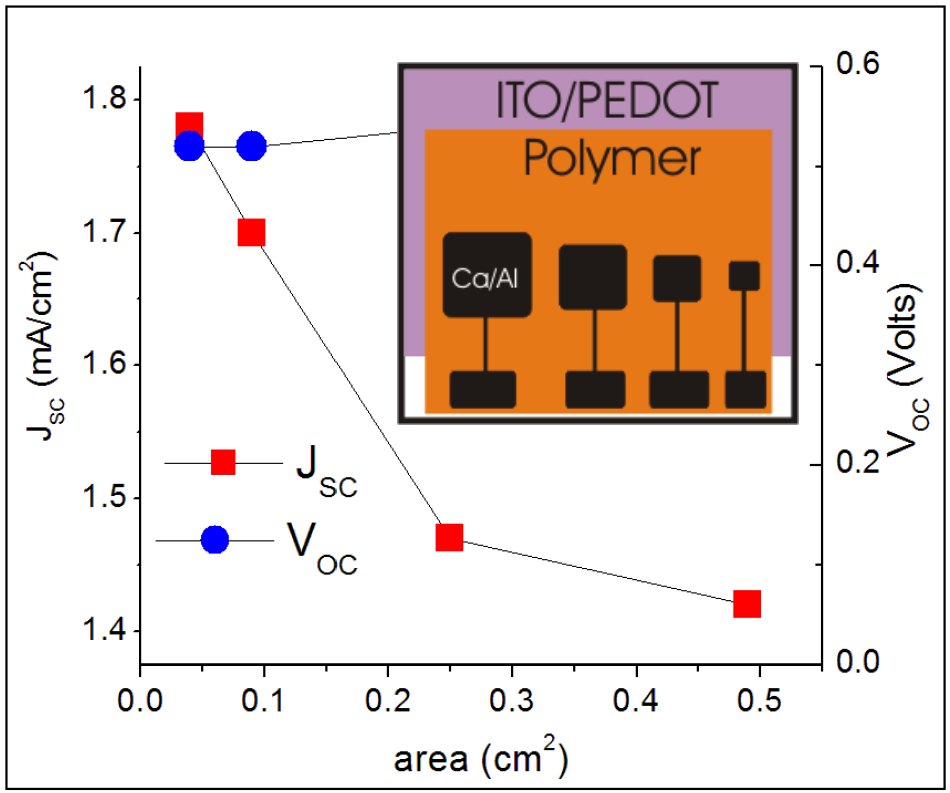

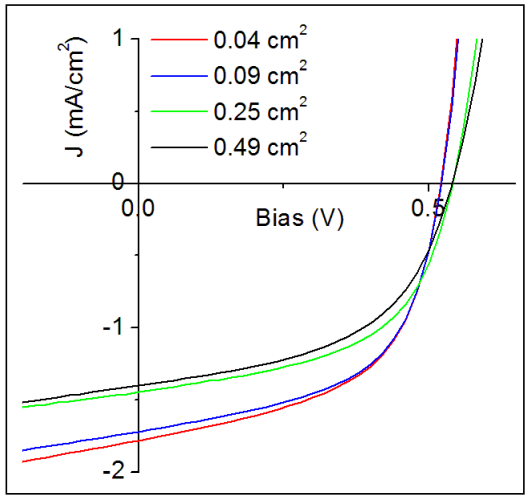

Appl. Phys. Lett. 2008
SPIE News 2009

Current density number shoots up as the cathode-area becomes smaller
Perimeter/Area varies as 1/x : The effect is pronounced for small area devices
Efficiency estimates can increase drastically for small area devices (< 0.01 cm^2)

To keep device area small top Al can be pixilated

Since it is just a single masking step

Lateral current contribution from the uncovered regions

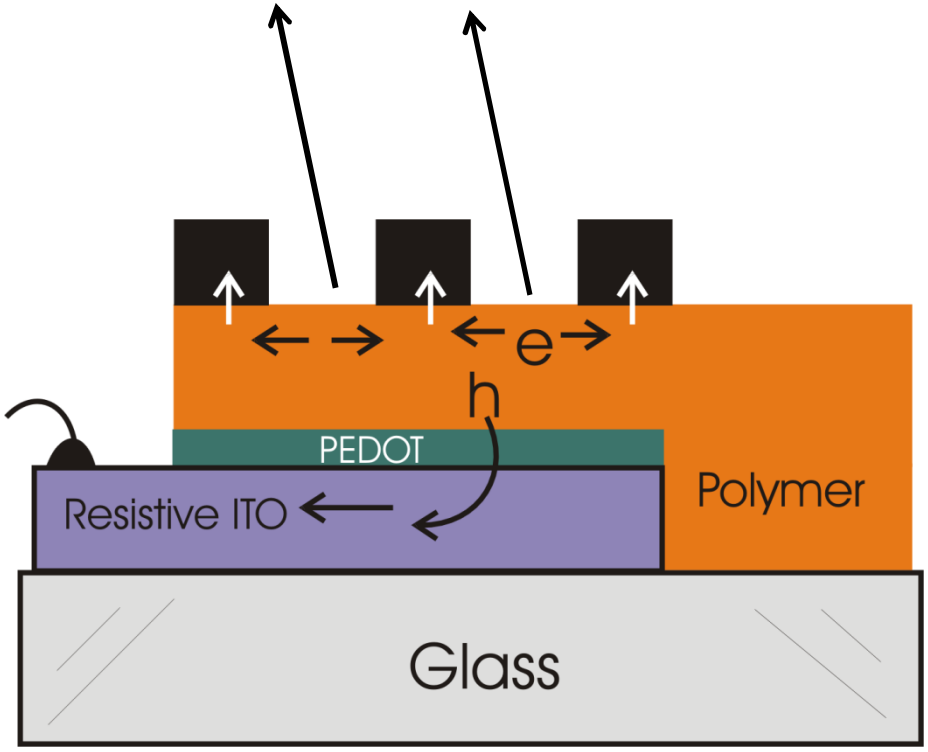

Photoactive region around the periphery

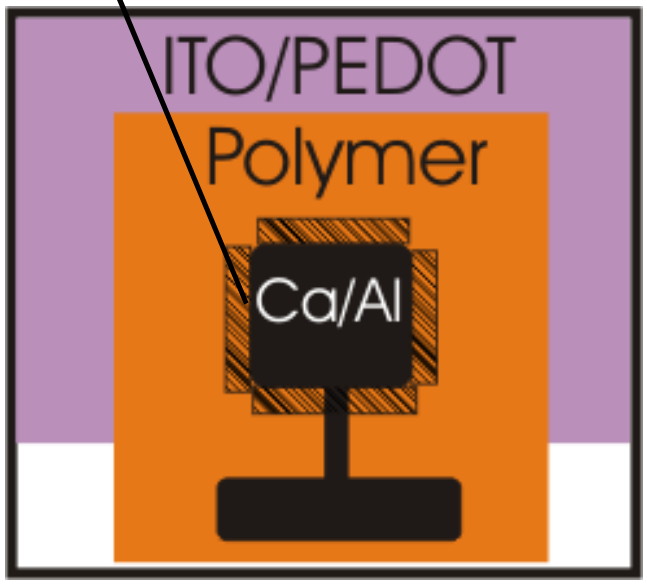

INTENSITY MODULATED PHOTOCURRENT MEASUREMENT

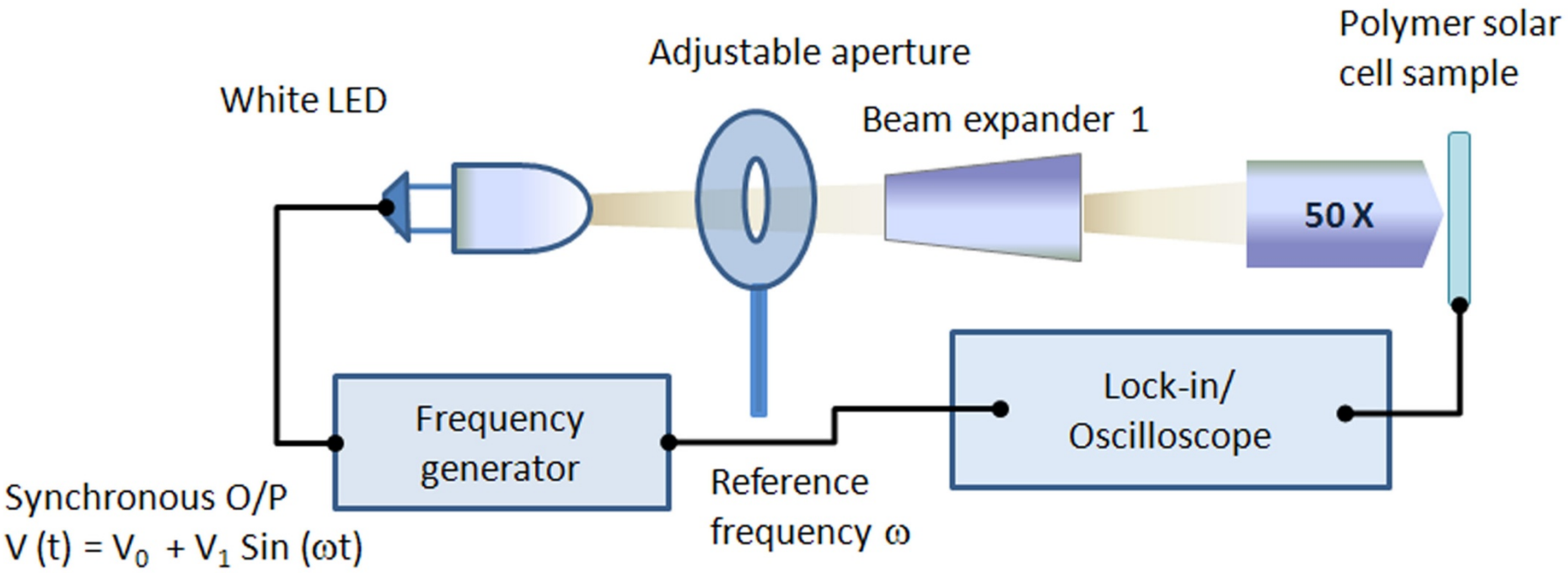

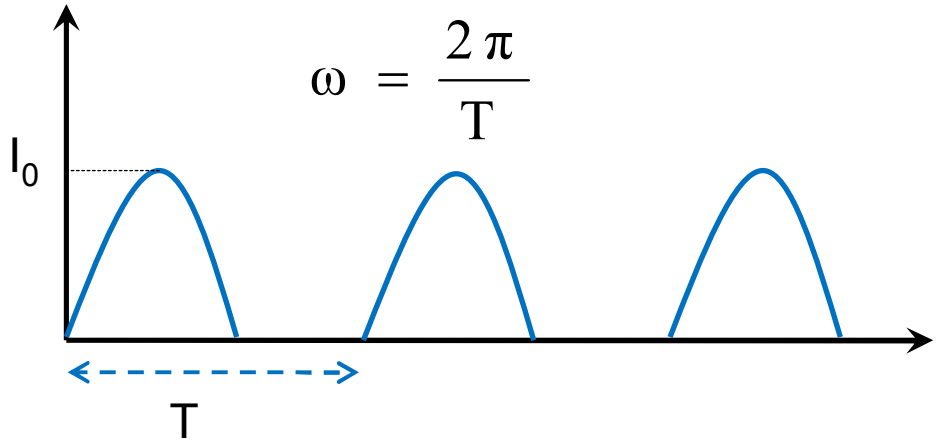

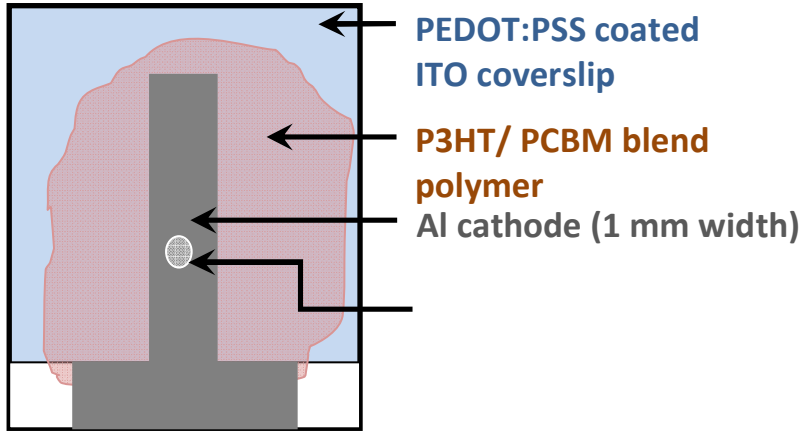

REAL TIME PHOTOCURRENT DATA FOR A FREQUENCY SWEEP FROM 100 HZ TO 100 KHZ

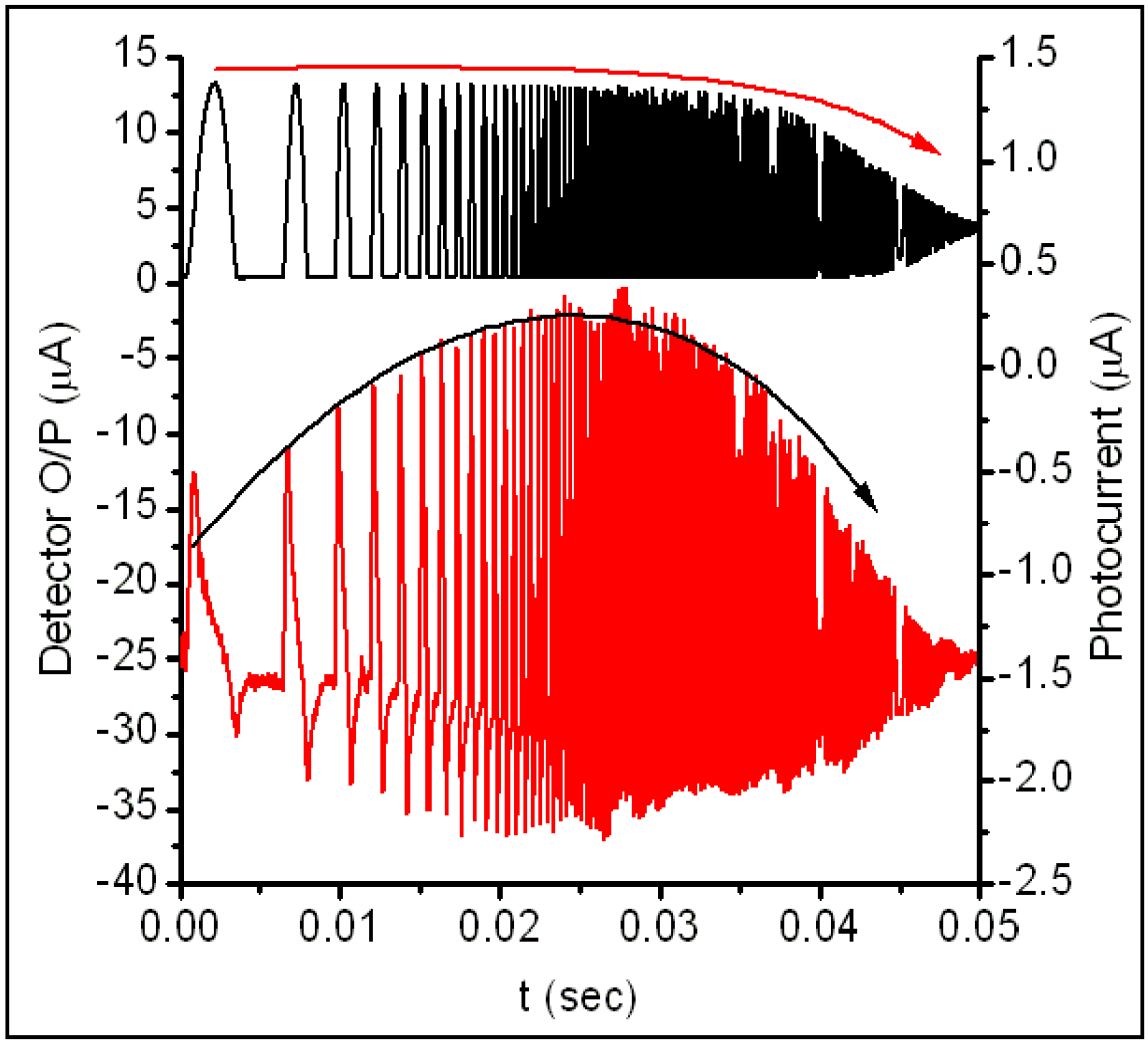

Device photocurrent is not purely sine wave (half wave) as the detector photocurrent is and there is always a phase lag between incident light and generated photocurrent.

PHOTOCURRENT FEATURES IN POLYMER BLEND SOLAR CELLS

- Low frequency regime (photocurrent independent of frequency)
- Photocurrent peak at ω_{max} between from 5 kHz -9 kHz.
- High frequency regime – photocurrent drops very sharply

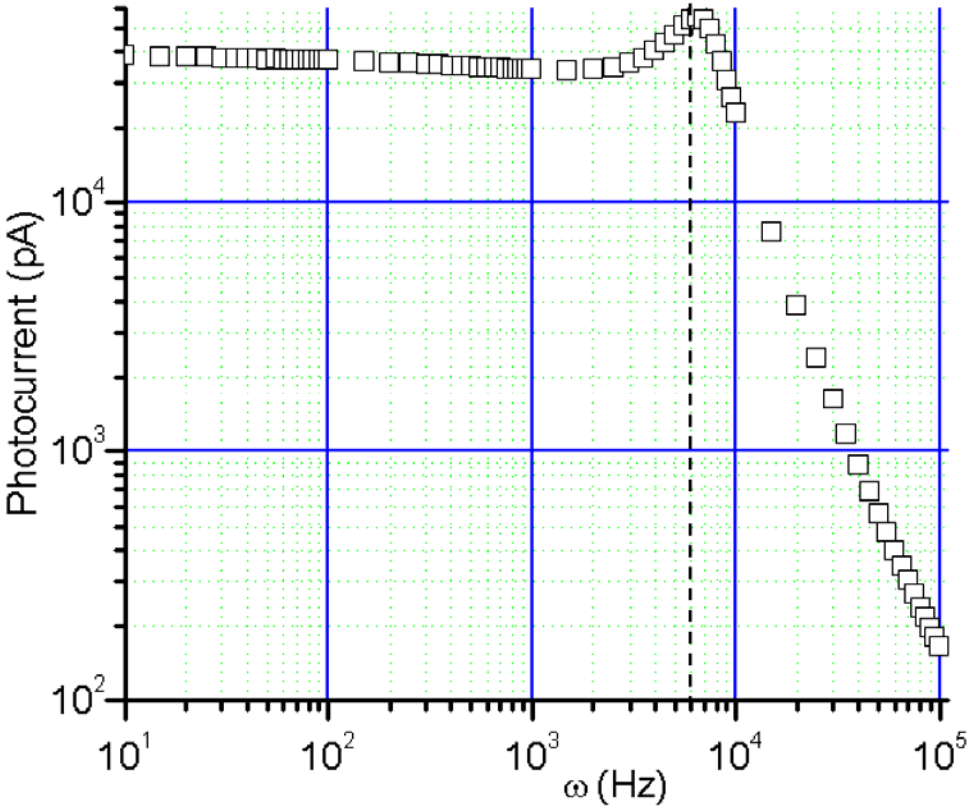

PHOTOCURRENT PEAK: A UNIVERSAL FEATURE IN POLYMER BLEND SOLAR CELL??

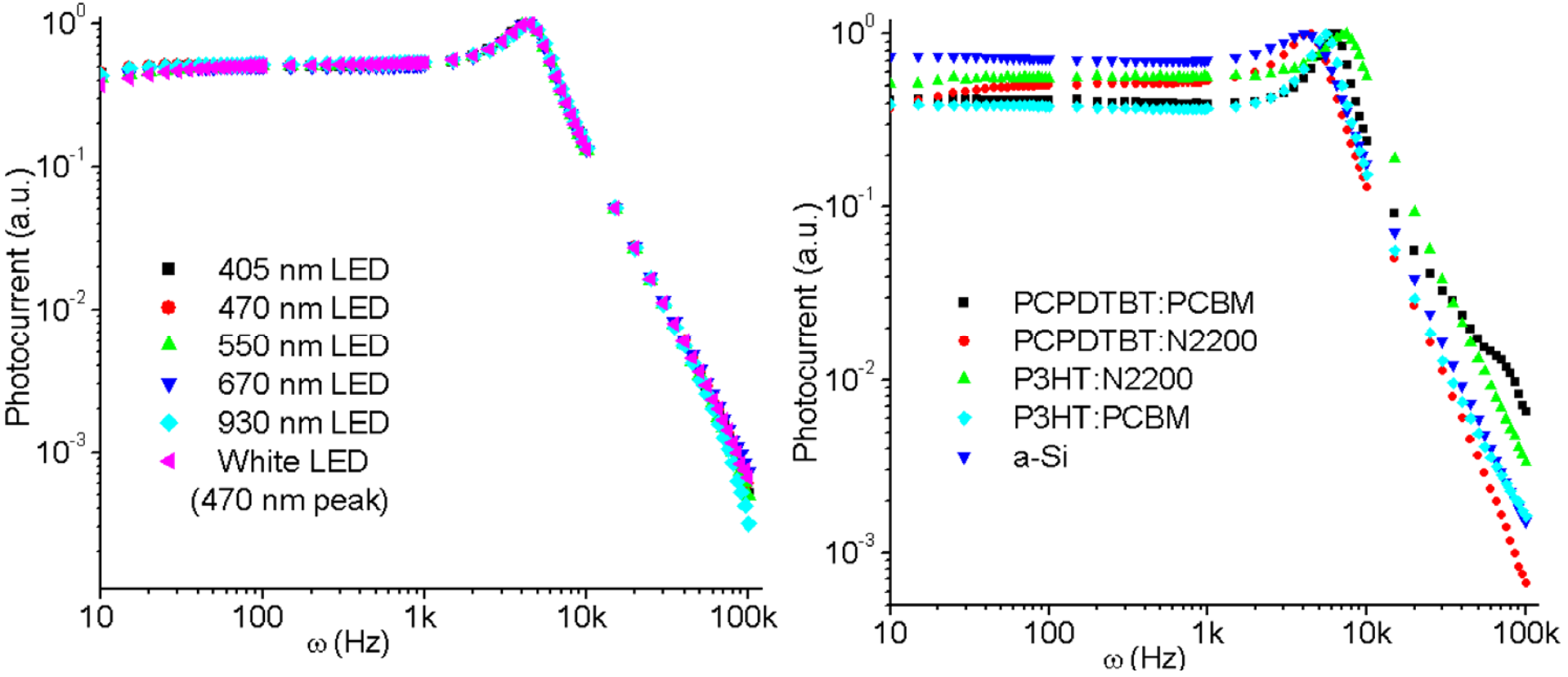

The origin of photocurrent peak is microscopic nature of the polymer blend solar cells. However macroscopic parameters modify it depending on the experimental condition.

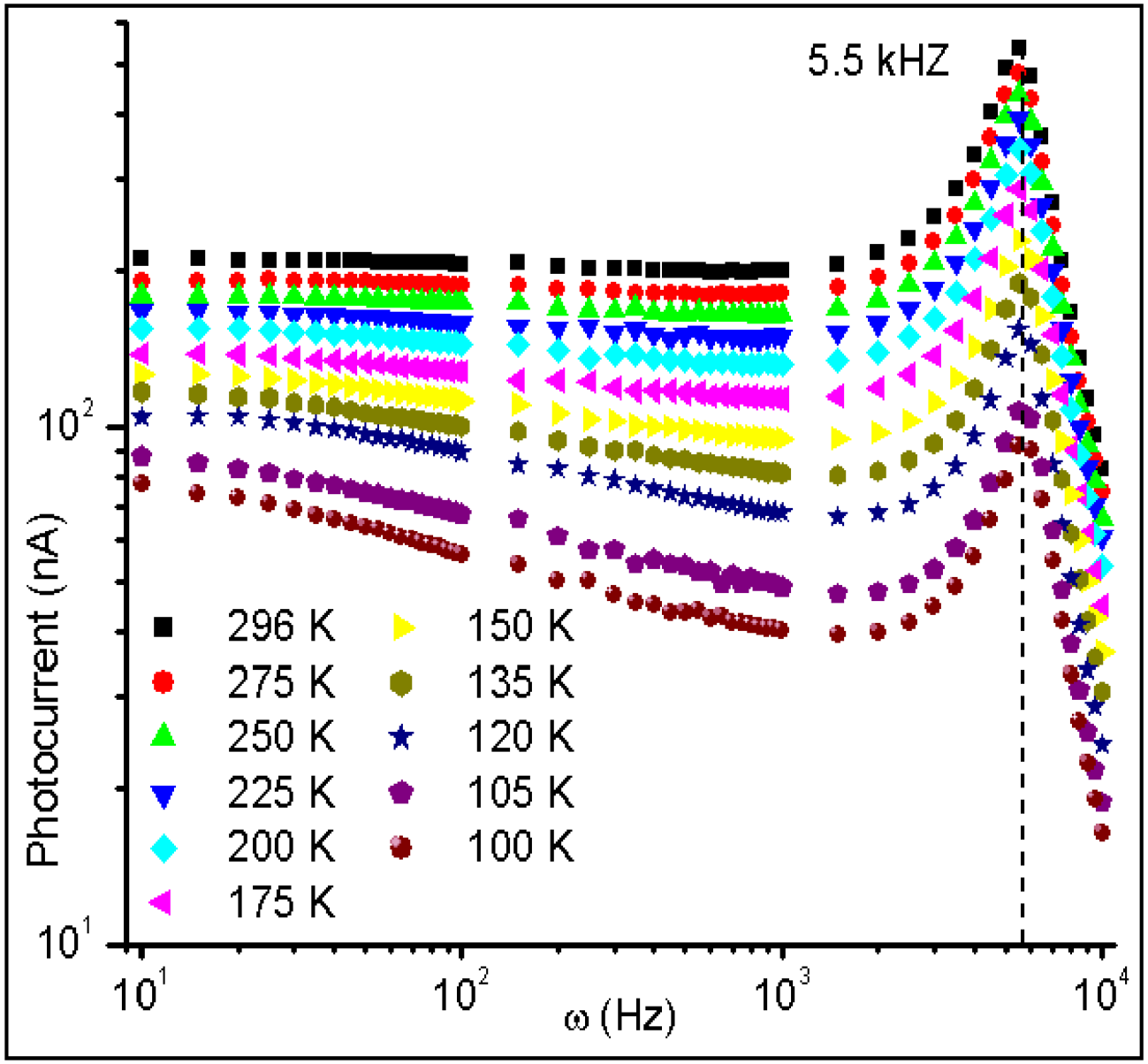
5.5 kHZ
Photocurrent (nA)
10^2
10^1
296 K
275 K
250 K
225 K
200 K
175 K
150 K
135 K
120 K
105 K
100 K
10^1
10^2
10^3
10^4
ω (Hz)

Step 1: Macroscopic model

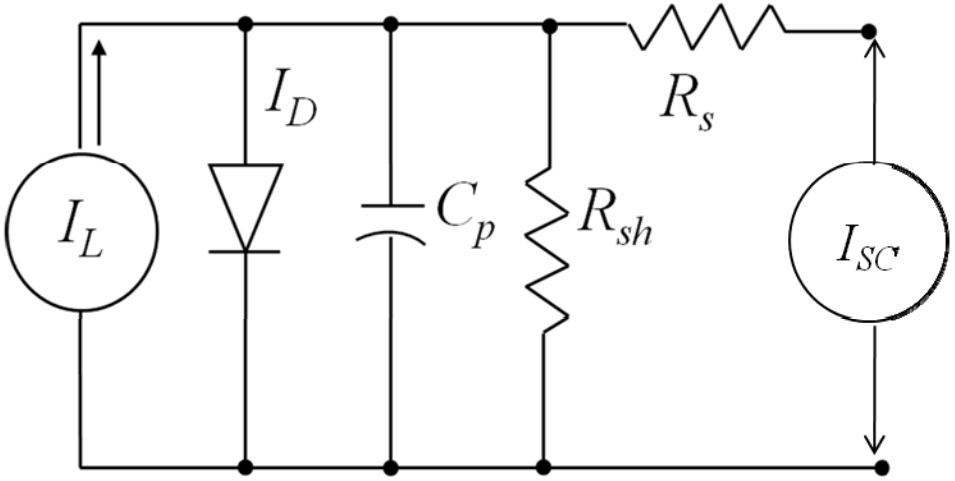

$$I_{SC} = CTF \times I_L$$

$$I_L = TF_{microscopic} G_L$$

$$I_{SC} = TF \times G_L$$

$$TF = CTF \times TF_{microscopic}$$

Step 2: Microscopic model

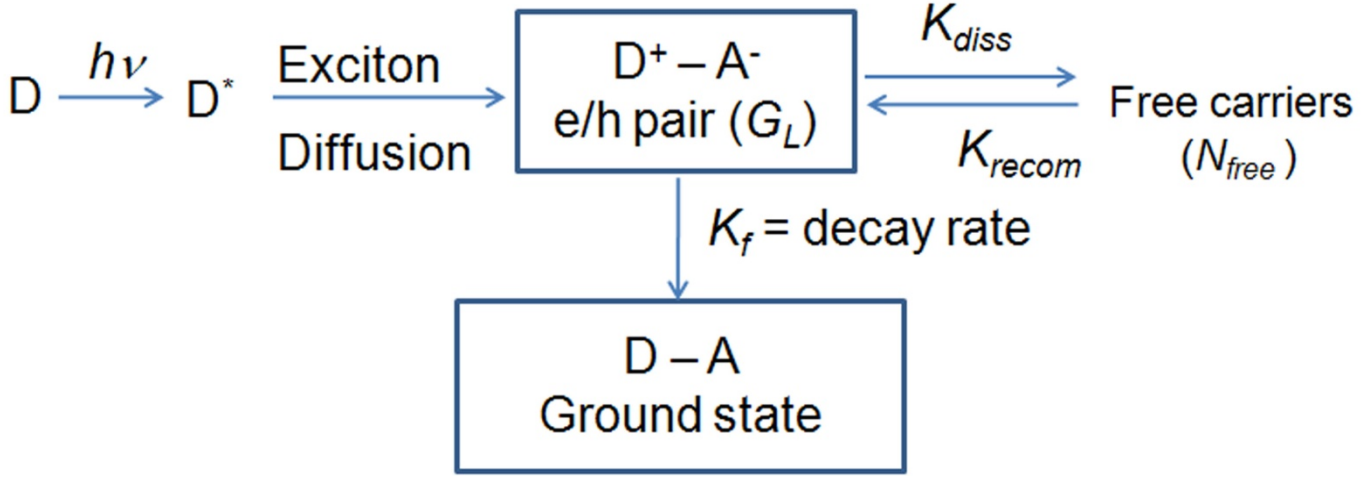

B. Mazhari, Solar Energy Mater. & Solar Cells, **90** (2006)
L. J. A. Koster *et. al*. Phys. Rev. B, **72** (2005)

MACROSCOPIC MODEL

$$I_{sc}(\omega) = \frac{R_{sh}}{\left[R_{sh}R_sC_p i\omega + (R_{sh} + R_s)\right]} I_L(\omega) \quad \text{.....(1)}$$

$$CTF = \frac{I_{sc}(\omega)}{I_L(\omega)} = \frac{R_{sh}}{\left[R_{sh}R_sC_p i\omega + (R_{sh} + R_s)\right]} \quad \text{.....(2)}$$

$$CTF = \frac{R_{sh}}{R_{sh} + R_s} \times \frac{(ai\omega + 1)}{(bi\omega + 1)} \quad \text{.....(3)}$$

$$C_p(\omega) = \frac{C}{(ai\omega + 1)}$$

$$b = a + \frac{R_{sh}R_sC}{R_{sh} + R_s}$$

MICROSCOPIC PROCESSES

$$\frac{dg_L(t)}{dt} = -\frac{g_L(t)}{\tau_1} + K_{recom} n_{free}(t) \quad \text{.......................................}(4)$$

$$\frac{dn_{free}(t)}{dt} = -\frac{n_{free}}{\tau_2} + K_{diss} g_L(t) - Q_{trp} \quad \text{.......................................}(5)$$

$$\frac{dn_{free}(t)}{dt} = -\frac{n_{free}}{\tau_2} + K_{diss} g_L(t) - \int \kappa_{eff} n_{free}(t) dt \quad \text{...............}(6)$$

Where $Q_{trp}\Big|_{t=t_0} = \int_{t_0-\Delta t}^{t_0+\Delta t} \kappa_{eff} n_{free}(t) dt$

MODEL CONTINUED.....

Solving coupled equation 4 and 6

$$K_1 \frac{d^2 n_{free}(t)}{dt^2} + K_2 \frac{dn_{free}(t)}{dt} + n_{free}(t) = -Qg_L(t) \quad \text{.....(7)}$$

$$K_1 = \frac{1}{\left(\kappa_{eff} - K_{recom} K_{diss}\right)} \qquad K_2 = \frac{1}{\tau_2 \left(\kappa_{eff} - K_{recom} K_{diss}\right)}$$

$$Q = \frac{K_{diss}}{\tau_1 \left(\kappa_{eff} - K_{recom} K_{diss}\right)}$$

$$g(t) = g_0 + g_1 \exp(-i\omega t) \qquad n(t) = n_0 + n_1 \exp(-i\omega t)$$

CONTINUED.....

$$N_{free}(\omega) = \frac{-Q}{\left[-K_1\omega^2 + K_2 i\omega + 1\right]} G_L(\omega)$$

$$I_L(\omega) \propto N_{free}(\omega)$$

$$I_{sc}(\omega) = CTF \times I_L(\omega) = CTF \times TF_{microscopic} G_L(\omega)$$

$$TF = K \frac{(as+1)}{(bs+1)\left(K_1 s^2 + K_2 s + 1\right)}$$

Where ‘s’ is a complex frequency ‘$i\omega$’

EXPERIMENTAL AND MODEL $I_{PH}(\omega)$ AND $\phi(\omega)$

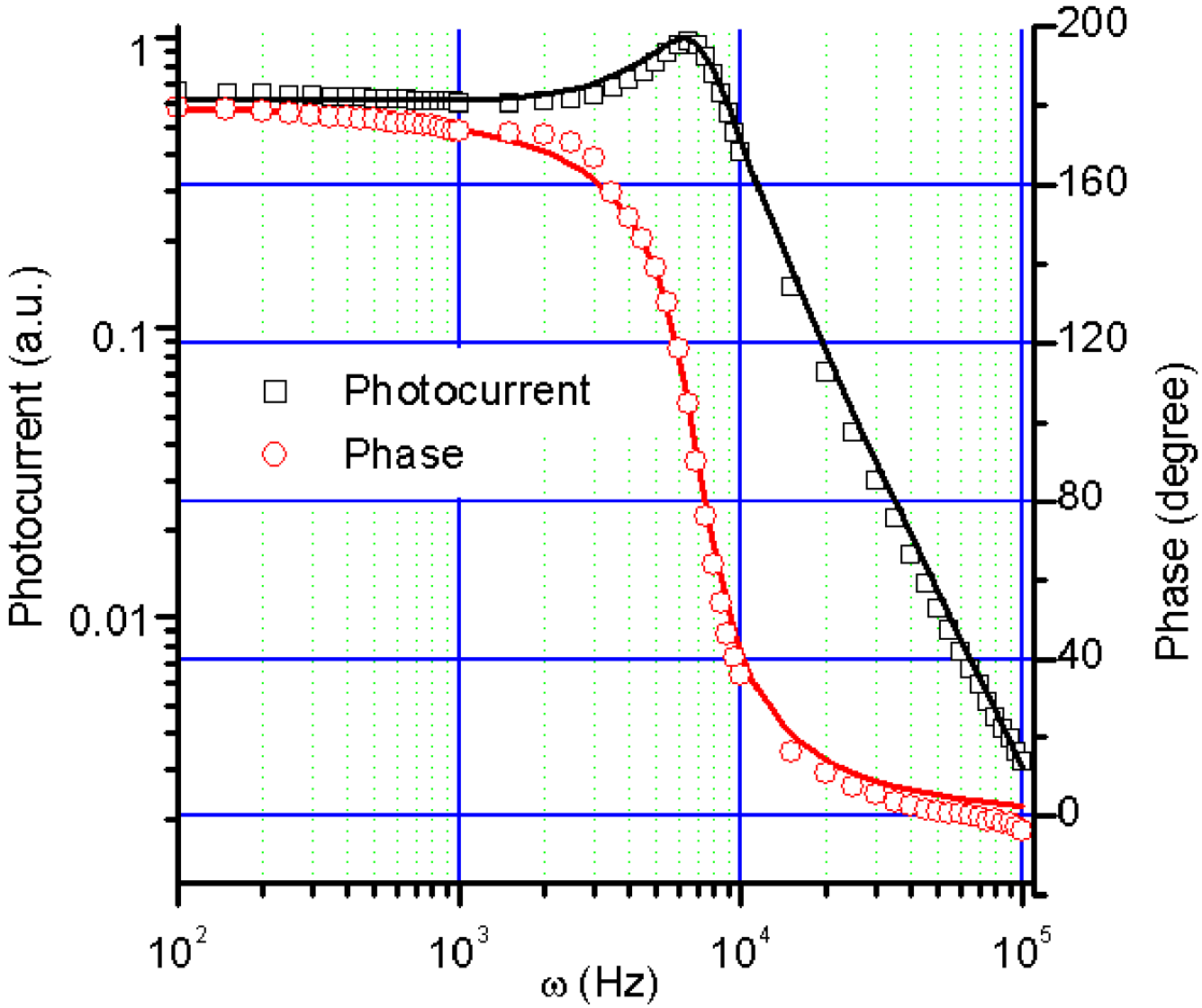

TEMPERATURE DEPENDENT STUDY FOR P3HT:PCBM SOLAR CELLS

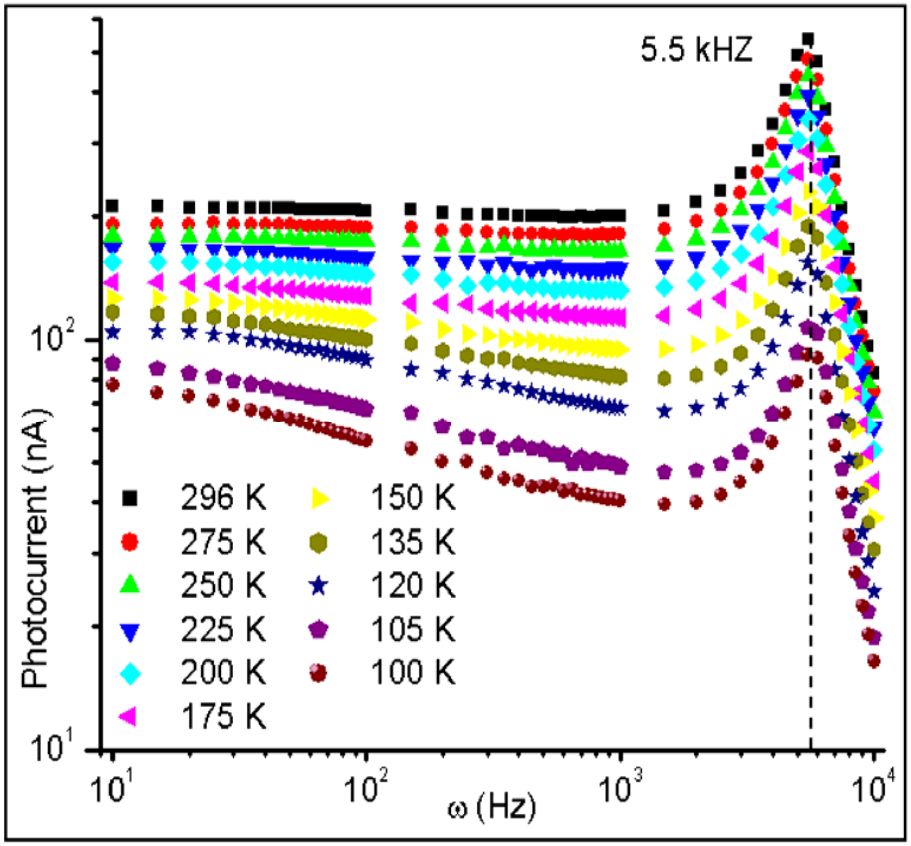

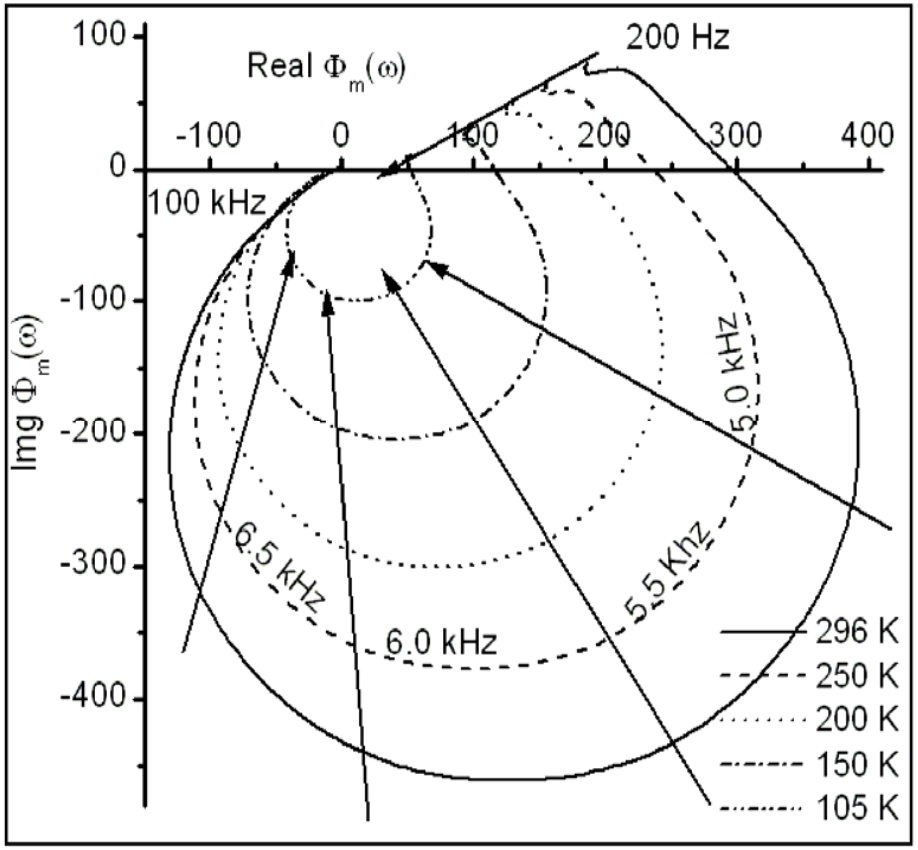

TEMPERATURE DEPENDENT MODULATE PHOTOCURRENT MODEL

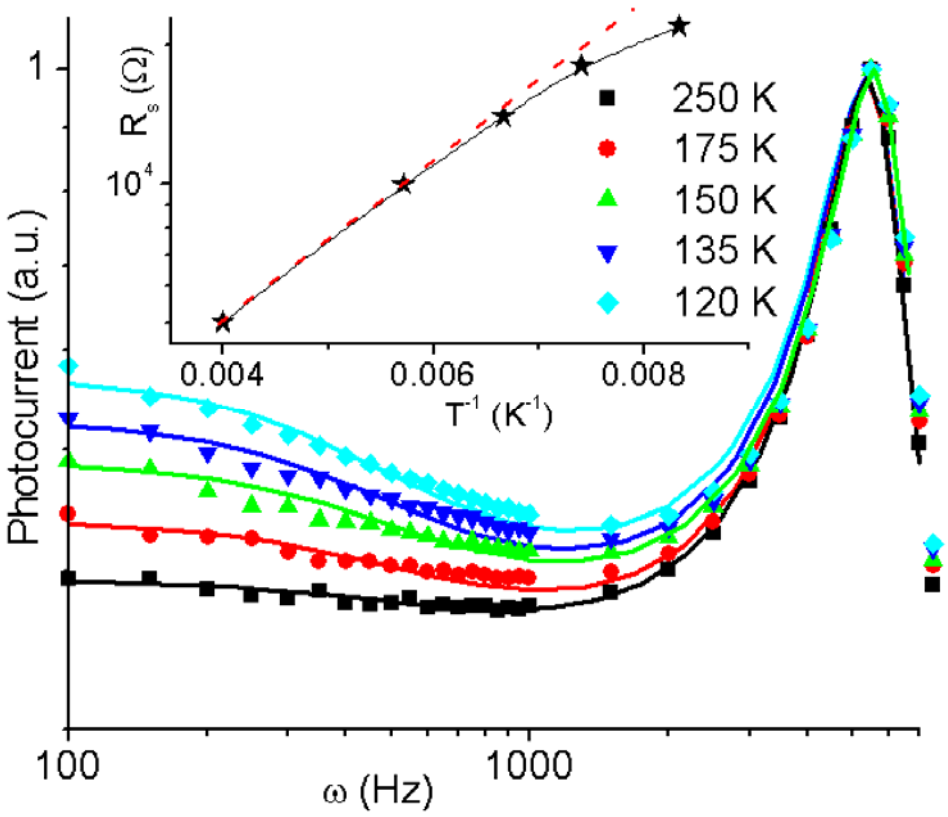

In our model we vary R_s as charge extraction is an activated process follows exponential dependence

$$R_s = R_0 \exp\left(E_a / k_B T\right)$$

From log (I_{sc}) Vs T^{-1} activation energy E_a = 21 meV which is of same order as simulated value 30 meV at room temperature

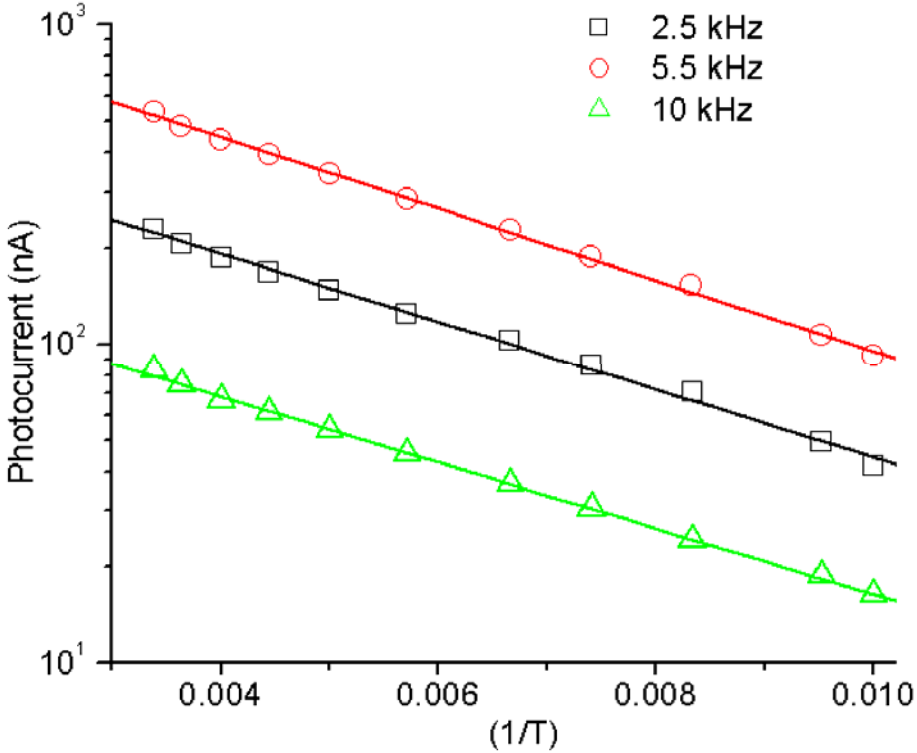

INTENSITY MODULATED PHOTOCURRENT WITH CW WHITE BACKGROUND LIGHT

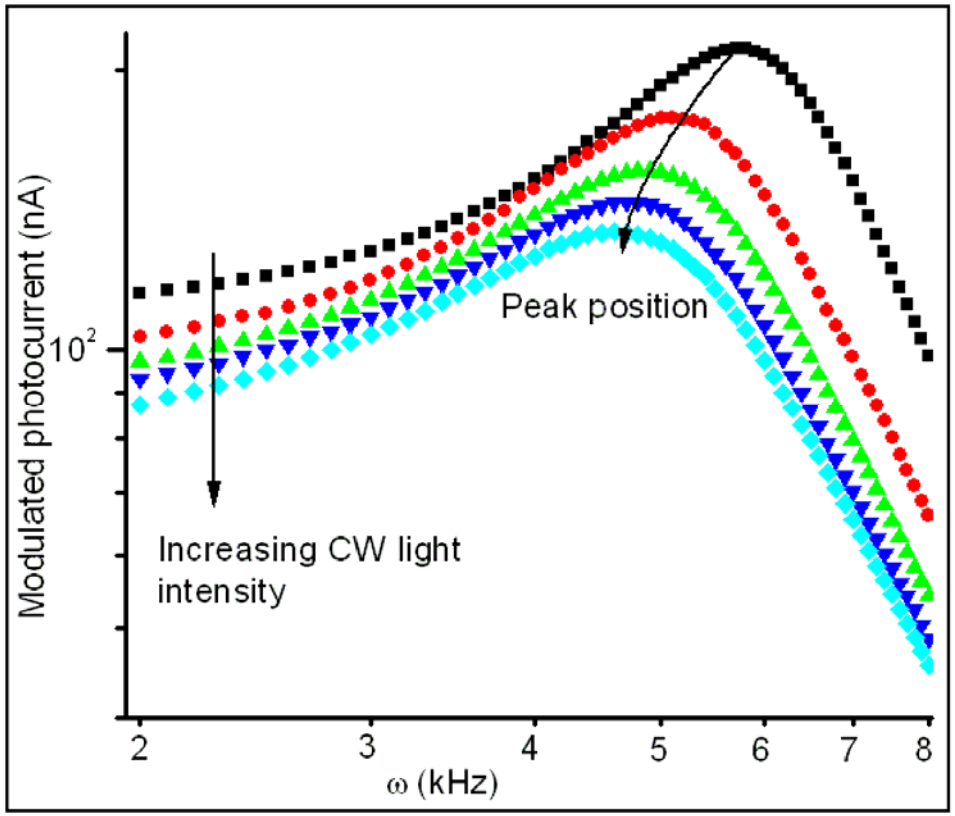

With background CW light charge carrier concentration increases and hence recombination rate increases which leads to decrease in modulated photocurrent

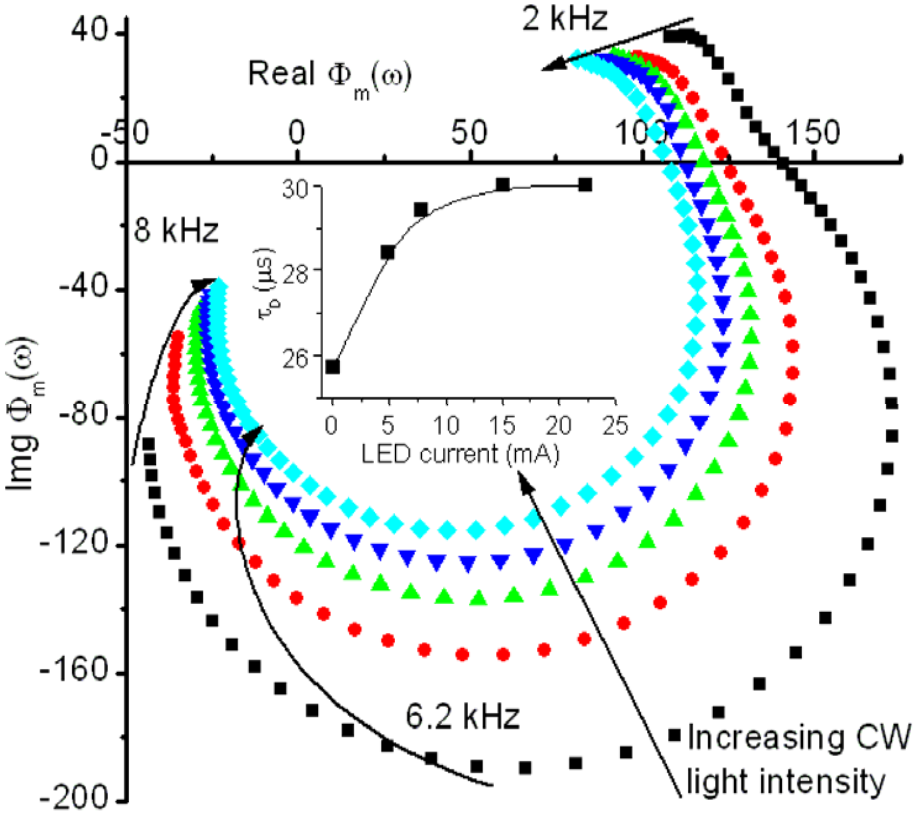

INCREASE IN INTENSITY OF MODULATED LIGHT SOURCE

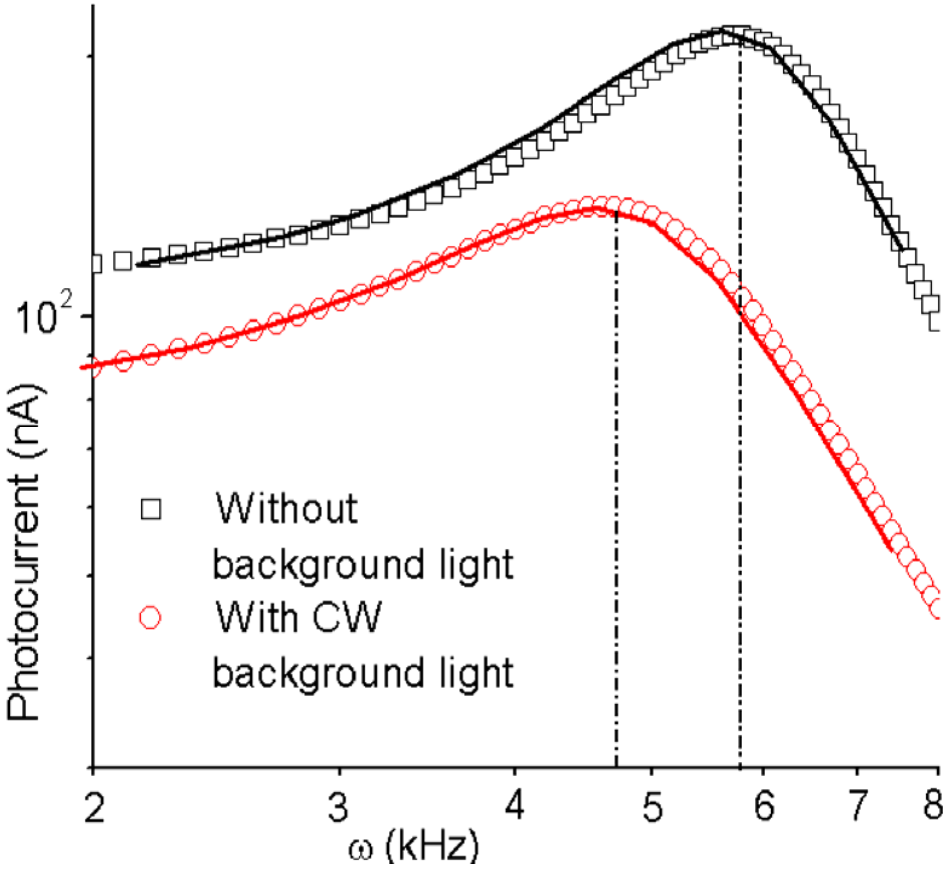

Symbols are for experimental

Lines are fit to the model

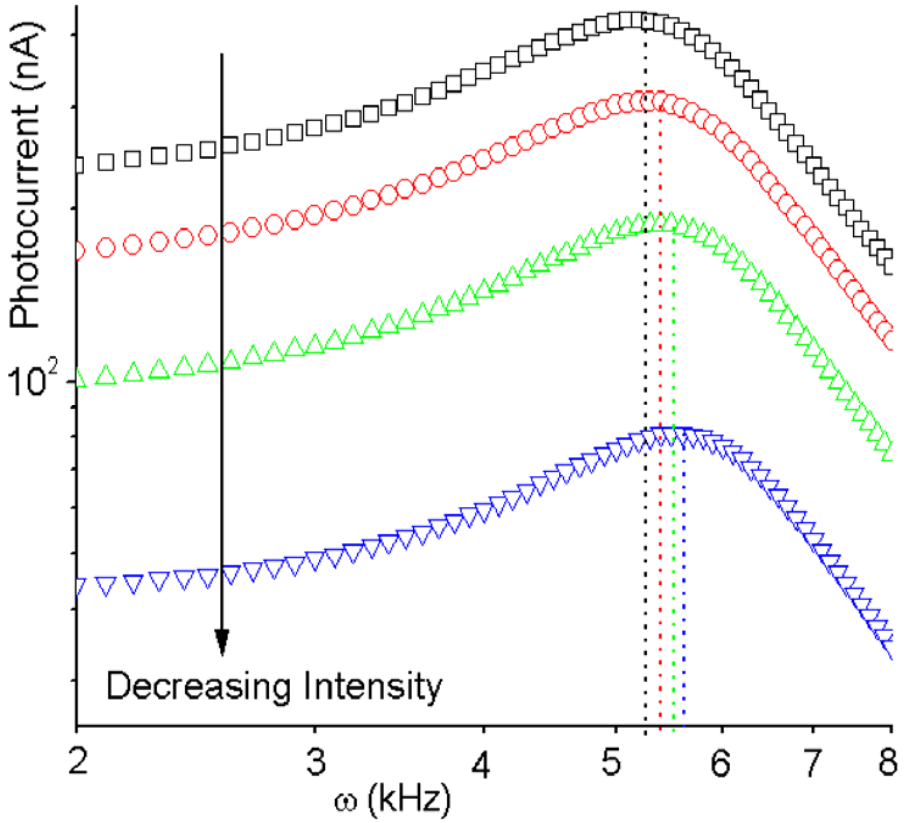

However increase in modulated intensity does not show significant peak shift except increase in modulated photocurrent

EFFECT OF MORPHOLOGY-FF DEPENDENCE

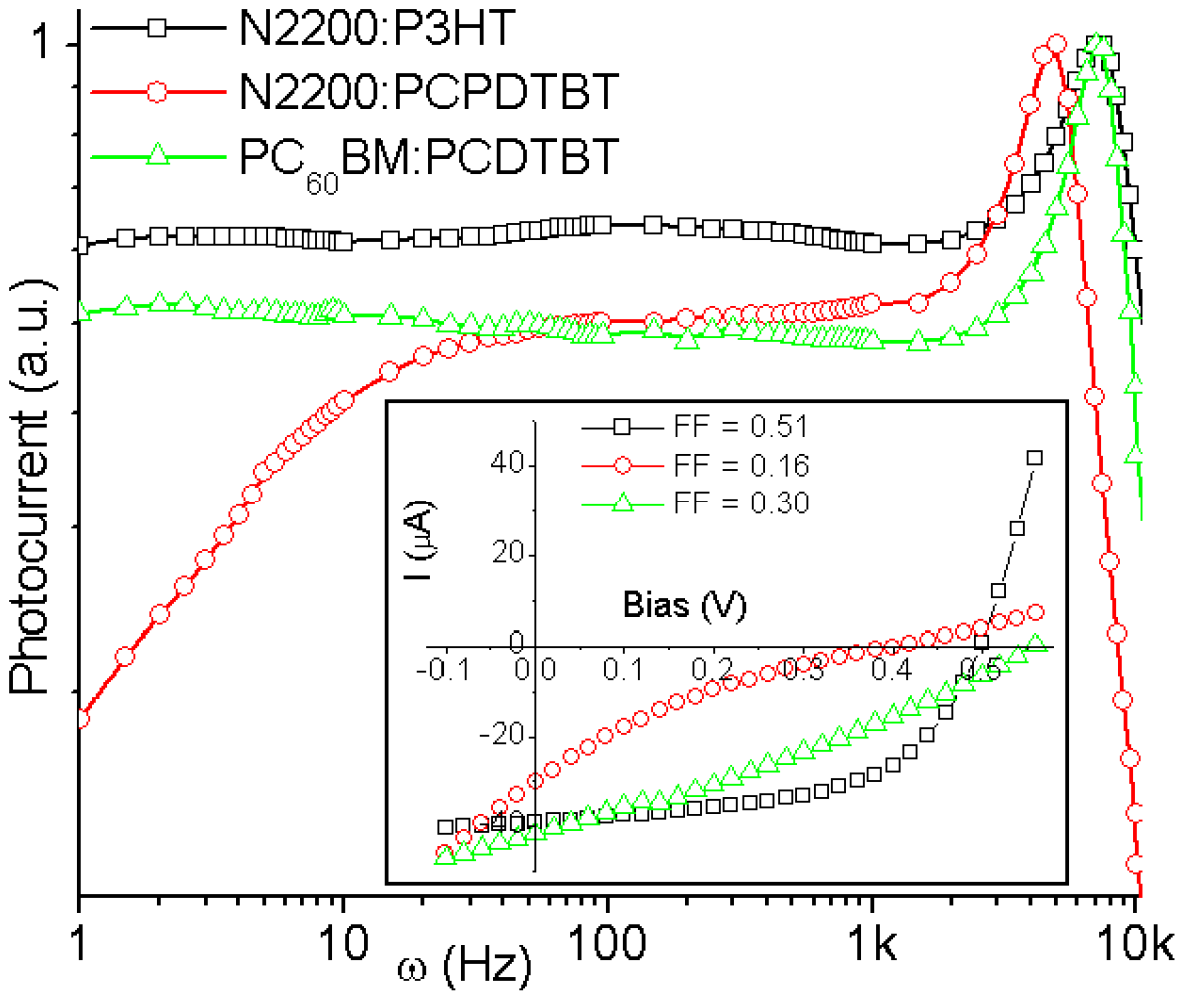

Recombination losses at low frequency is more dominating when morphology/ interface is not perfect; leading to reduced fill factor

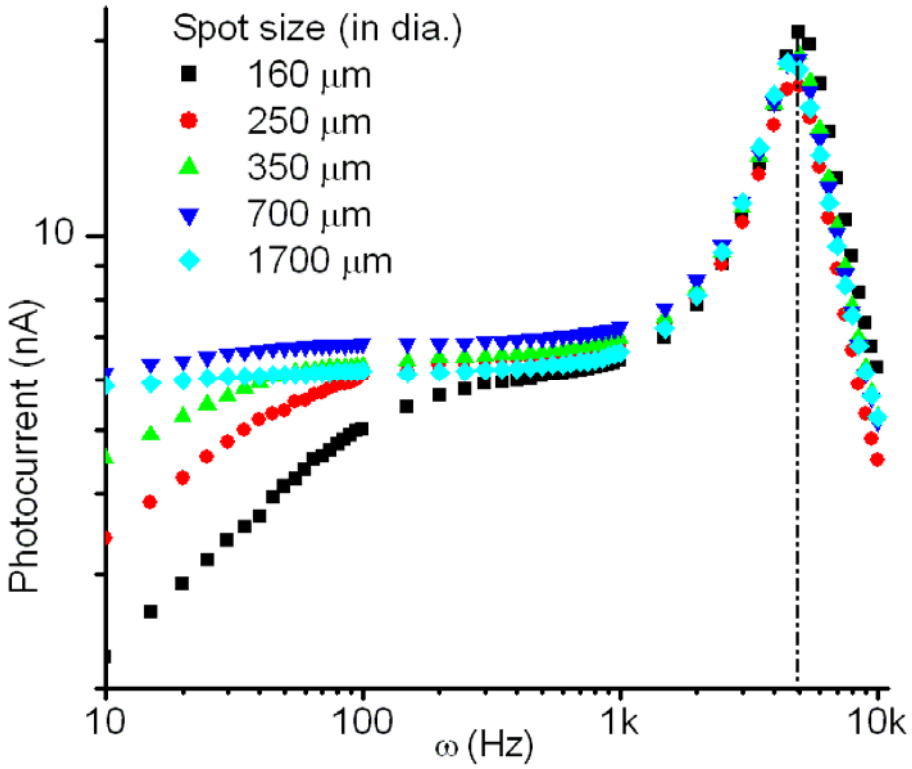

Photocurrent peak has been observed in relatively less efficient solar cells. However these devices show intensity dependent at low frequency regime.

Photocurrent from the peripheral region also shows photocurrent peak at same position when illumination is on overlap region, but absolute photocurrent drops at low frequency regime.

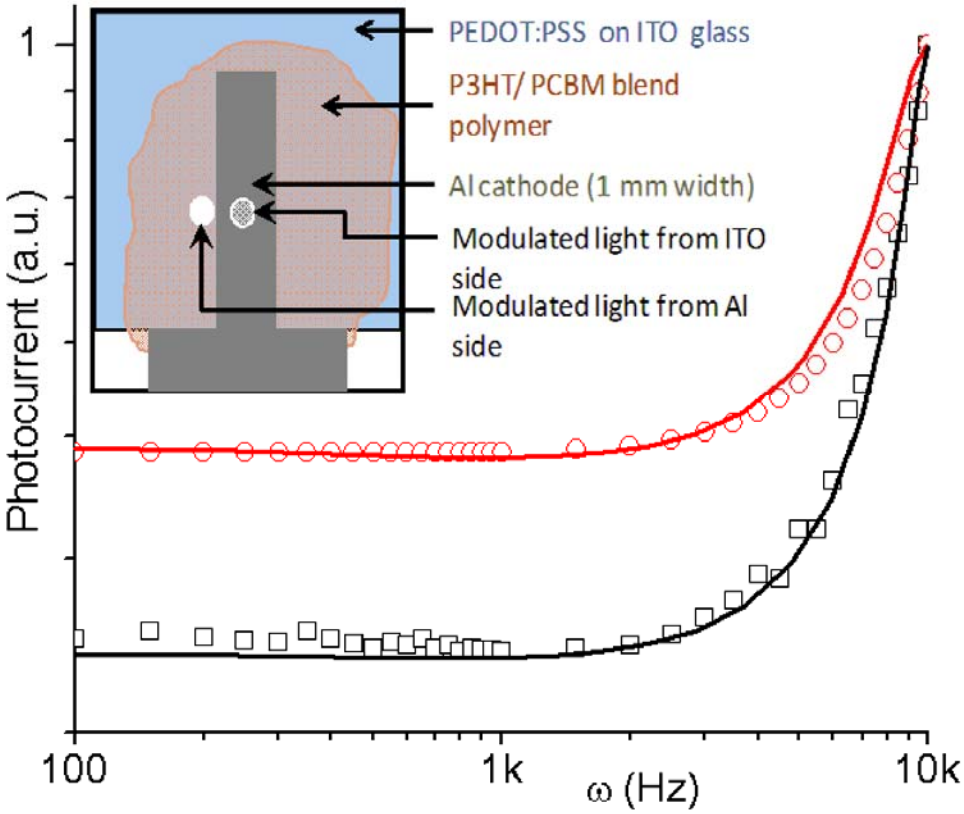

PHOTOCURRENT PEAK: A UNIVERSAL FEATURE IN POLYMER BLEND SOLAR CELL??

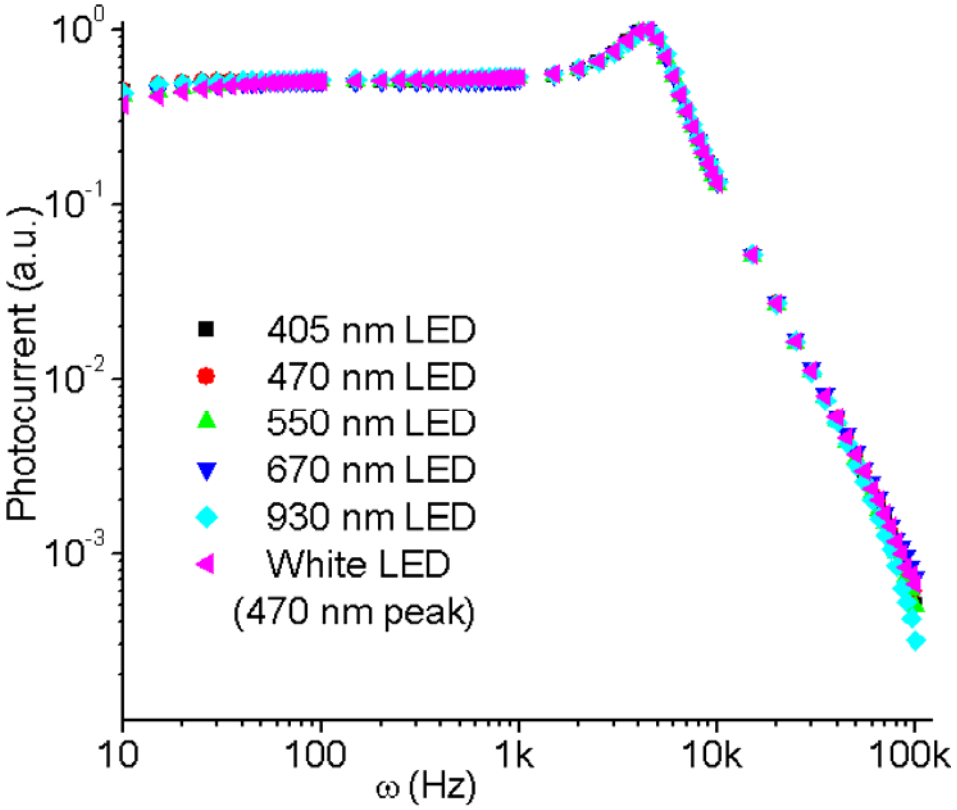

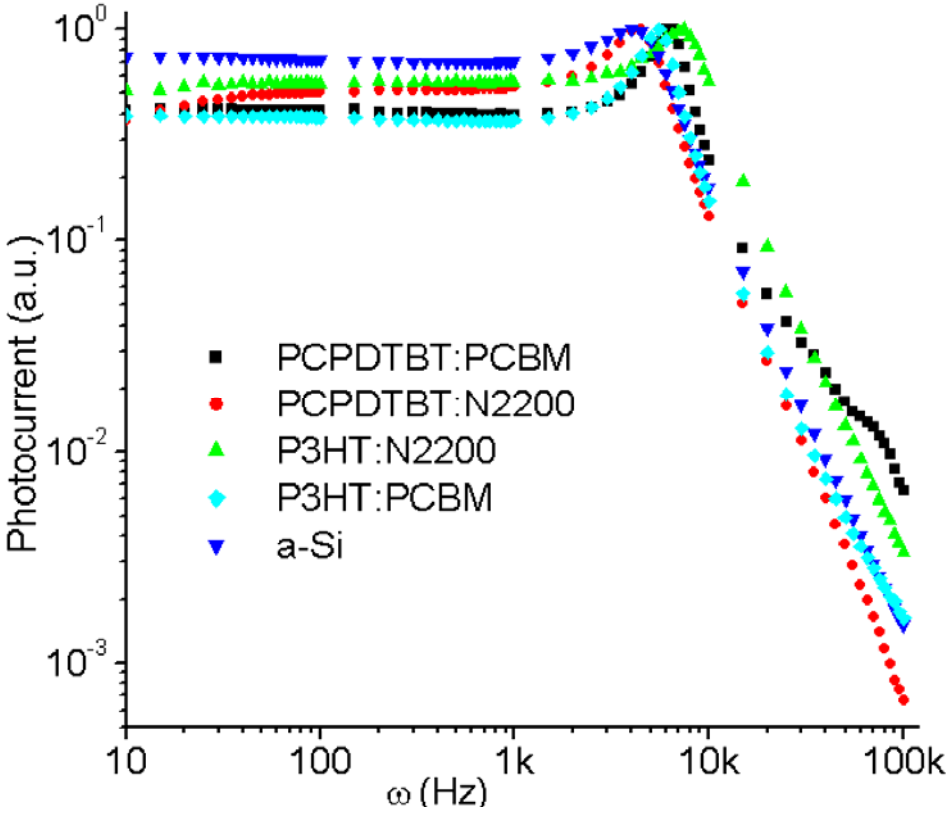

The origin of photocurrent peak is microscopic nature of the polymer blend solar cells. However macroscopic parameters modify it depending on the experimental condition.

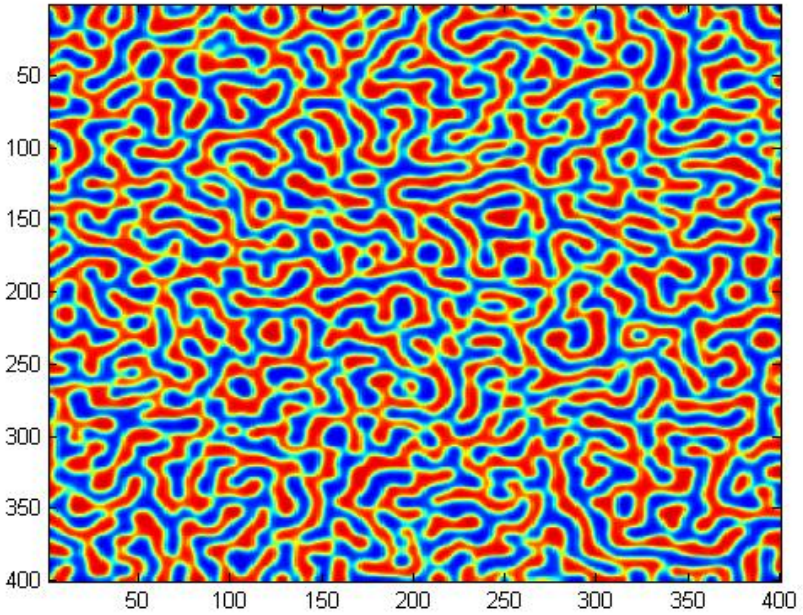

- Universal response in BHJ-PSCs

- Low frequency response is related to the morphology and fill factor

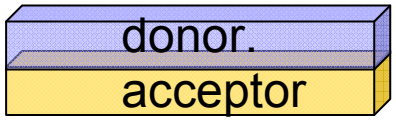

To probe D-A interface, in a non-invasive manner

Effect of Electrostatic field on the interfacial processes

FETs of stable Acceptor systems can be fabricated

Transfer Printing Method

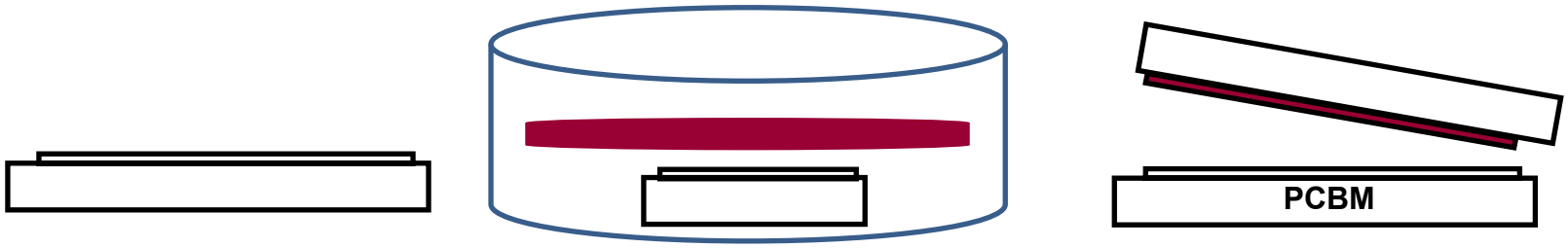

PDMS coated
glass substrate

P3HT dropped
on water solution.

Dry film transfer
On PCBM surface.

Depositing P3HT film on spin coated PCBM film is not solution processible.

P3HT films were suspended on water and transferred onto PDMS substrate and then laminated onto PCBM film.

P3HT on PCBM laminates giving rise to good structural film.

Bilayer configuration has well defined D-A interface as opposed to D-A interface formed in blend morphology.

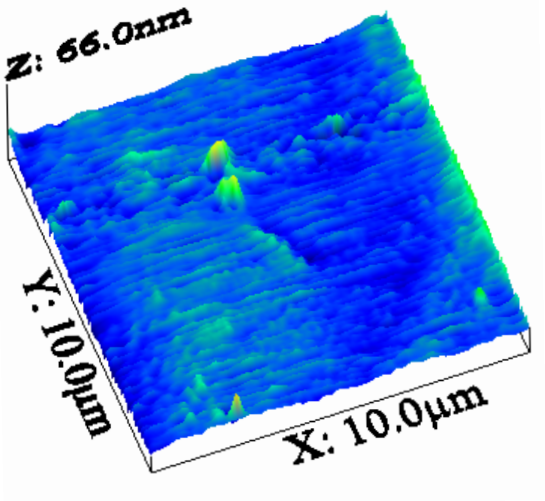

PCBM rms roughness: 1.9 nm

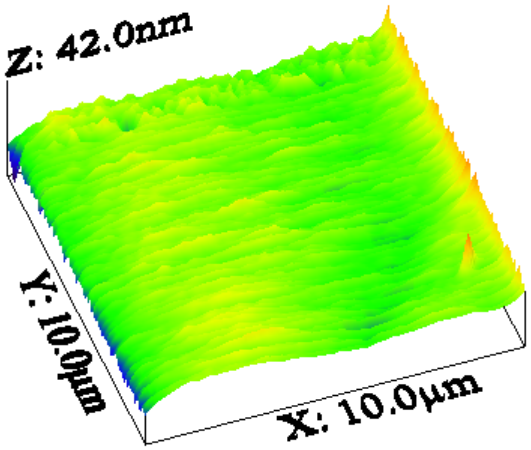

P3HT rms roughness 2.9 nm

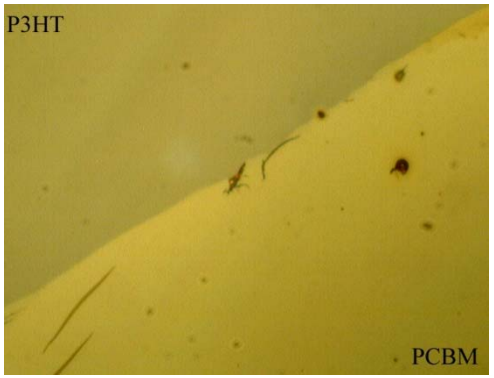

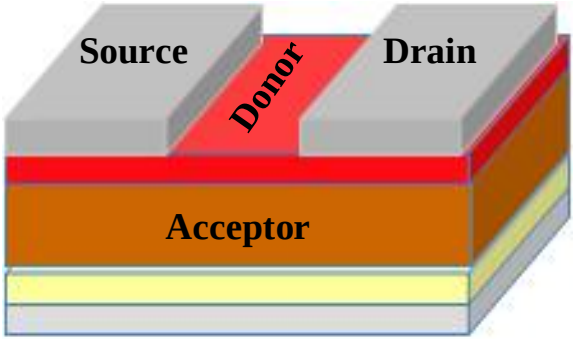

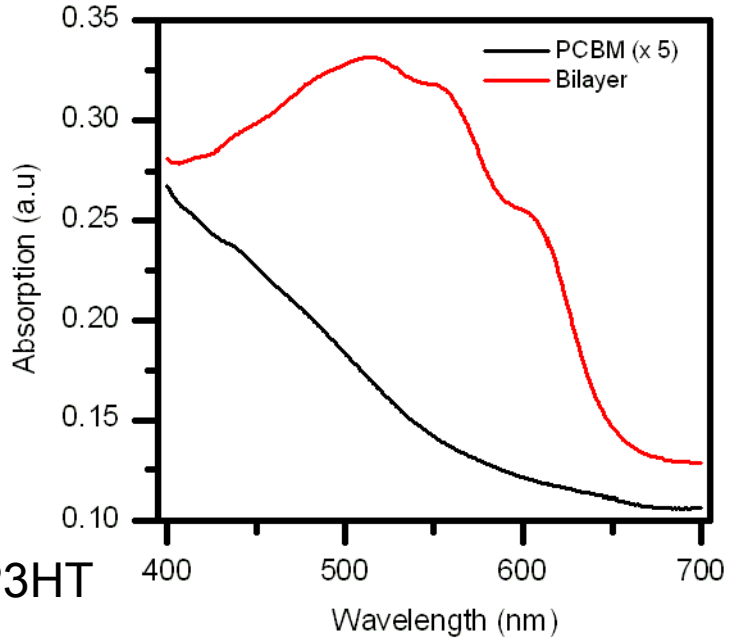

PCBM absorption is not optically active, whereas P3HT is optically active.

Based on energy symmetry level HOMO-LUMO optical transition are not allowed allowing weak absorption above 500 nm for PCBM.

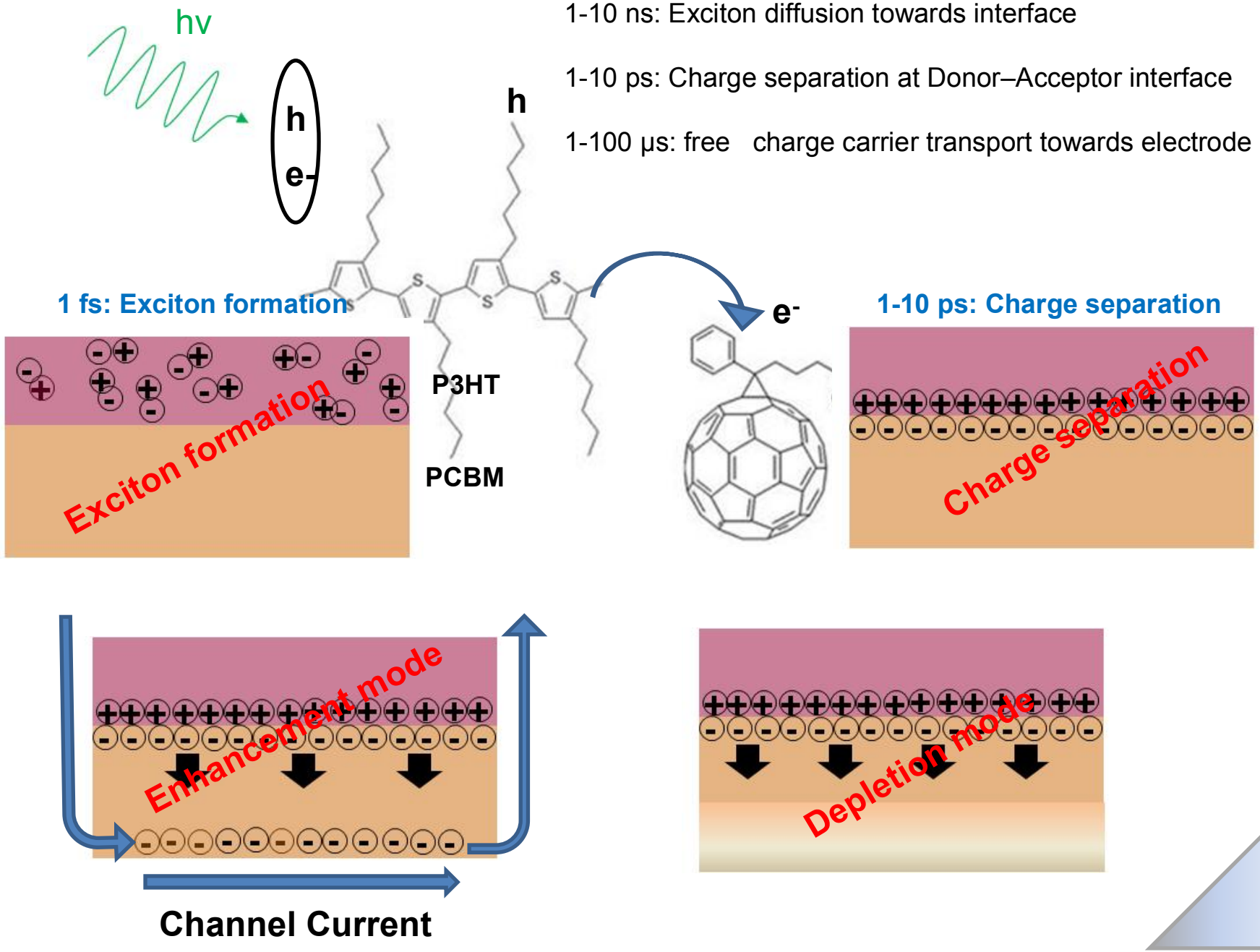
Time Scales
1-10 ns: Exciton diffusion towards interface
1-10 ps: Charge separation at Donor–Acceptor interface
1-100 µs: free charge carrier transport towards electrode
hv
h
e-
h
1 fs: Exciton formation
Exciton formation
P3HT
PCBM
e-
1-10 ps: Charge separation
Charge separation
Enhancement mode
Channel Current
Depletion mode

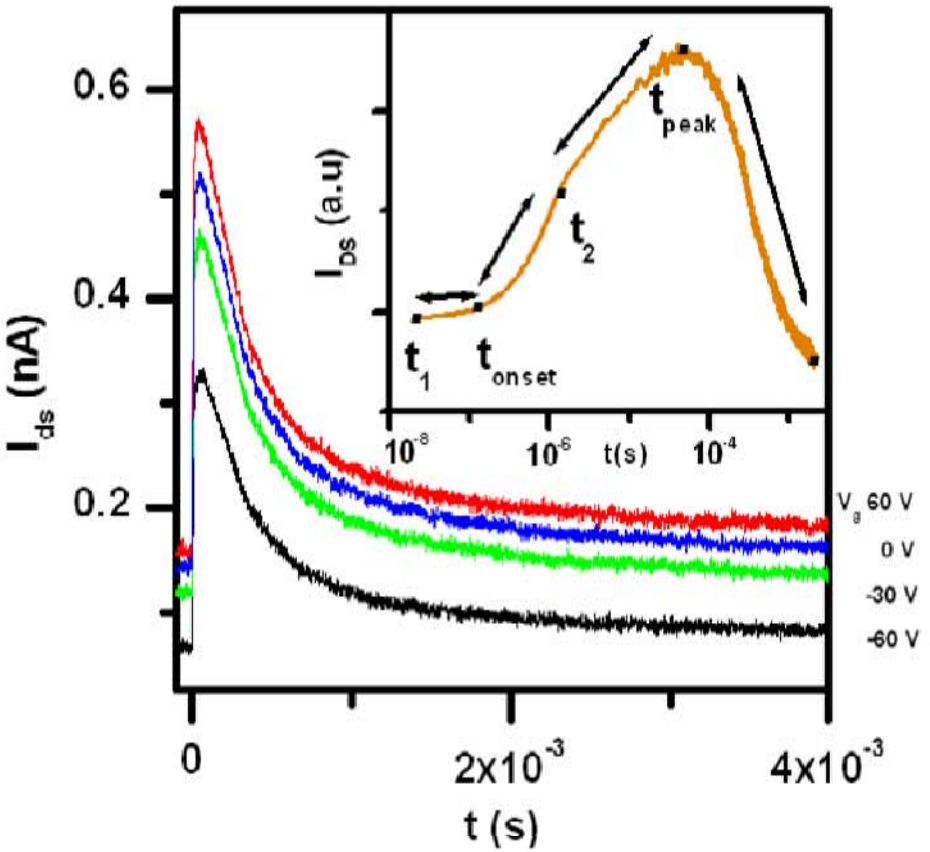

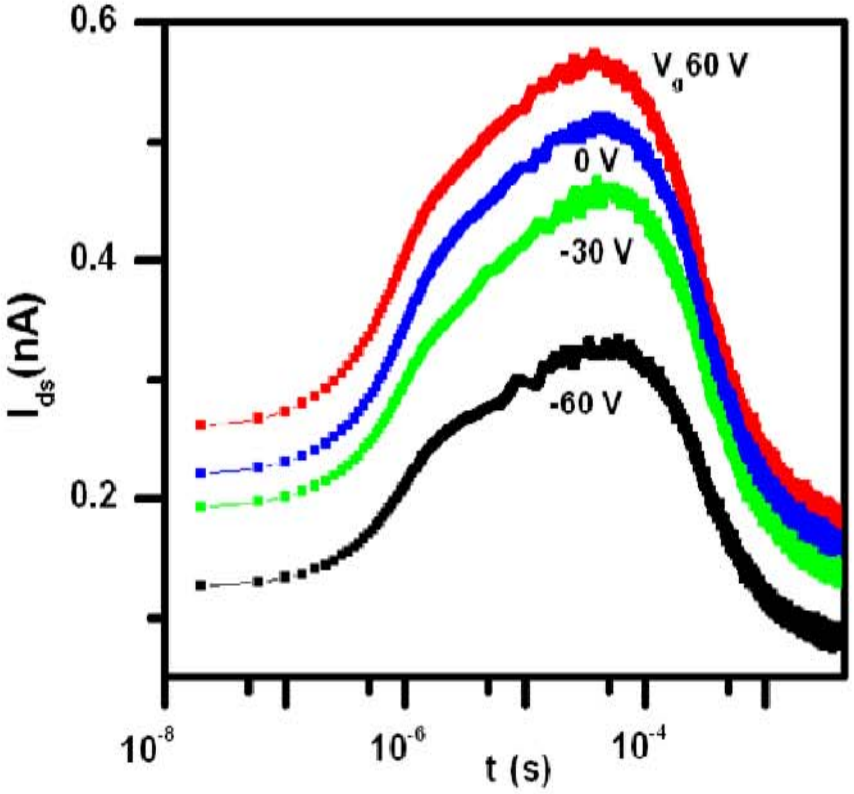

APPLIED PHYSICS LETTERS **95**, 183306 (2009)

Studies of charge transfer processes across donor-acceptor interface using a field effect transistor geometry

Manohar Rao and K. S. Narayan[a)]
Jawaharlal Nehru Centre for Advanced Scientific Research, Jakkur P. O., Bangalore 560 064, India

High mobility electron transporting polymer

Electron depleted core has been used for n-channel polymer building block.
Electron poor NDIR core has been used because of large electron affinity and T2(dithiophene) because of stability resulting in highly conjugated, planar and rod like polymers.

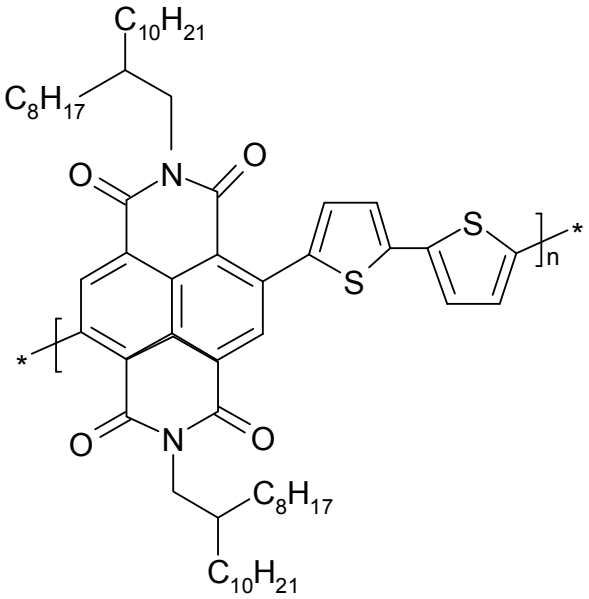

P(NDI20D-T2)

poly{[N,N'-bis(2-octyldodecyl)-napthalene-1,4,5,8-bis(dicarboximide)-2,6-diyl—alt-5,5'-(2,2'-bithiophene)}, (P(NDI20D-T2)

Air stable electron transporting Polymer FET can be fabricated

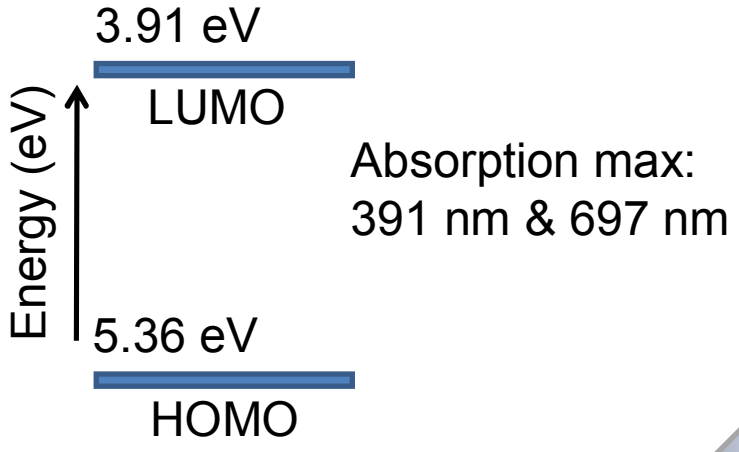

Absorption max:
391 nm & 697 nm

Fachetti et. al. JACS, 131, (2009)
Nature, 457, 679, (2009)

N2200 & P3HT based bilayer FET on Al gate electrode with BCB as dielectric and AL as source drain injecting electrode.

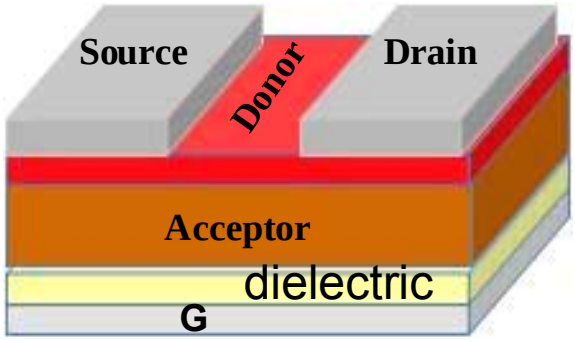

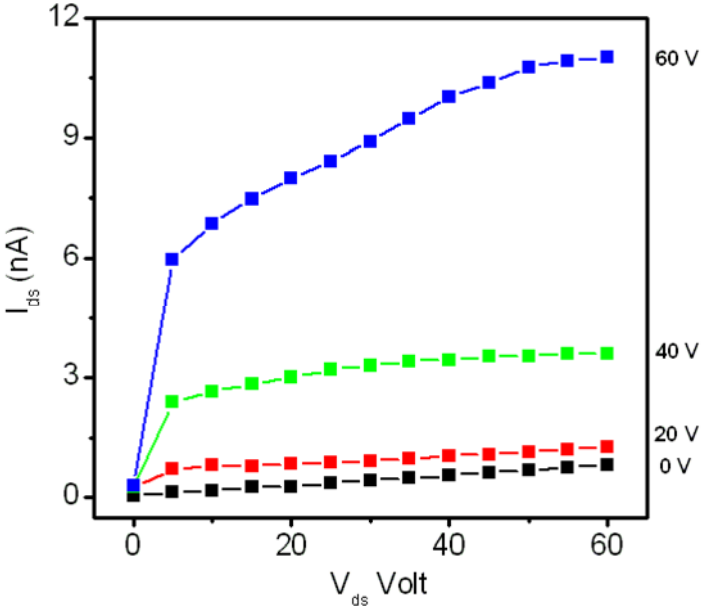

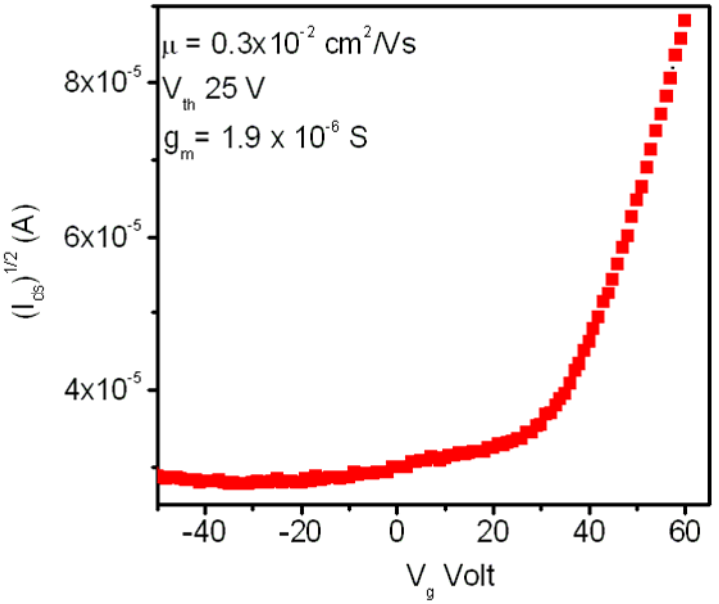

On-Off ratio: 20-100
Mobility ~ 10^{-3} cm^2 /Vs
Threshold voltage: ~20 volt

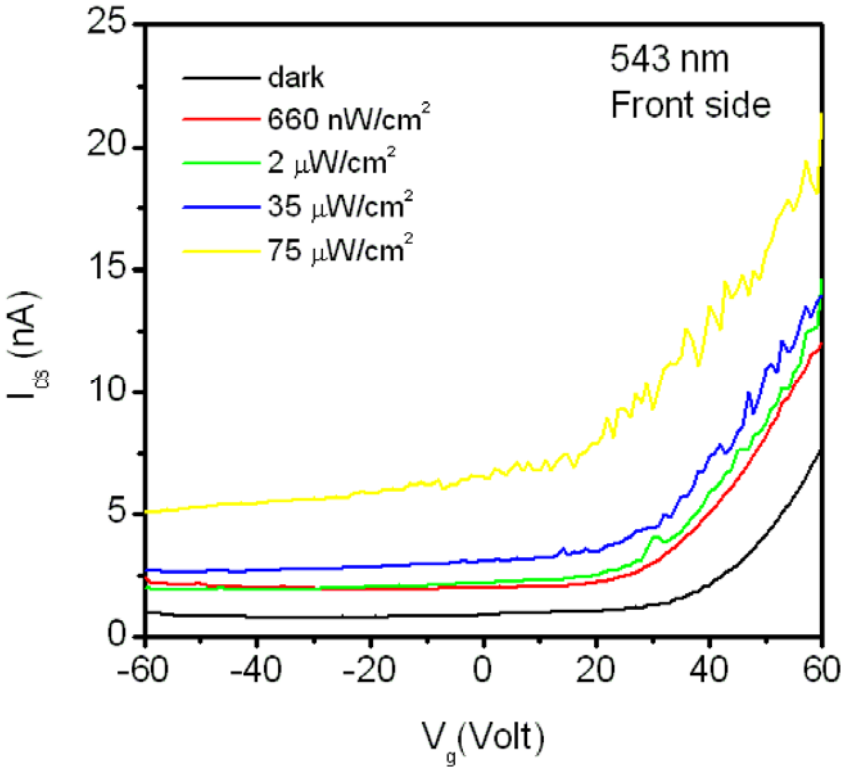

DA-FET with 543 nm excitation from D side

Its shows linear change in I_{ds} in both depletion and enhancement mode of operation.

ΔV_{th} shift with increasing light intensity is in negative V_g

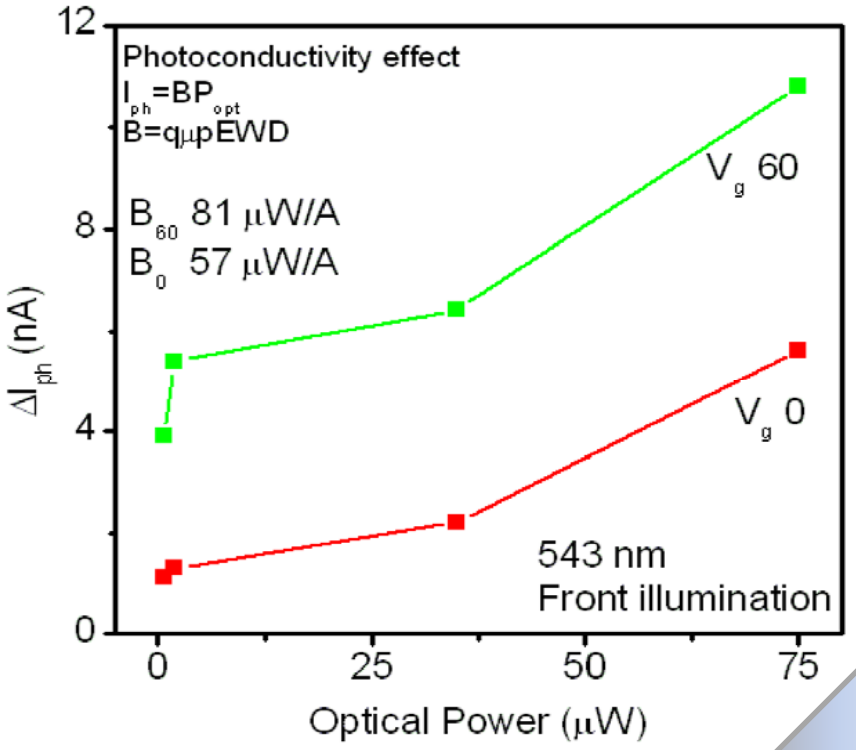

For DA-FET upon channel illumination from D-side
PC effects were observed.

Photocurrent Spectrum

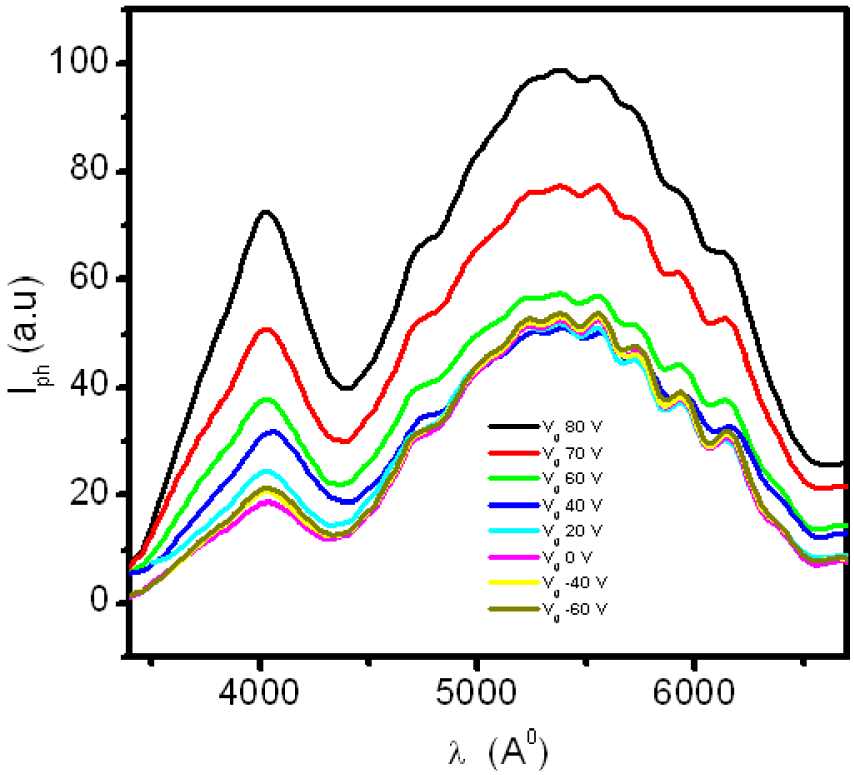

V_g dependent spectral features for DA-FET, illuminated from Front.

400 nm features exclusively originates from N2200, while spectral features from 540 nm contribution is from P3HT.

For 400 nm I_{ph} scales uniformly with V_g.

Negligible changes for 542 nm with V_g, since photoactivity is restricted to Donor interface, while transport occurs through acceptor channel region.

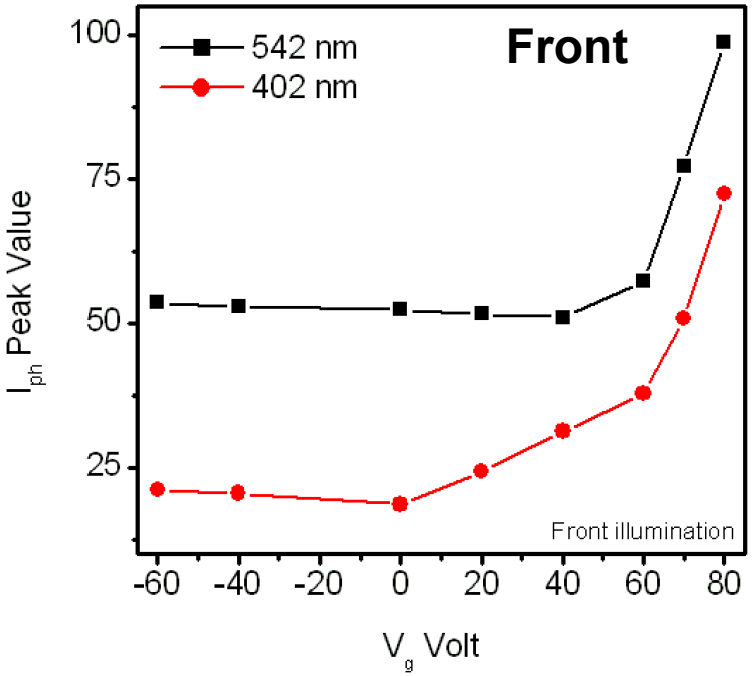

For 540 nm, the change is large since bulk of N2200 also absorbs 540 nm, thus large contribution to I_{ph}.

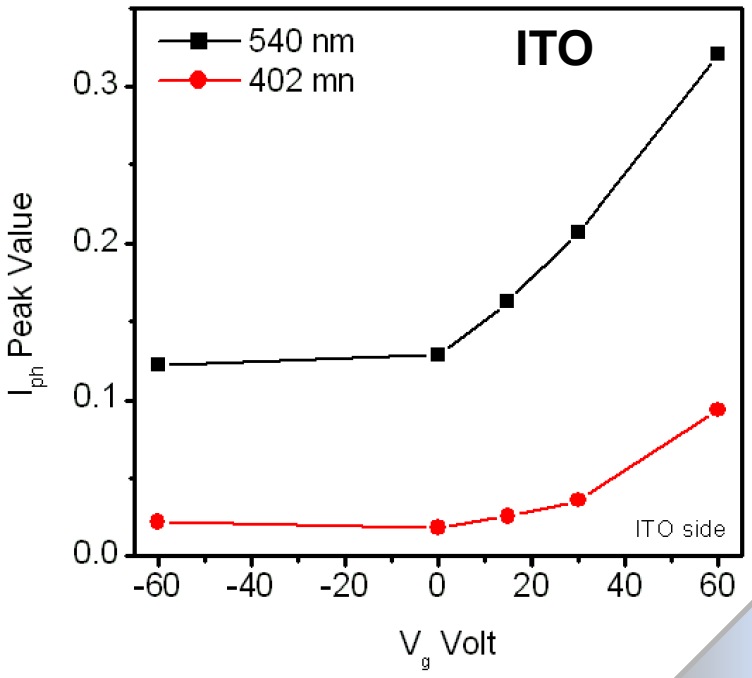

Illumination from ITO allows for charge carrier generation close to dielectric interface, which can be modulated through V_g.

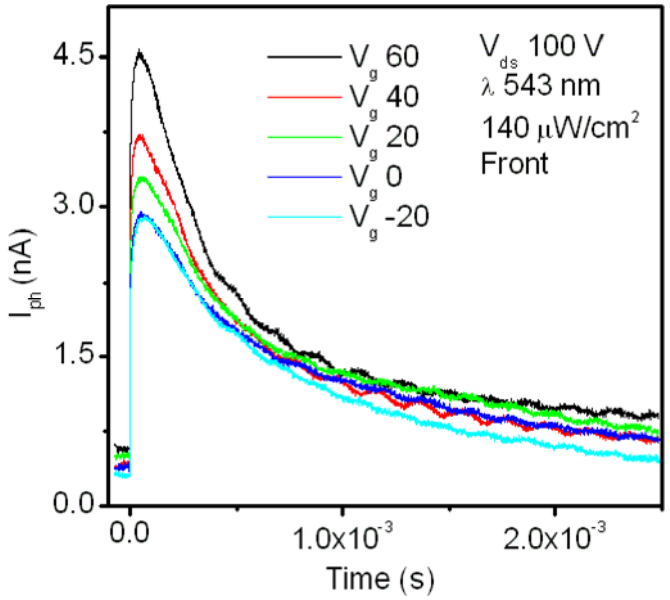

Transient-TOF measurement N2200-P3HT DA-FET, for Front & ITO side illumination.

Decay constant increases, when illuminated from ITO side, for both mode of operation.

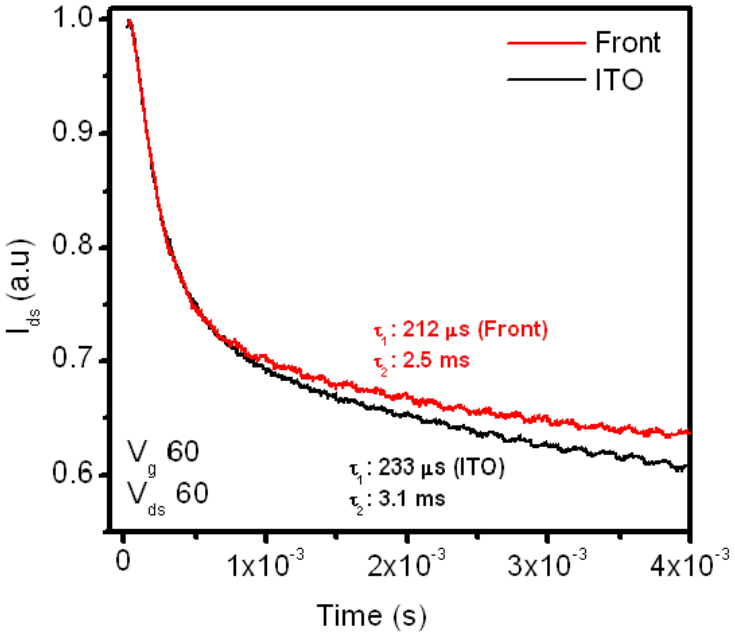

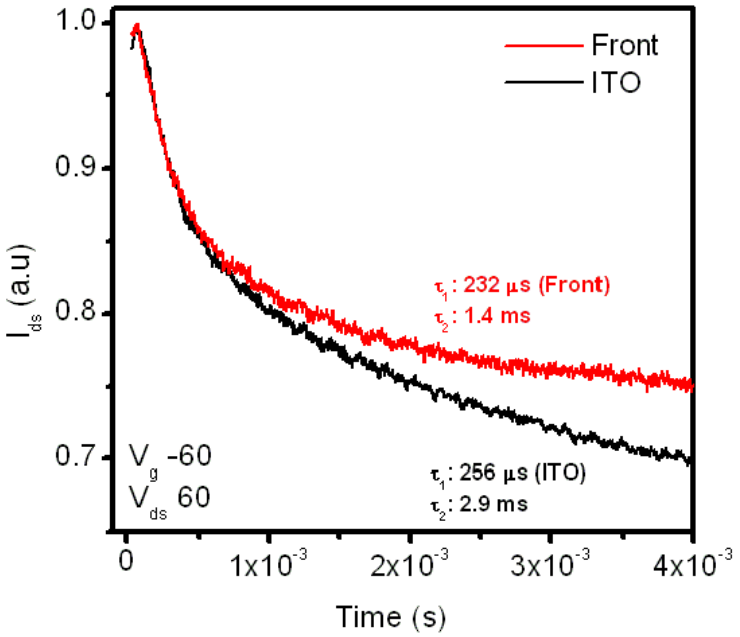

Bilayer FET Response after a light pulse

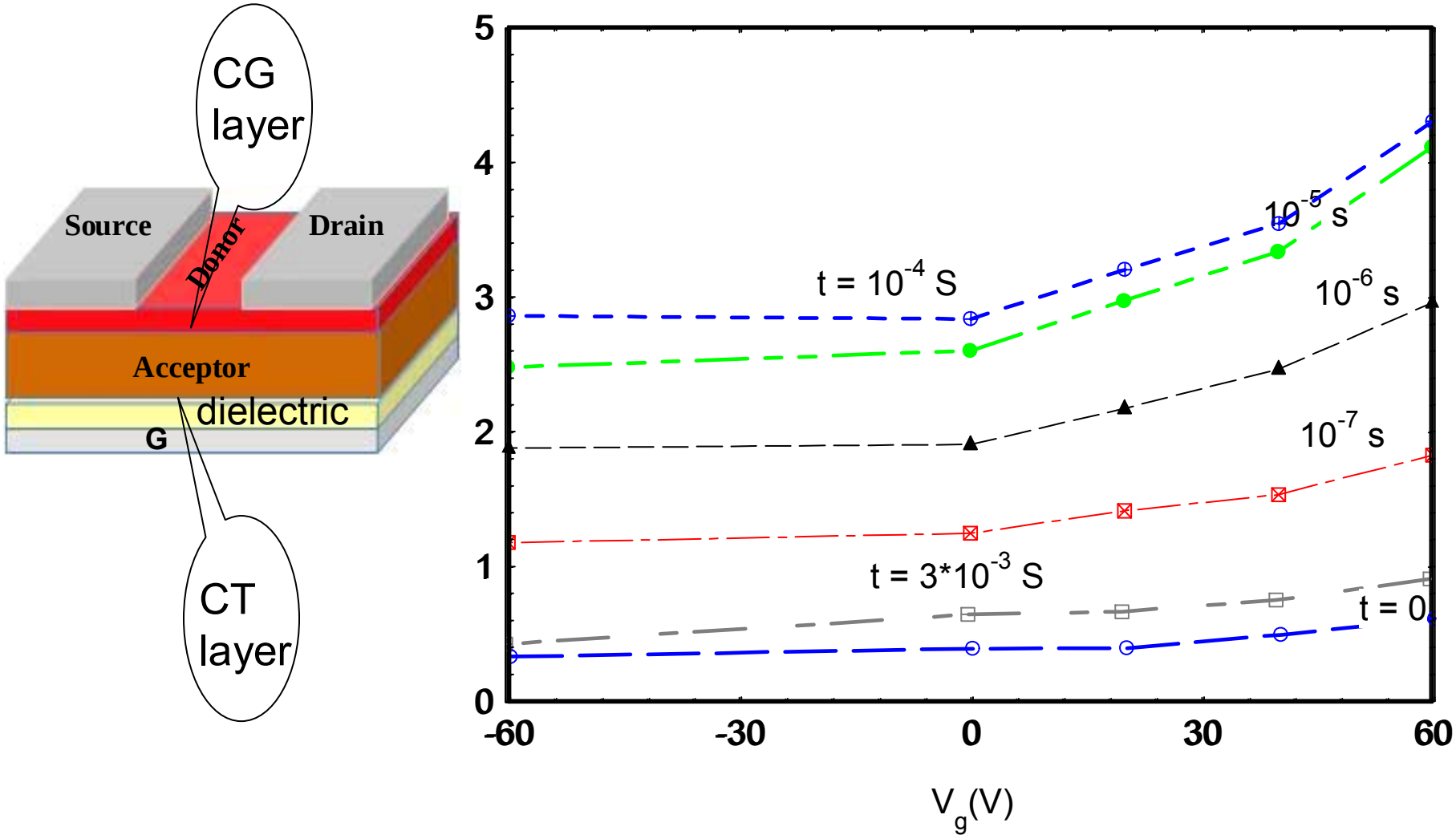

Simultaneous measurement of Field Effect mobility and bulk mobility (TOF) !!

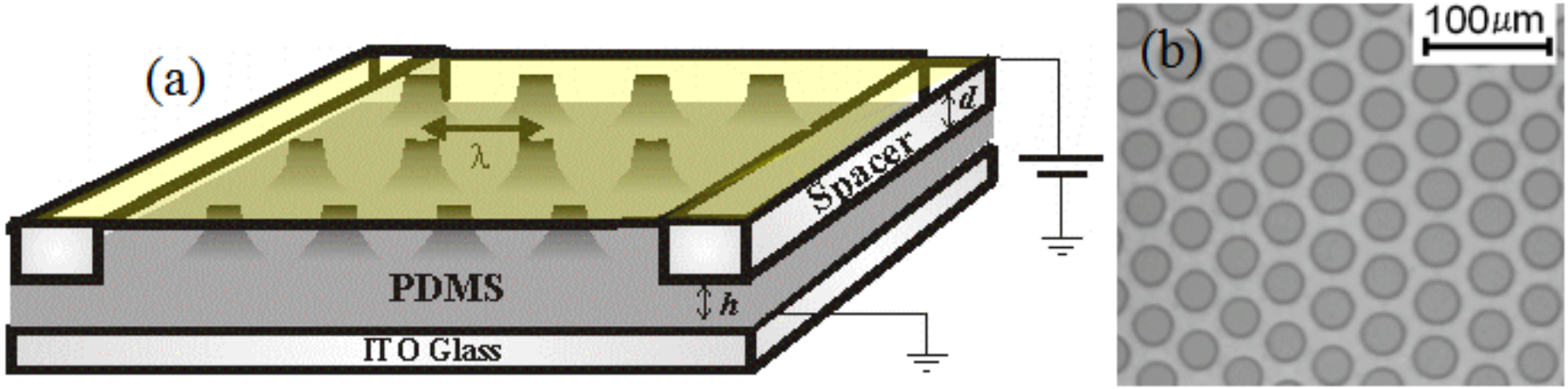
(a)
λ
d
Spacer
PDMS
h
ITO Glass
(b)
100μm

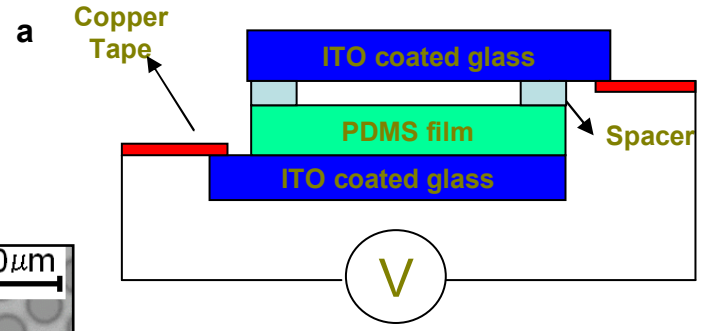

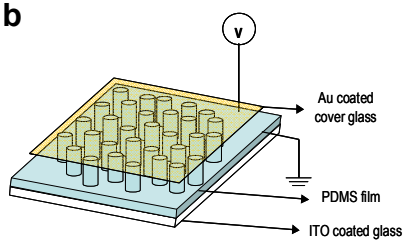

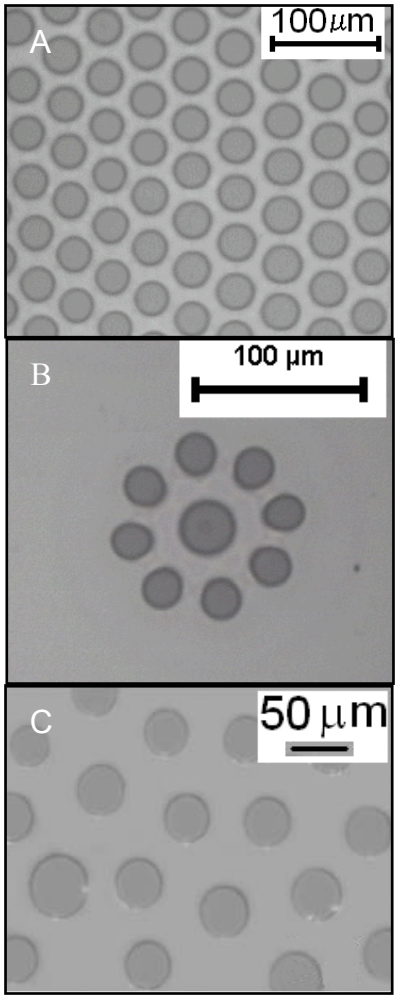

h = 6.25, V = 35V, 1.5% crosslinker

h = 6.78 μm, V=50 volts, 1.5% crosslinker

h=75 μm, 32V, 3 % crosslinker.

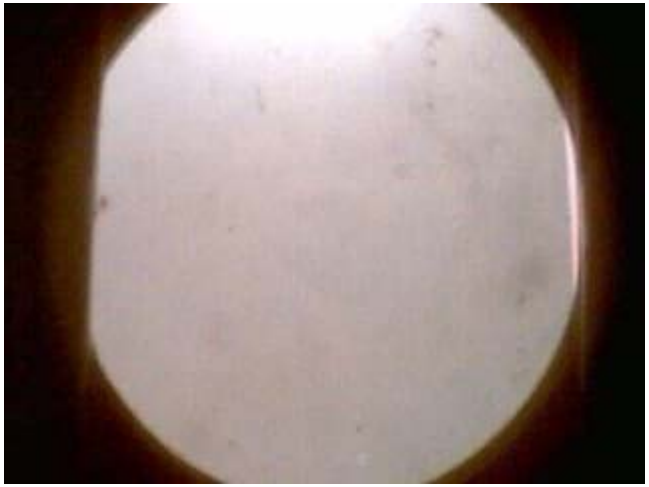

$$\lambda = 2\pi\sqrt{\frac{2\gamma}{-\partial p/\partial h}} = 2\pi\left(\frac{2\gamma}{\varepsilon_0\varepsilon_p\left(\varepsilon_p - 1\right)^2}\right)^{\frac{1}{2}}\left(V\left[\frac{\varepsilon_p d - \left(\varepsilon_p - 1\right)h}{V}\right]^{-3}\right)^{\frac{1}{2}}$$

$$\lambda = C\left[VE^{-3}\right]^{\frac{1}{2}}$$

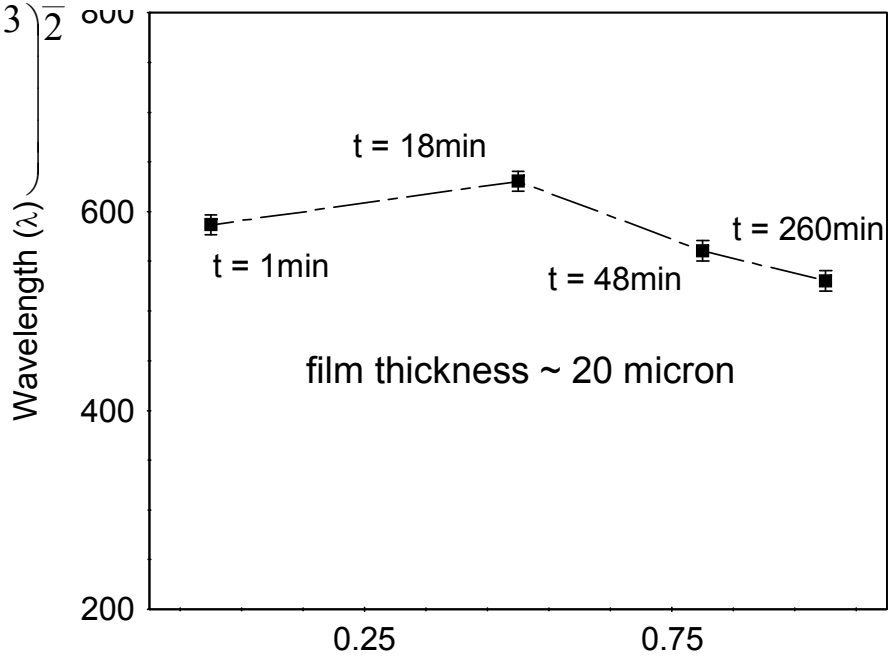

λ Independent of intrinsic props.

λ Dependent on external factors

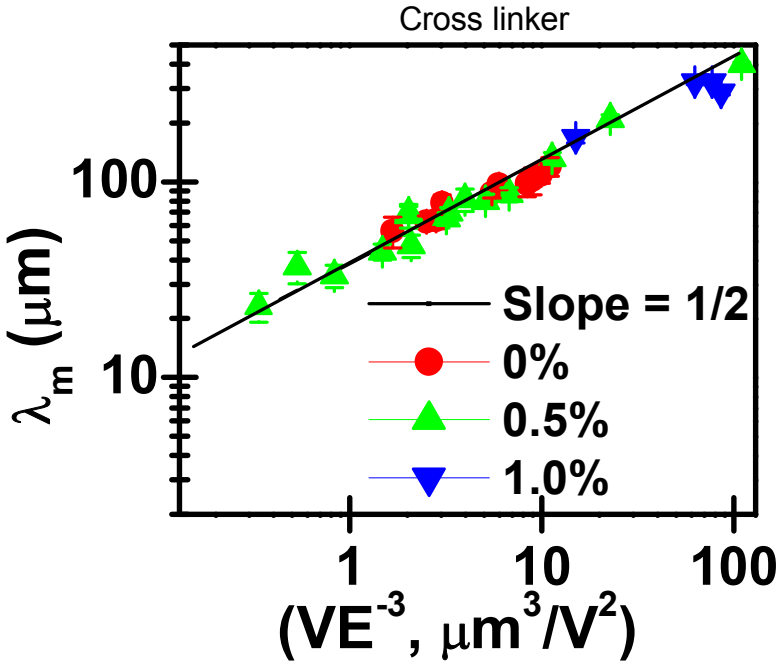

Arun,Sharma,Banerjee, Dixit, K. S. Narayan
Phys. Rev. Lett. 102, 254502 (2009)

What are Bessel beams?

Gaussian Beams

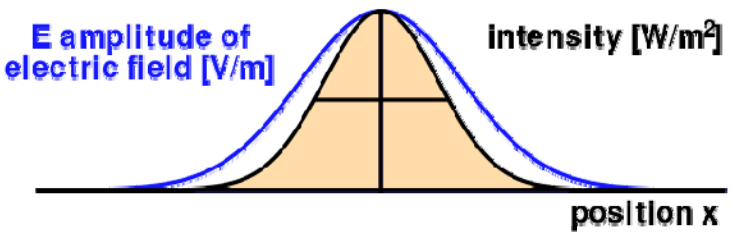

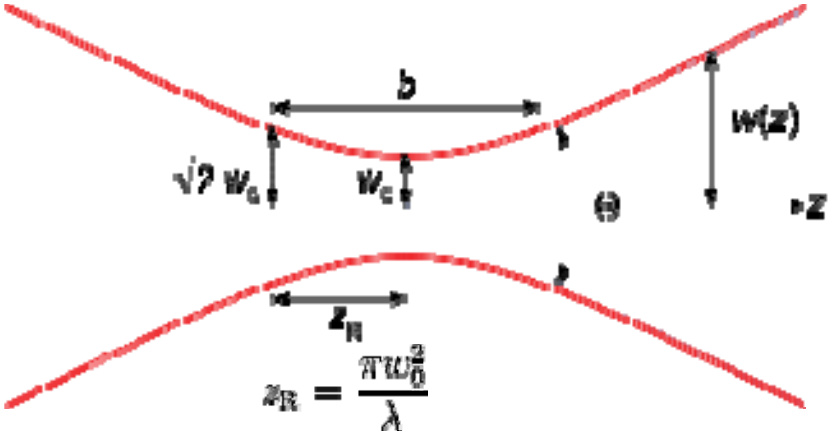

Gaussian beam width $w(z)$ as a function of the axial distance z. w_0: beam waist; b: depth of focus; z_R: Rayleigh range; Θ: total angular spread

$$E(r,z) = E_0 \frac{w_0}{w(z)} \exp\left(\frac{-r^2}{w^2(z)}\right) \exp\left(-ikz - ik\frac{r^2}{2R(z)} + i\zeta(z)\right)$$

Siegman, Anthony E. (1986). Lasers. University Science Books. Chapter 16.

What are Bessel beams?

$$I(\rho,z) = \frac{4Pk\sin\alpha_0}{w_0}\frac{z}{z_{\max}}J_0^2(k\rho\sin\alpha_0)\exp\left(-\frac{2z^2}{z_{\max}^2}\right) \equiv I_0(z)J_0^2\left(2.4048\frac{\rho}{\rho_0}\right)$$

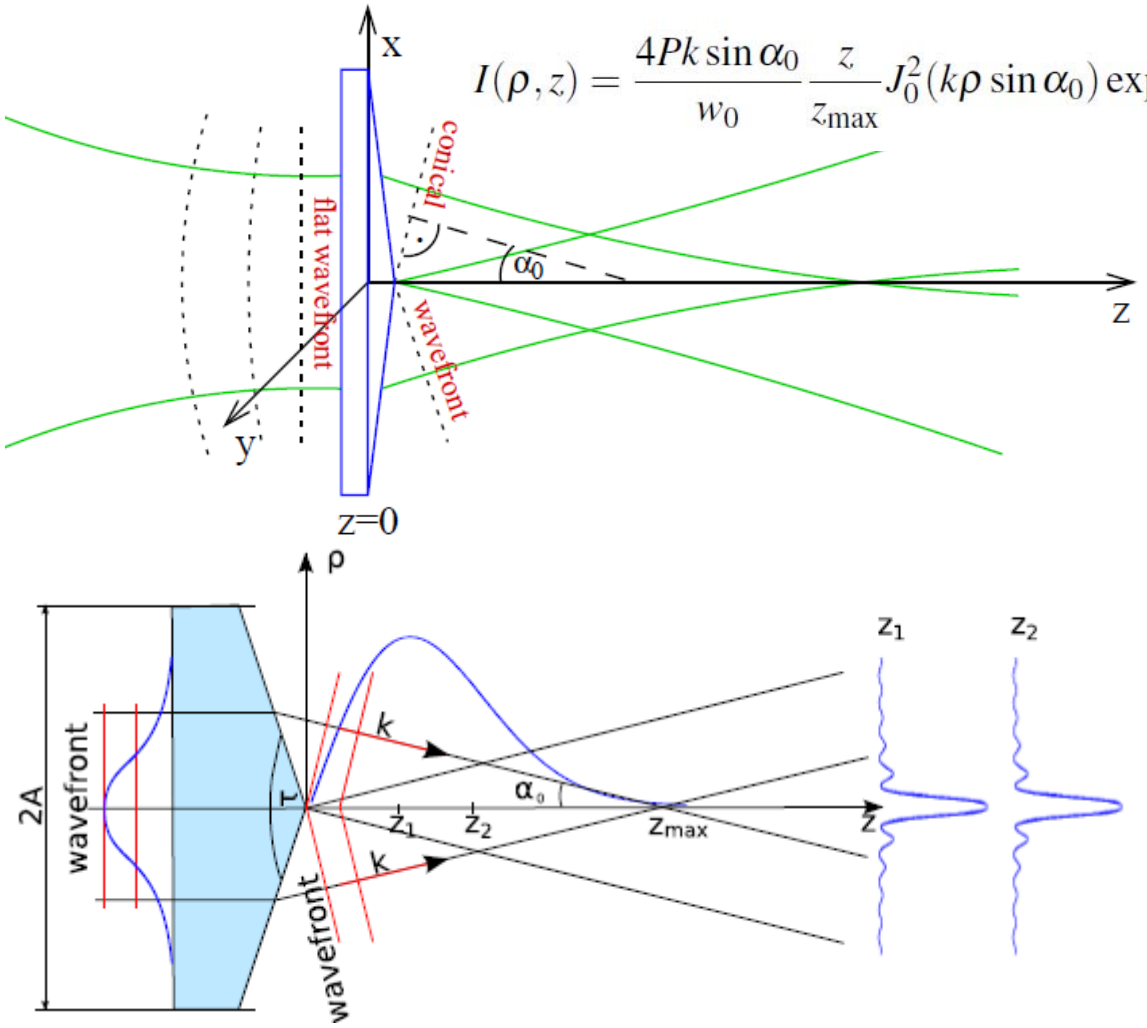

Non-spherical optics:
e.g. Conical lens
Axicons: **Bessel beam Generators**

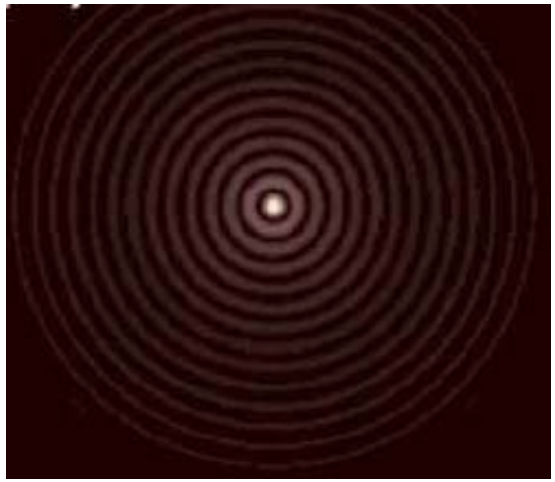

O. Brzobohaty, et. al, Opt. Exp.16, 12688 (2008)

Non-Diffracting type beams and Gaussian beams - A comparison

Non-diffracting	Diffracting
Eg. Bessel beams, Airy beams etc.	Gaussian Beams
Large depth of focus- ~100mm	Small depth of focus ~few mm
Self-healing, self-regeneration properties	No such properties

Applications:
Corneal Surgery, Optical Coherence Tomography, Atom Traps, Laser Resonators

Relevant References:

1. J.H. McLeod, J. Opt. Soc. Am**. 44,** 592 – 597 (1954).
2. J. Durnin, J.J. Miceli and J.H. Eberly, Phys. Rev. Lett. **59,** 2612 –2612 (1987).
3. Durnin, J.,Miceli, J. J. Jr & Eberly, Phys. Rev. Lett. **58**, 1499–1501 (1987).
4. J. Durnin, J. Opt. Soc. Am**.** A **4,** 651 – 654 (1987).
5. R. Grunwald et. al., Opt. Lett. **25**, 981–983 (2000).
6. V. Garces-Chavez et. al.,Nature **419**, 145-147 (2002).

Properties of Bessel beams

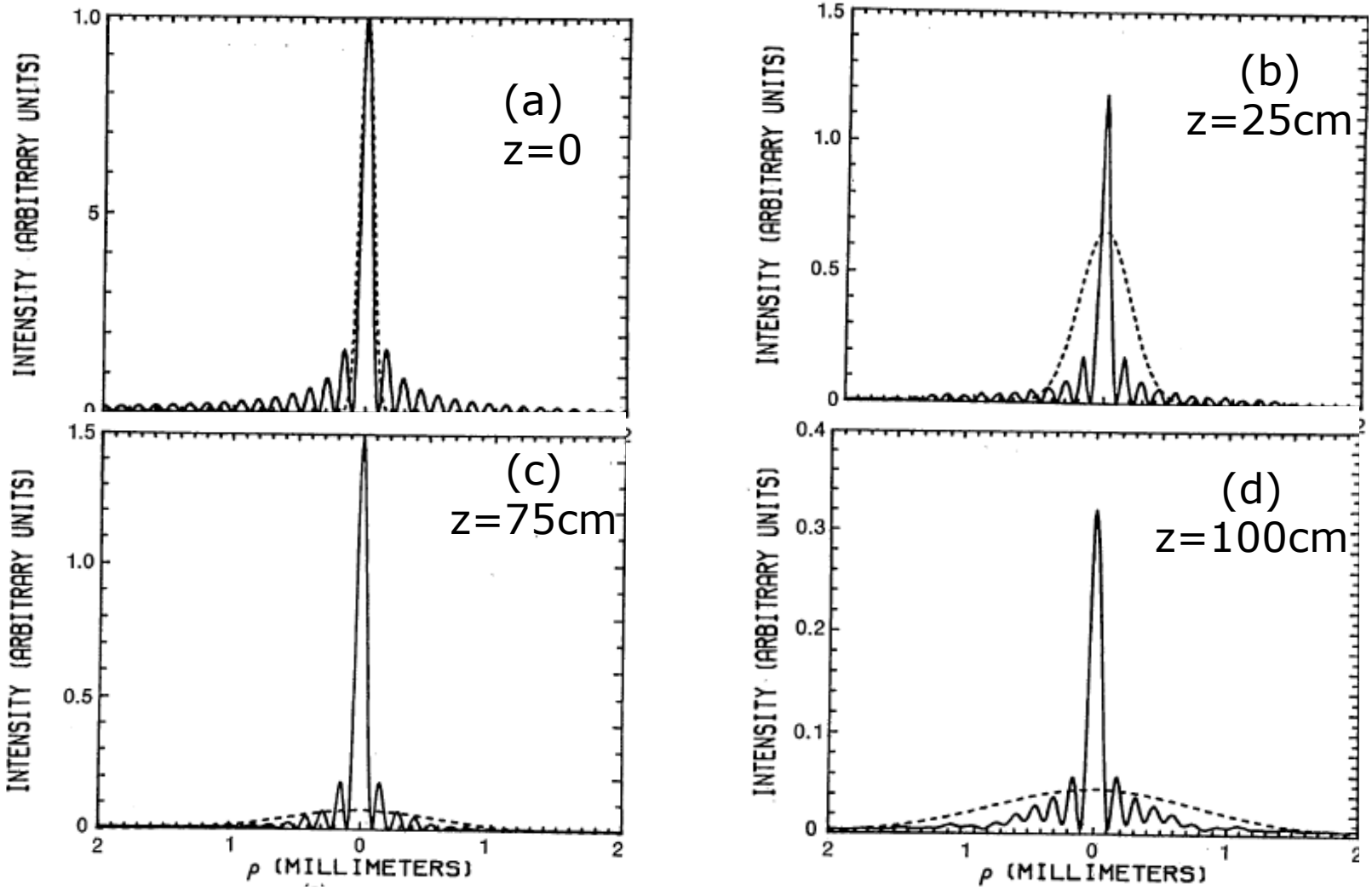

J. Durnin, J. Opt. Soc. Am. A ***4,*** *651 – 654 (1987).*

"One way of thinking about the Bessel beam is to consider a set of plane waves propagating on a cone. Each propagating wave undergoes the same phase shift, kD_z over a distance D_z.
This decomposition of the Bessel beam into plane waves manifests itself in the angular spectrum of the beam, which is a ring in k-space. Thus the optical Fourier transform of a ring will result in a Bessel beam, and this is how Durnin et al. first experimentally observed an approximation to a Bessel beam"

Fabrication of Micro-axicons

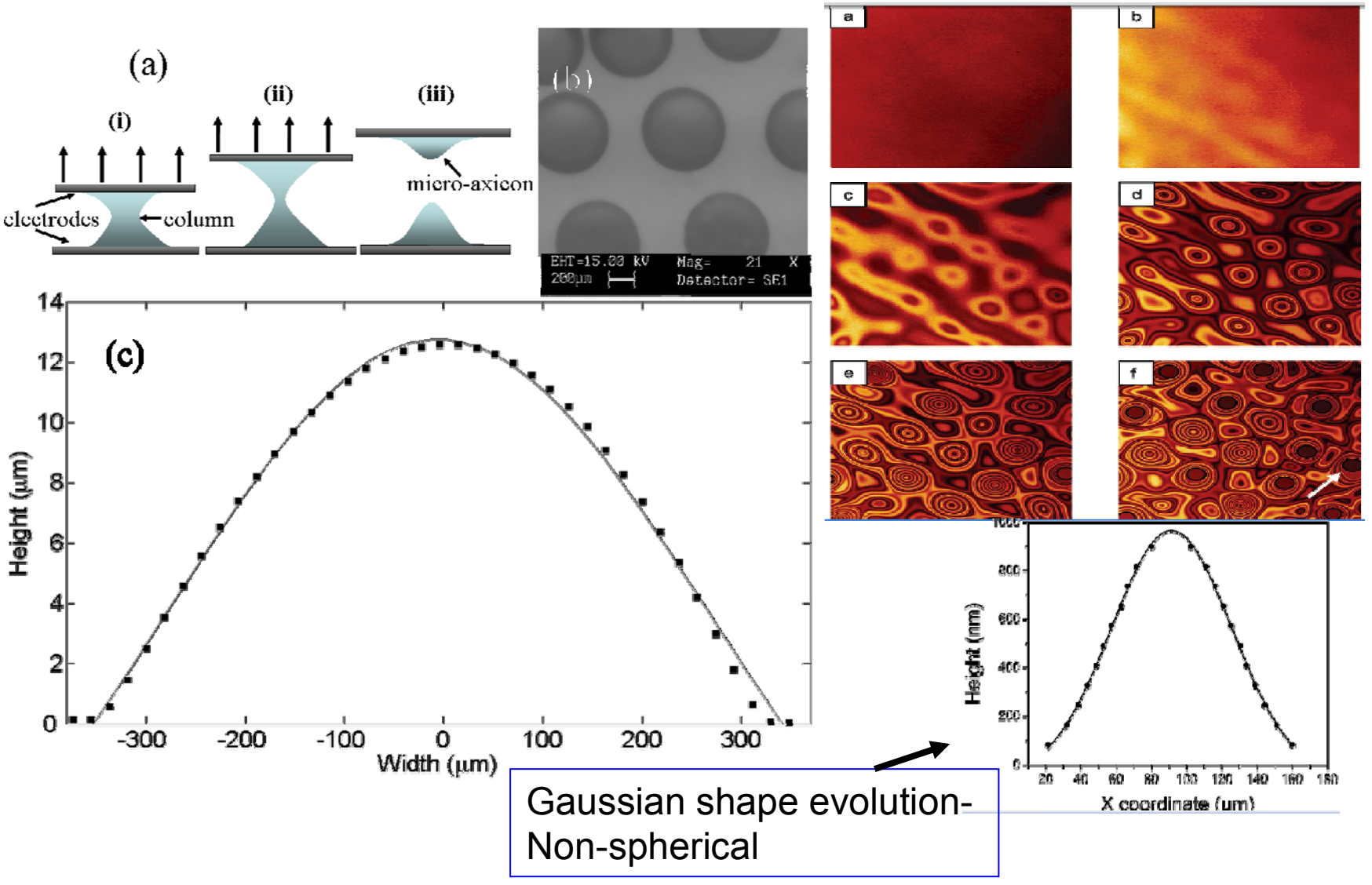

Gaussian shape evolution-
Non-spherical

Non-Diffracting type beams

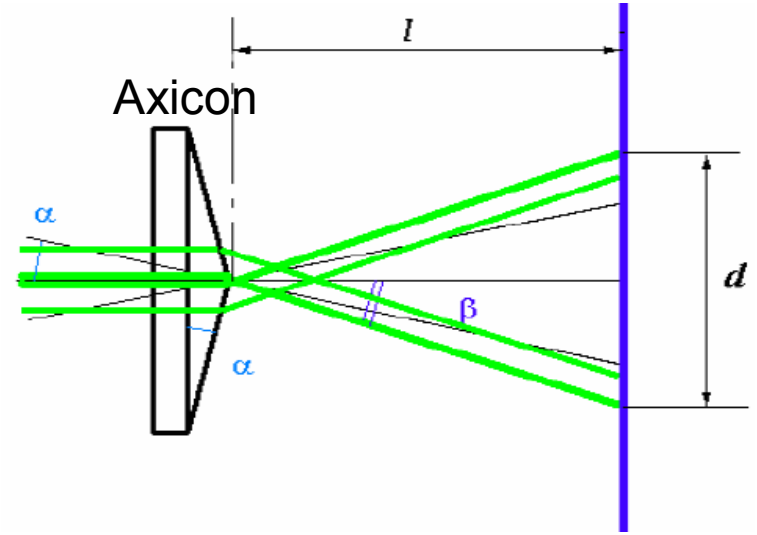

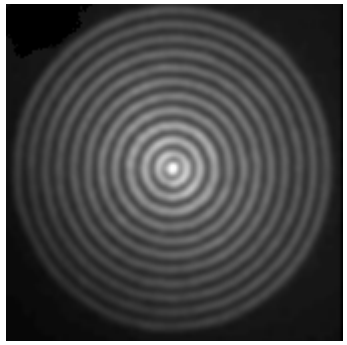

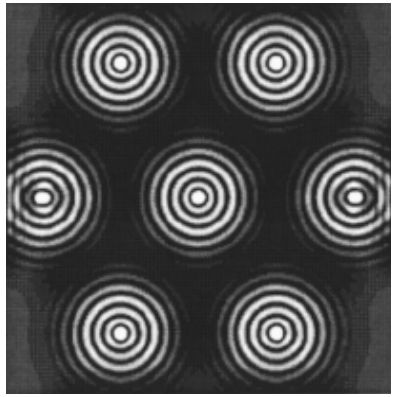

Array of Bessel beams using micro-axicon arrays

Bessel Beams obtained using an *axicon* lens

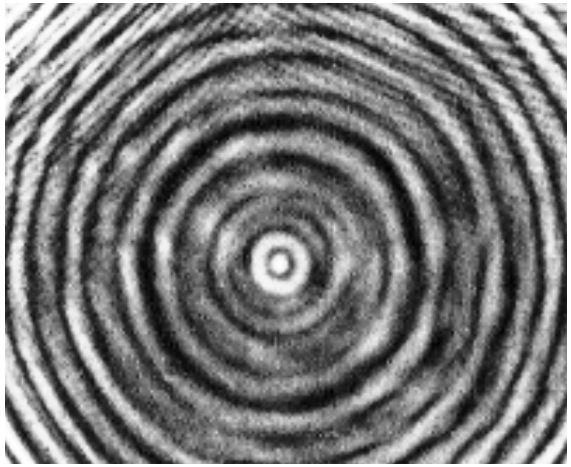

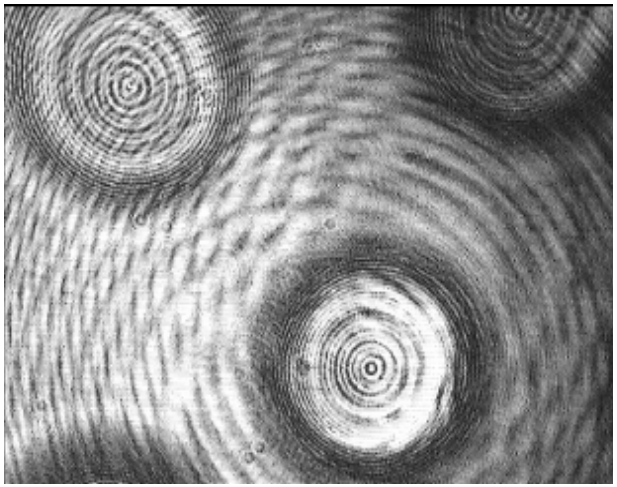

Experimentally observed Bessel like beams with PDMS micro-axicons

Array of Bessel beams

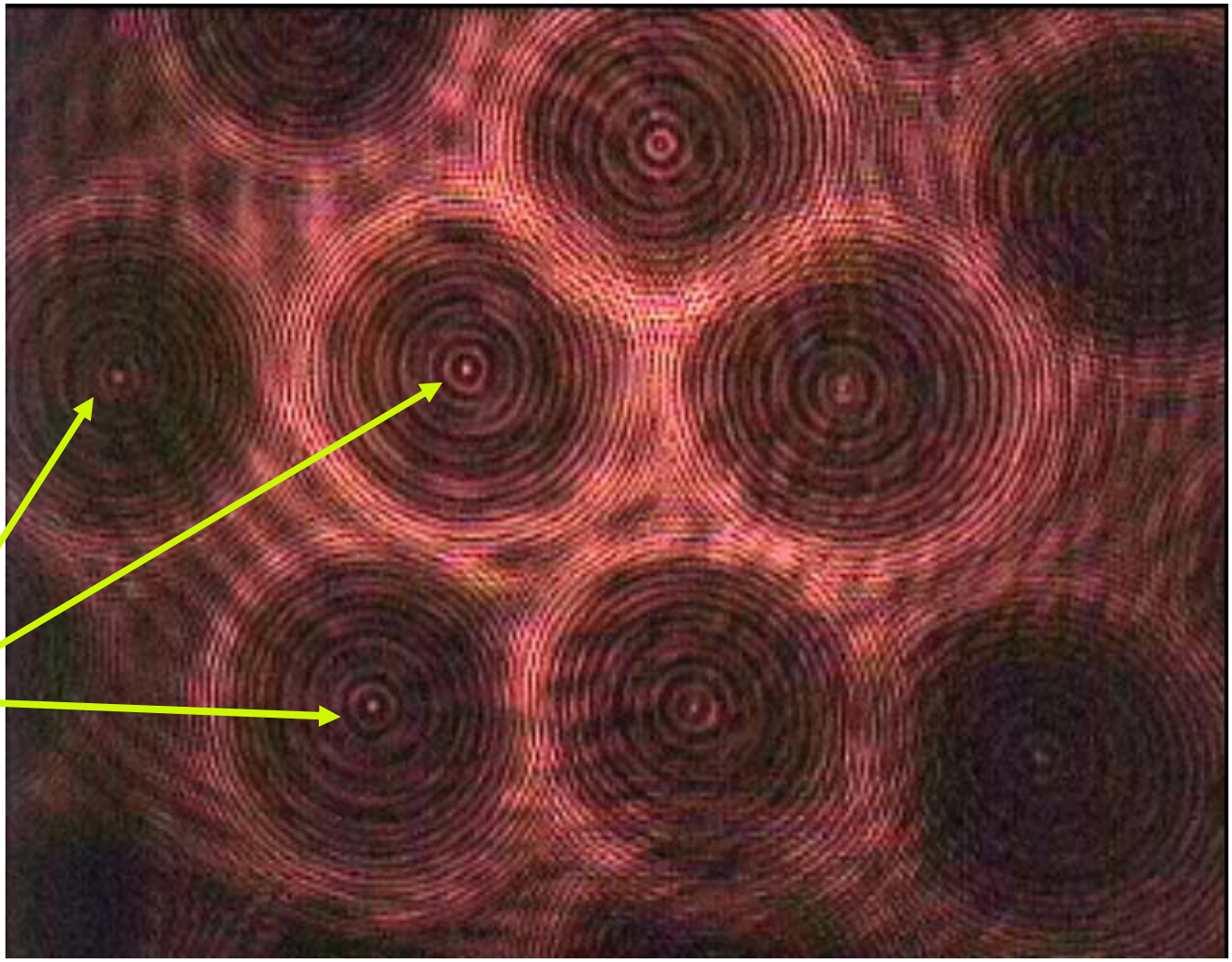

CCD image of Bessel beam array

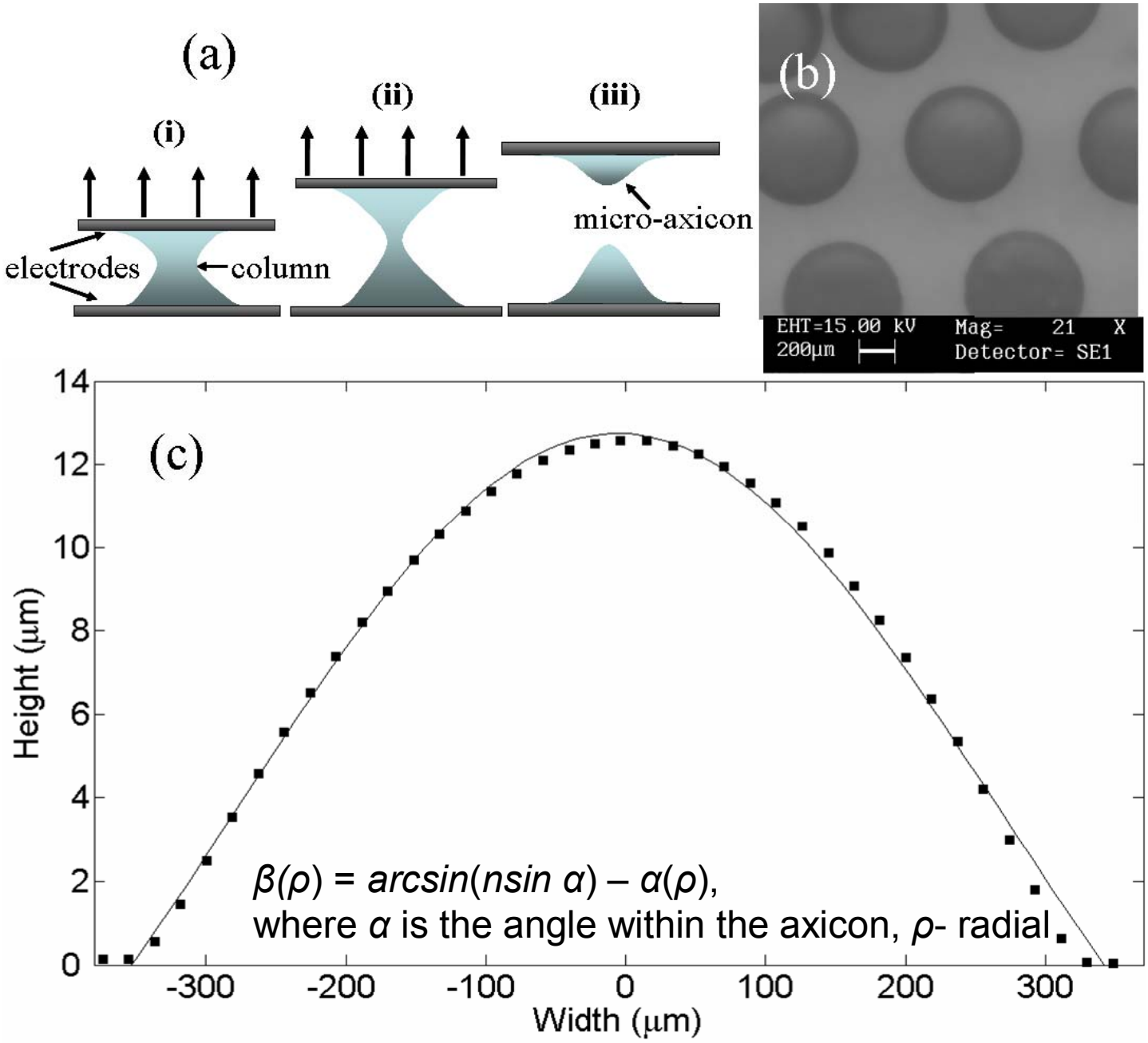

Anshuman and Narayan - Optics Letters 2009

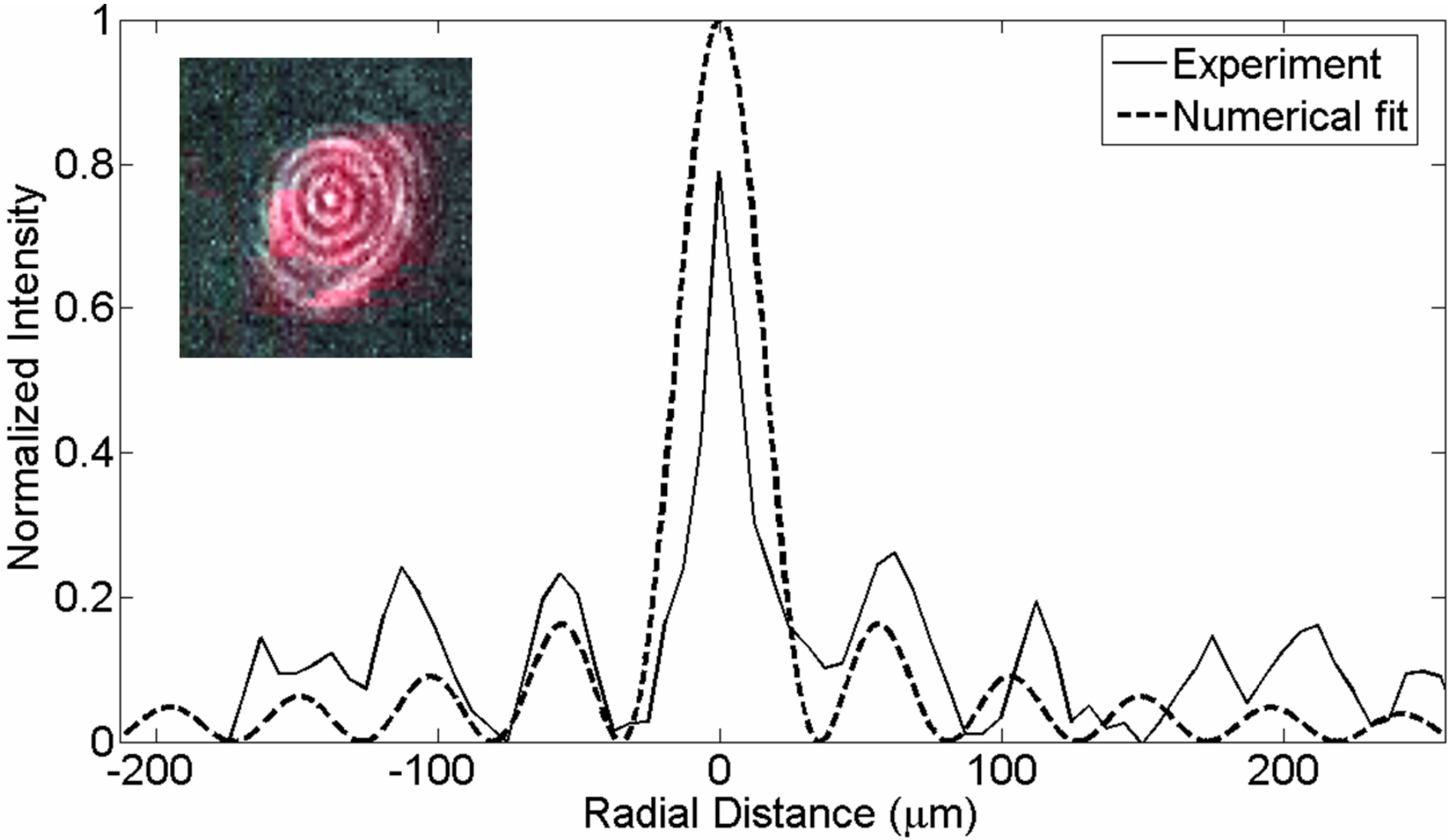

$$A(r,z) = \frac{a_0 k}{iz} \int_0^\infty e^{-\frac{\rho^2}{\omega^2} - i\beta\rho + \frac{ik(r^2+\rho^2)}{2z}} J_0(\rho)\rho d\rho$$

Anshuman and Narayan - Optics Letters 2009

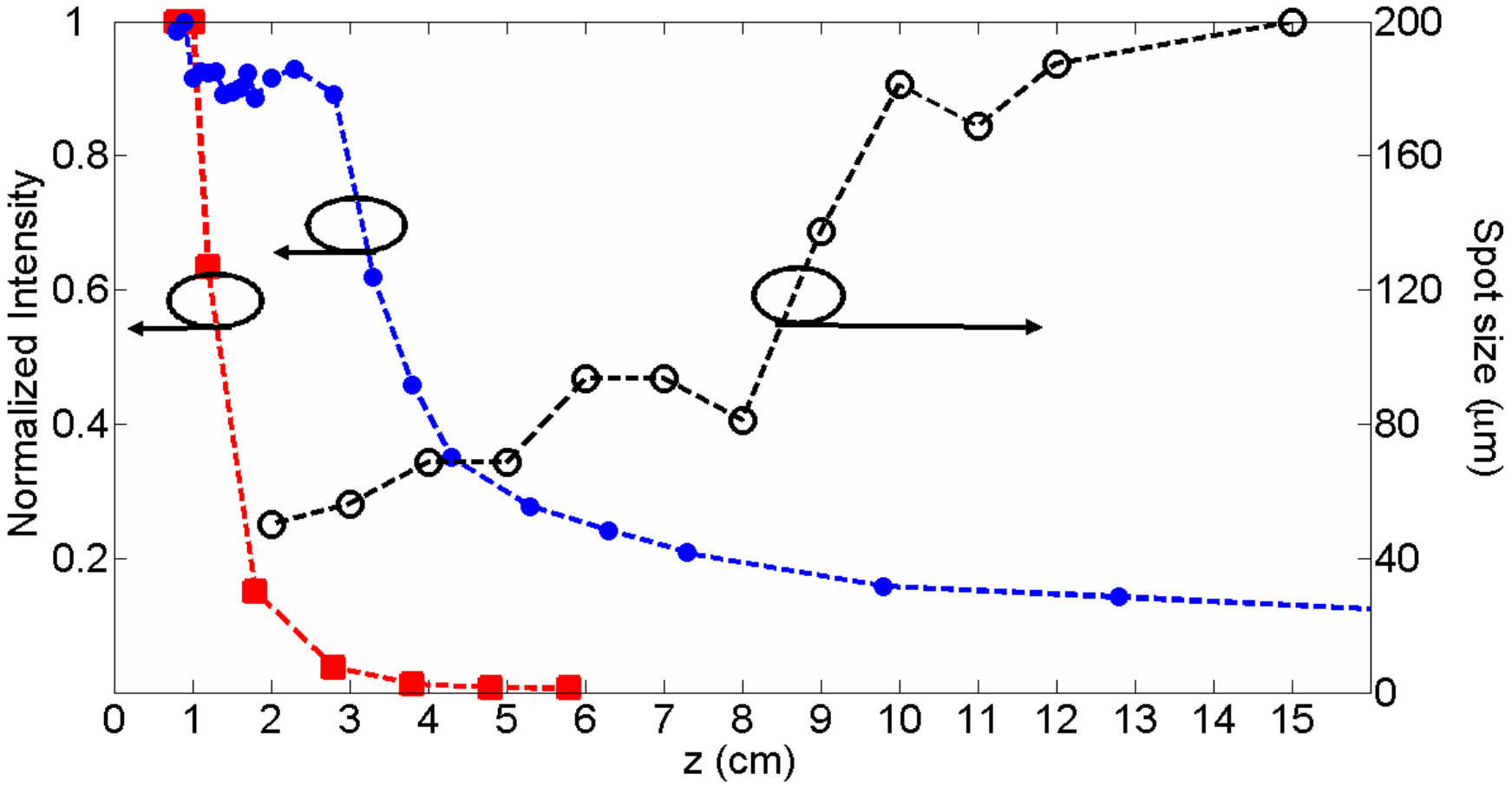

Comparison of on-axis intensity of Bessel beam (blue curve) with a Gaussian beam (red curve)as a function of axial distance z. Spot size variation as a function of axial coordinate (black curve).

Non-Diffracting type beams

Pillar Side View

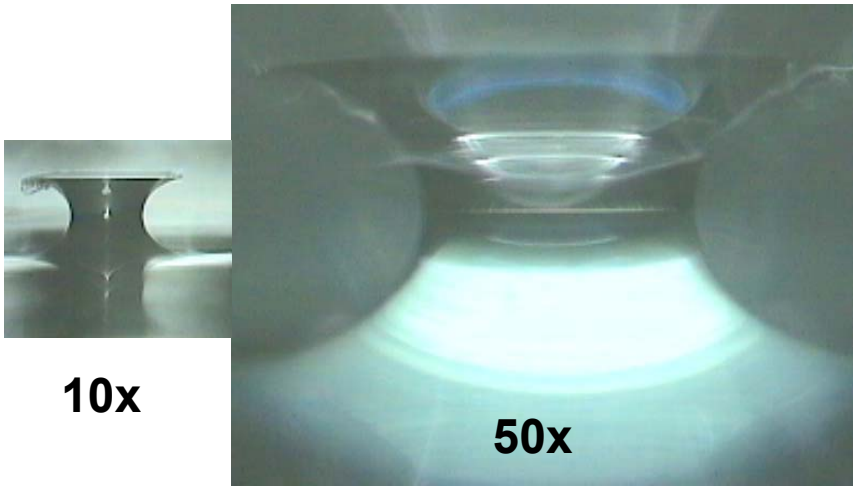

Some clips

Gaussian beam blocked by obstacle

Self-reconstruction of Bessel like beams from the above structures

Self Reconstruction

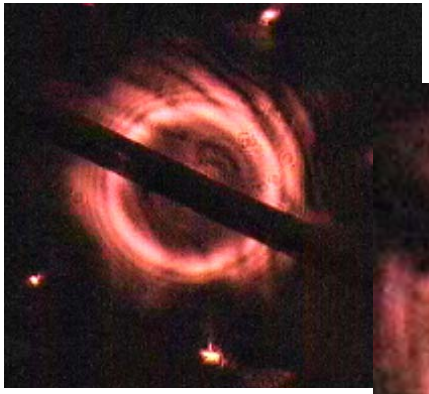

8mm

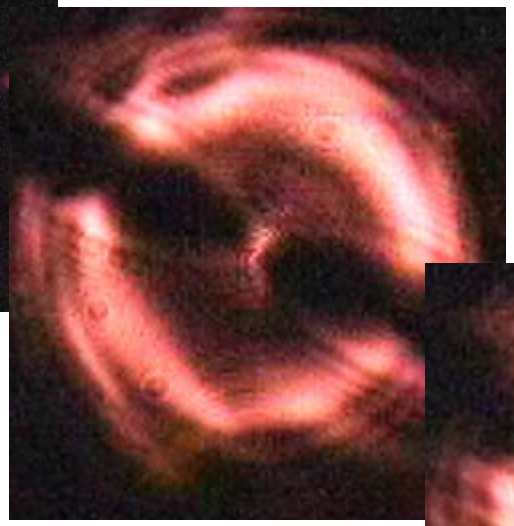

16mm

28 mm

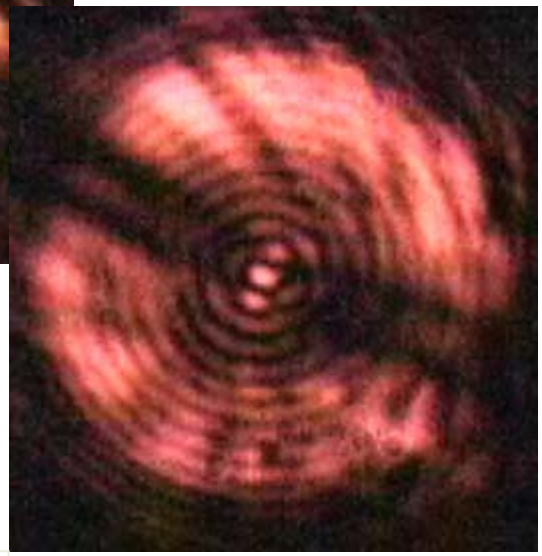

64 mm

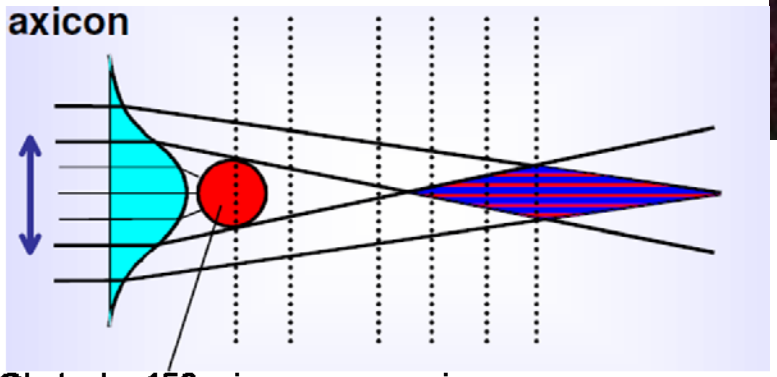

The beam is not affected by the obstacle !!!

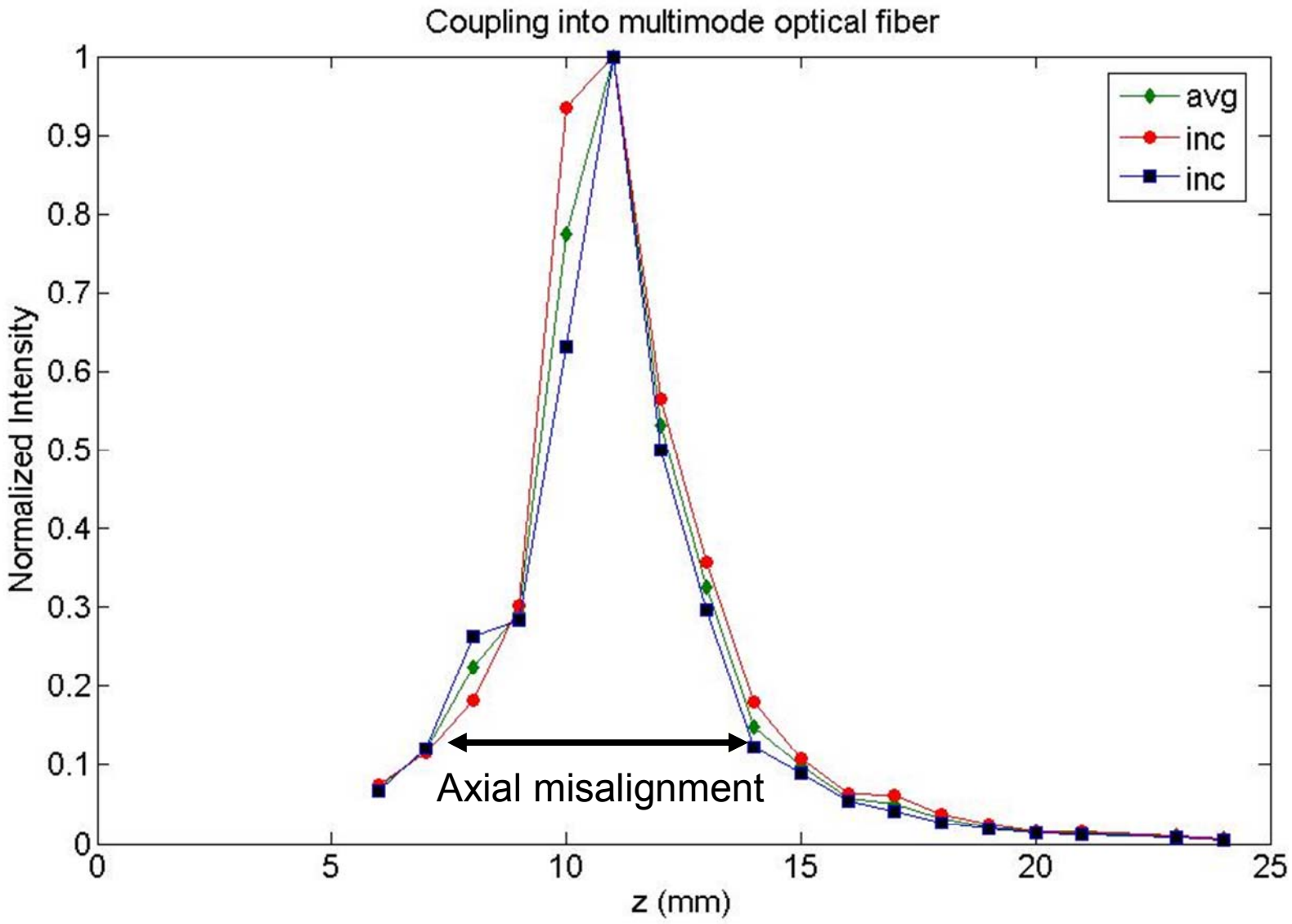

Better tolerance to axial misalignment

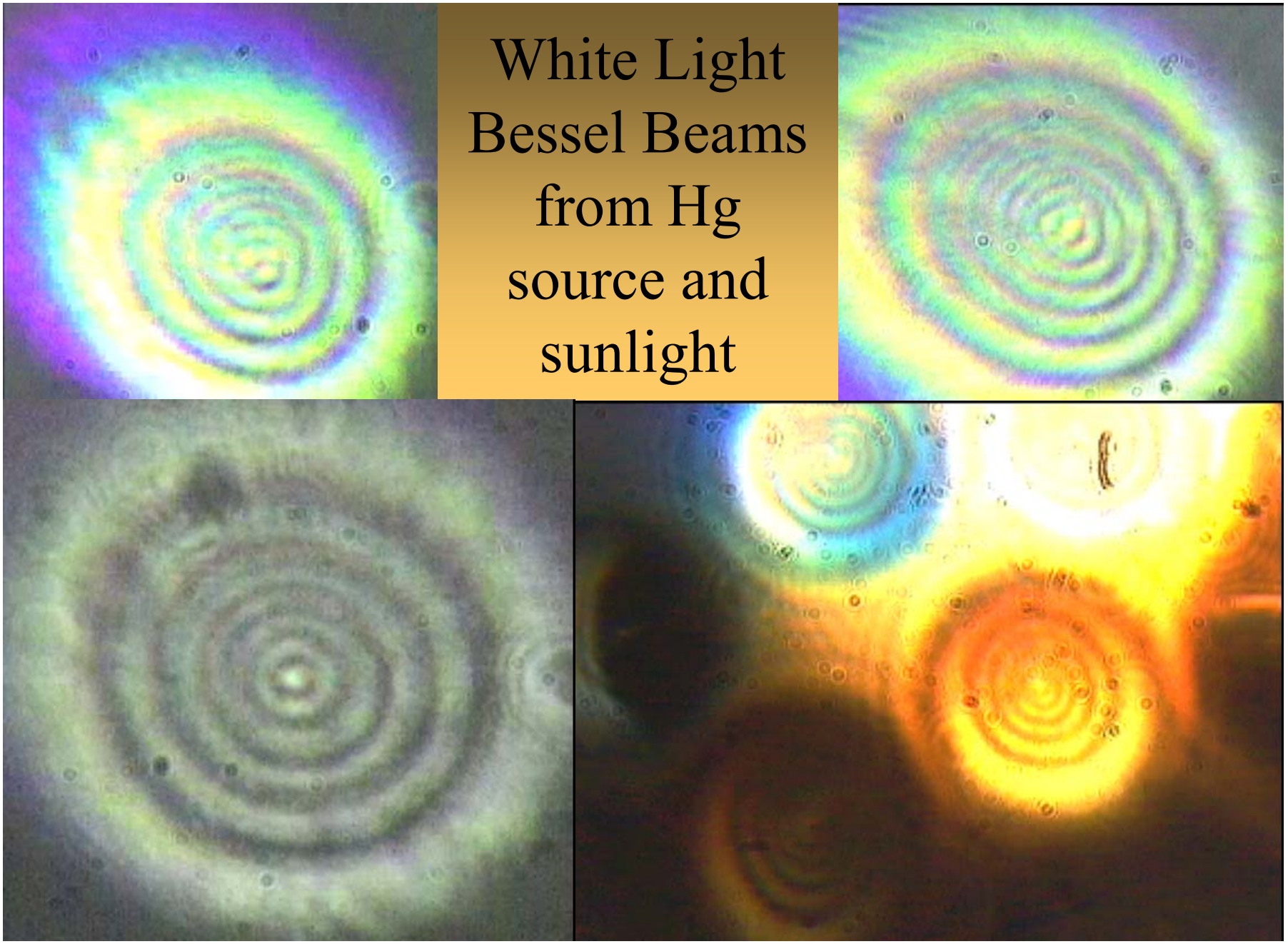
White Light
Bessel Beams
from Hg
source and
sunlight

- The results demonstrate a facile method to manipulate beam characteristics.

- The beam from the EF induced deformation exhibited all the basic features of a Bessel beam in terms of the nondiffracting distance and spot size variation with axial distances including the self reconstruction characteristics.

- The possibility of fabricating polymer microaxicon arrays using a simple and reproducible lithography free technique and using EF strength with controllable geometrical parameters should have a wide range of applications.

- Light Management in Photovoltaic Structures
- Ring patterns – Lithography
- …..

Deformation of a metal-drop induced by electric-field for organic-electronics and molecular electronics

Origin:

•Metallic Drop on conducting substrate or on dielectric substrate
(Landau Lifshitz – Electrodynamics Home Assignment)

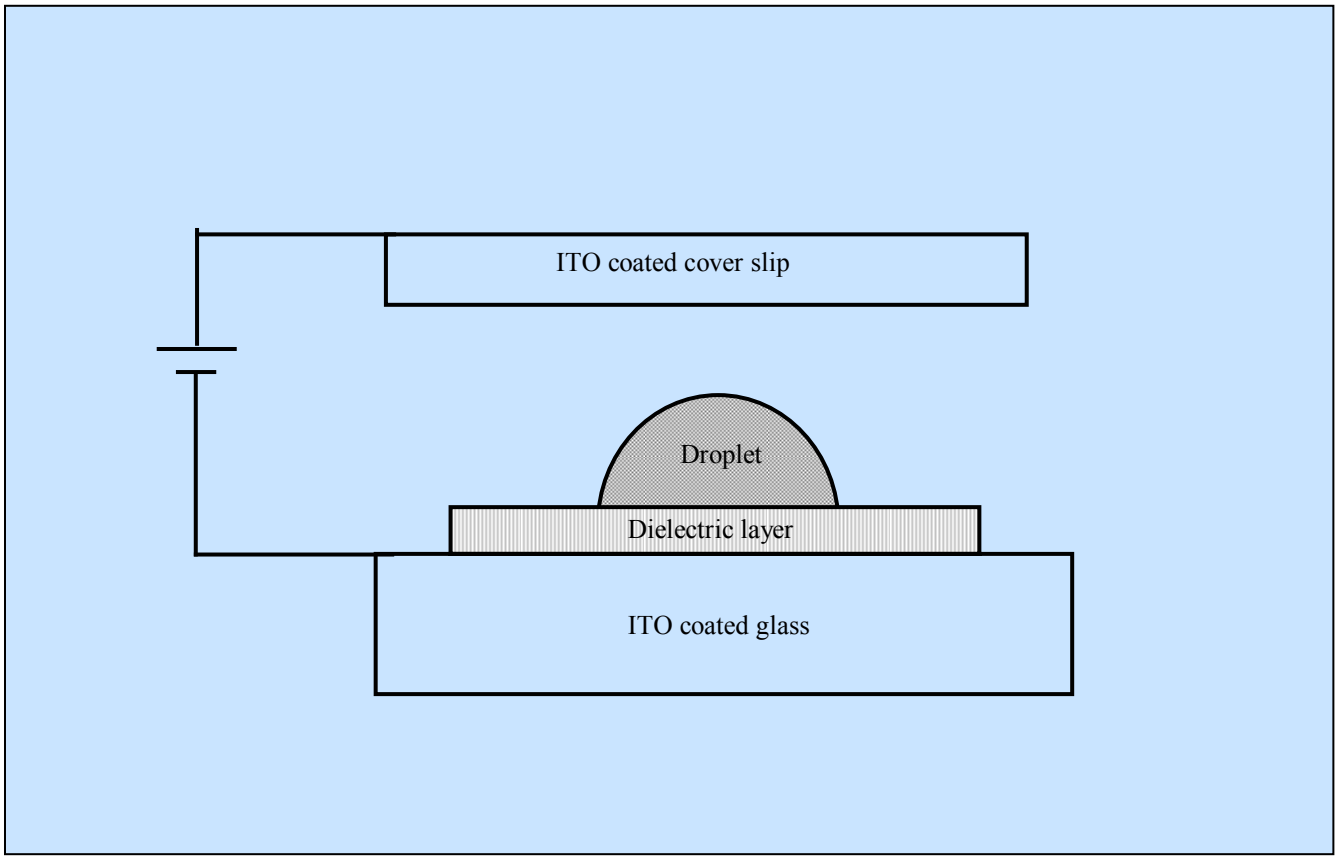
ITO coated cover slip
Droplet
Dielectric layer
ITO coated glass

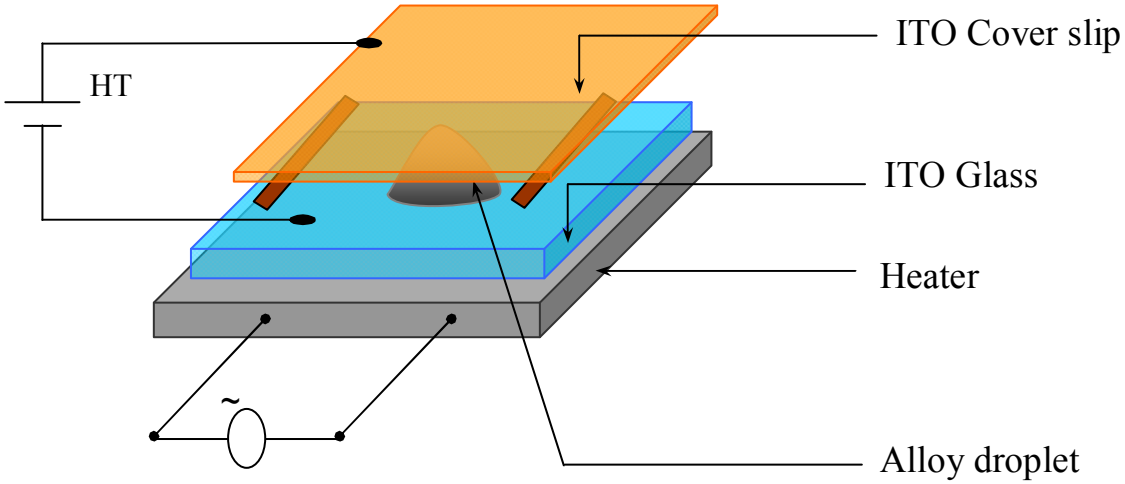
HT
ITO Cover slip
ITO Glass
Heater
~
Alloy droplet

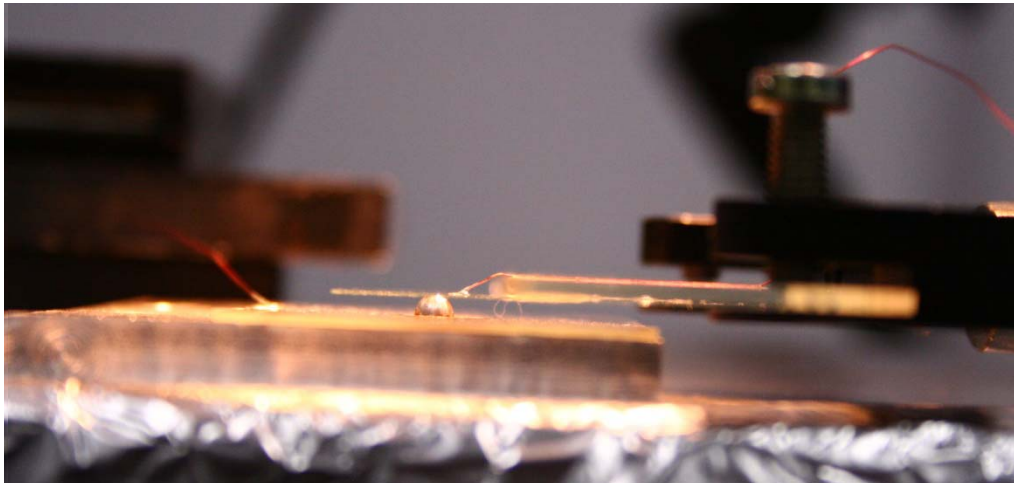

Charged deformable conducting-drop

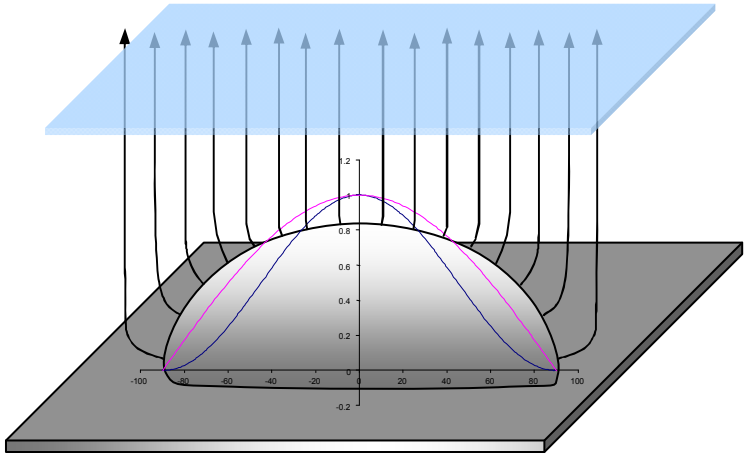

$$\vec{E} = -\frac{\partial \phi}{\partial r}\hat{r}\bigg|_{r=R} = (3E\cos\theta)\hat{r}$$

$$\vec{F}_s = \frac{E^2}{8\pi}\hat{r} = \frac{9E^2\cos^2\theta}{8\pi}\hat{r}$$

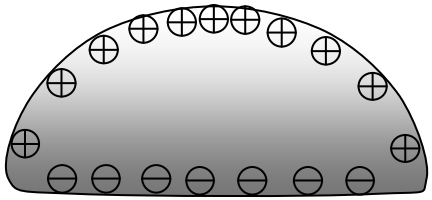

Uncharged droplet under constant electric field

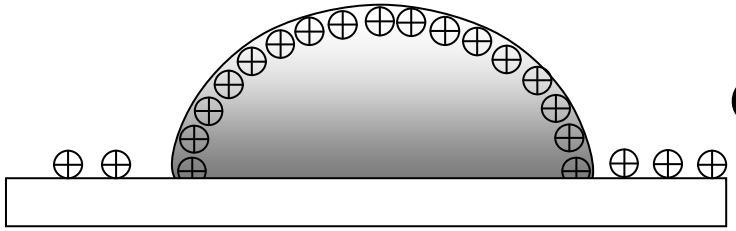

Charged conductor

$$\left(\vec{E}^2/8\pi\right)\hat{r} + \rho_0 = \left(2\gamma/r\right)\hat{r}$$

- For low Bond number and assuming spheroid

$$\vec{F}_{el} = \left(\vec{E}^2/8\pi\right)\hat{r} = \frac{9E^2\cos^2\theta}{8\pi}\hat{r}$$

$$\vec{F}_s = \left(2\gamma/r\right)\hat{r} \qquad E \geq \frac{4}{3\cos\theta}\sqrt{\frac{\gamma\pi}{r}}$$

For charged conductor

- Electrostatic pressure

$$F_{el} = e\phi / 6V$$

Where V is the volume of the droplet

$$\phi \geq \sqrt{\frac{12\gamma V}{Cr}}$$

C is the capacitance of the droplet

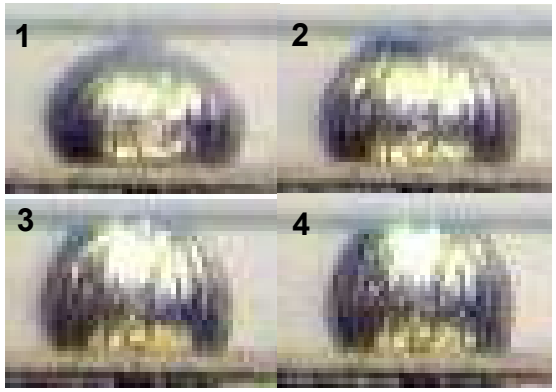

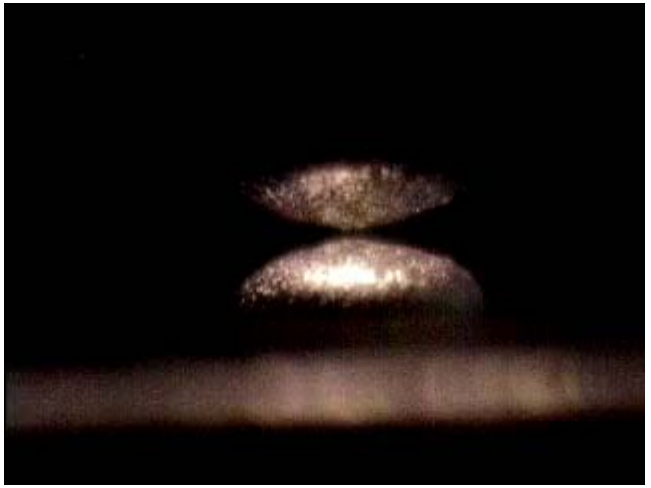

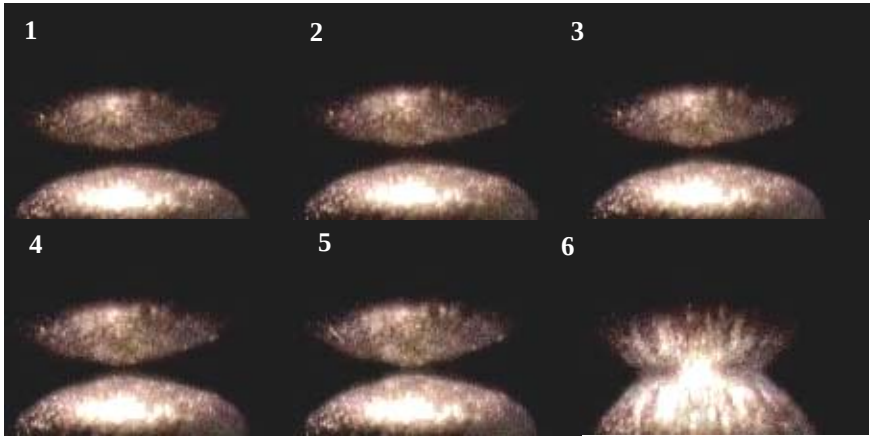

Monojit and Narayan Proc. Of Royal Soc. 2008

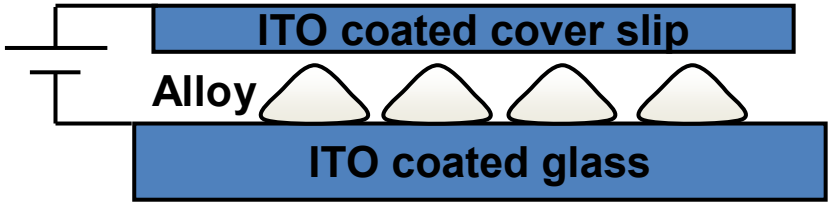
ITO coated cover slip
Alloy
ITO coated glass

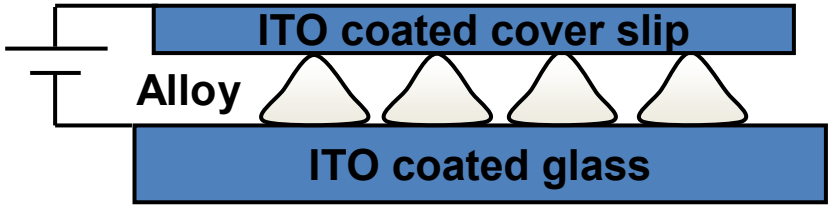
ITO coated cover slip
Alloy
ITO coated glass

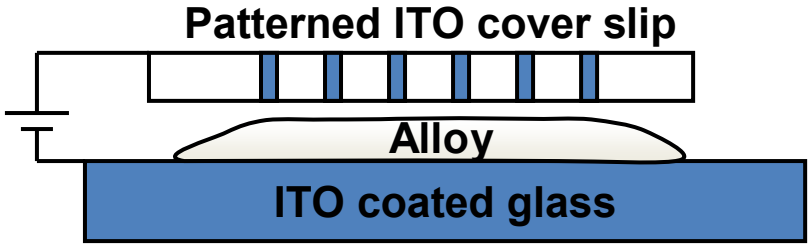
Patterned ITO cover slip
Alloy
ITO coated glass

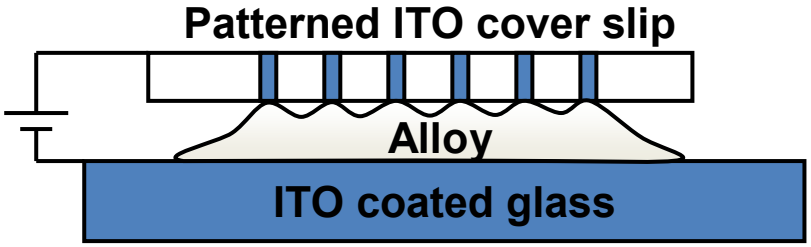
Patterned ITO cover slip
Alloy
ITO coated glass

“Organic Solar Cells”

Energy input from the sun in a single day could supply the needs for all of the earth's inhabitants for a period of about 3 decades.

Needs to be affordable: money wise + CO_2 emission wise + …

Energy Payback Time

Renewable-energy technologies promise to liberate us from fossil fuels. But this implies that their energy payback periods—the time it takes for a system to recover the energy used to produce it—is just as important as financial payback

Polymer Solar Cells with Low Melting Alloys

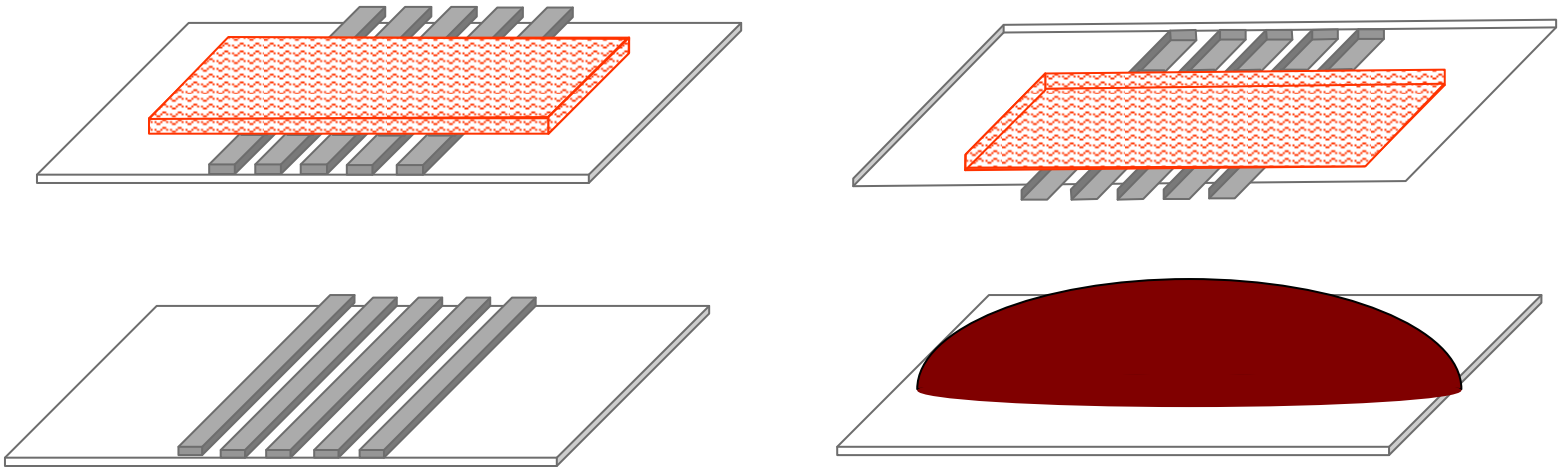

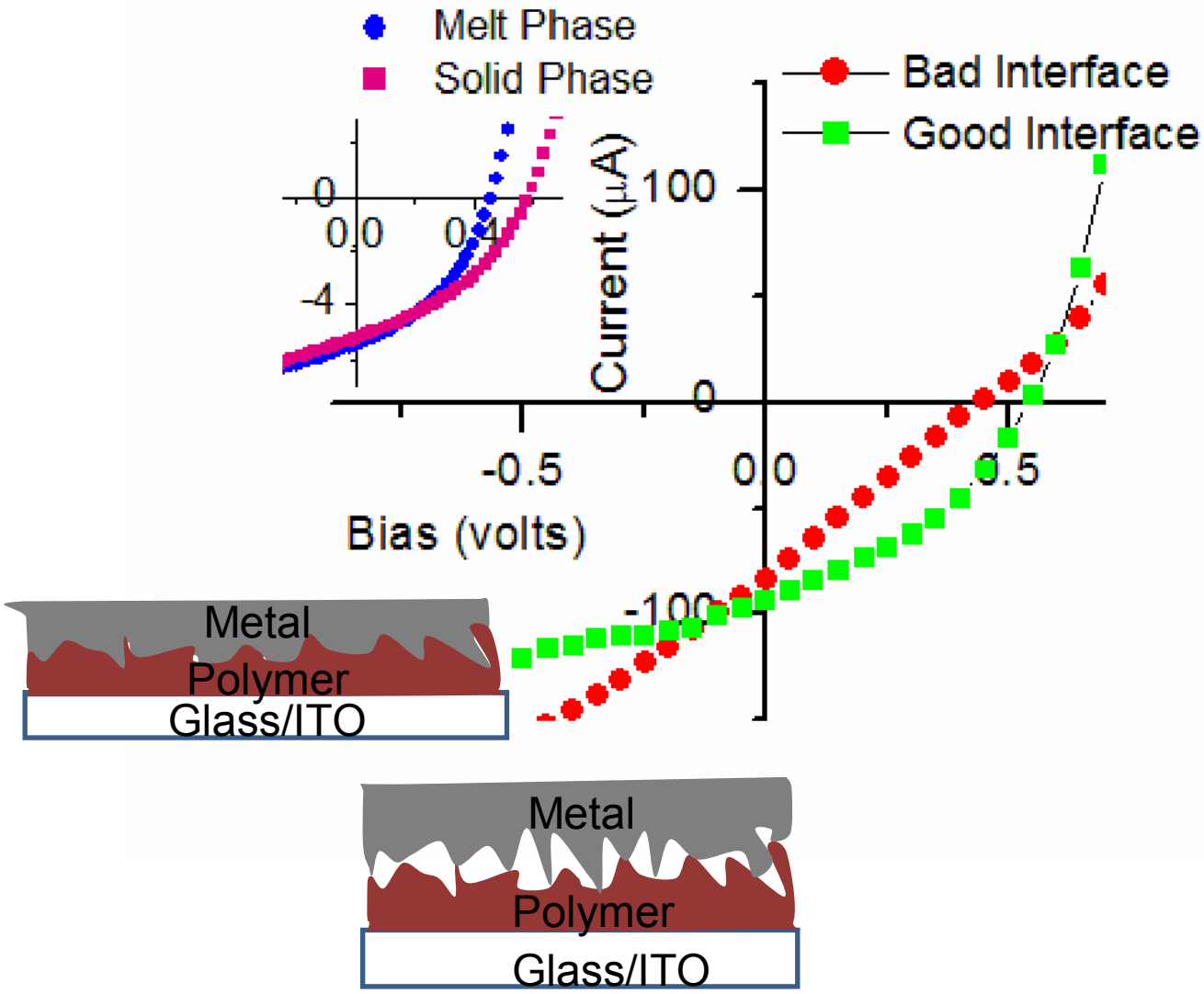

Gupta and Narayan – Appl. Phys. Lett. 2008

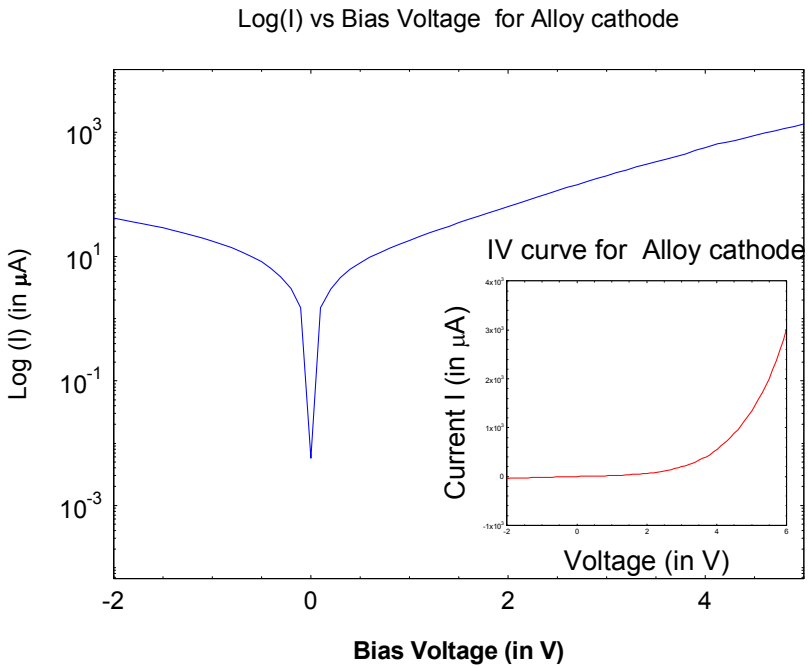

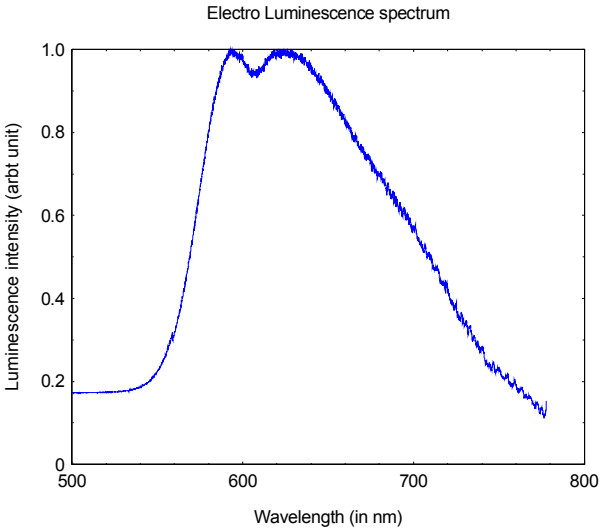

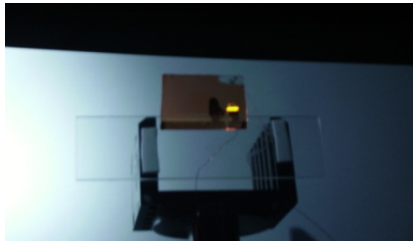

PV/OLED fabrication technology without vacuum requirement

सर्वदेवात्मको ह्येष तेजस्वी रश्मिभावनः ।

एष देवासुरगणाँल्लोकान् पाति गभस्तिभिः ॥ ७ ॥

He indeed represent the totality of all celestial beings. He is self-luminous and sustains all with his rays. He nourishes and energizes the inhabitants of all the worlds.

- Thank You -